# Process monitoring and quality assessment in extrusion-based bioprinting: Defect formation, identification strategies, and the role of artificial intelligence

**Md Asif Hasan Khan[1], Md Anisur Rahman[1], and Jinki Kim[1]**

*1 Department of Mechanical Engineering, Georgia Southern University, Statesboro, GA, USA 30458*

## Abstract

Bioprinting has emerged as a transformative technology in tissue engineering and regenerative medicine, enabling the precise fabrication of three-dimensional biological constructs. The bioprinting process is governed by a complex interplay among material behavior, complex design of bioconstructs, and printing parameters. Any mismatch among these factors can introduce diverse structural defects, thereby compromising the structural integrity, dimensional accuracy, and cell viability of the bioprinted samples. Therefore, ensuring structural integrity requires a robust process monitoring and defect detection approach to produce reliable and functional bioconstructs. This review provides an analysis of sources and impacts of different types of anomalies found in the extrusion-based bioprinting process. Moreover, it discusses the most widely adopted structural health monitoring (SHM) techniques, and assesses their sensitivity, effectiveness, and practical integration within bioprinting processes. The role of artificial intelligence (AI) and machine learning (ML) is further explored, highlighting how the traditional structural health monitoring techniques utilize AI and ML to enable defect detection and predictive quality control. The review also critically examines the key challenges and limitations in bioprinting, including the scarcity of standardized defect datasets and difficulties in sensor integration, and identifies research gaps that must be bridged to advance reliable, intelligent monitoring systems. Collectively, this review aims to provide a structured foundation for developing SHM frameworks capable of supporting the translation of bioprinting from laboratory research toward consistent, clinically viable fabrication.

**Keywords**: Extrusion-based bioprinting; Structural health monitoring; Defect detection; Process Monitoring; Quality assessment

# 1. Introduction

## 1.1. Background

Organ transplantation represents one of the major advancements of modern biomedical science, with the number of transplants increasing steadily over the last two decades, as illustrated in Figure 1 [1]. Nevertheless, the organ shortage remains a critical challenge worldwide. In the United States alone, more than 108,482 people are waiting for an organ transplant as of 2026 [2], and an estimated 13 people die every day due to organ shortages [3]. Three-dimensional bioprinting has emerged as a transformative technology to tackle this challenge by enabling the fabrication of complex tissue and organ constructs using bioinks composed of living cells, hydrogels, and biochemicals, deposited in a precise, layer-by-layer manner [4, 5].

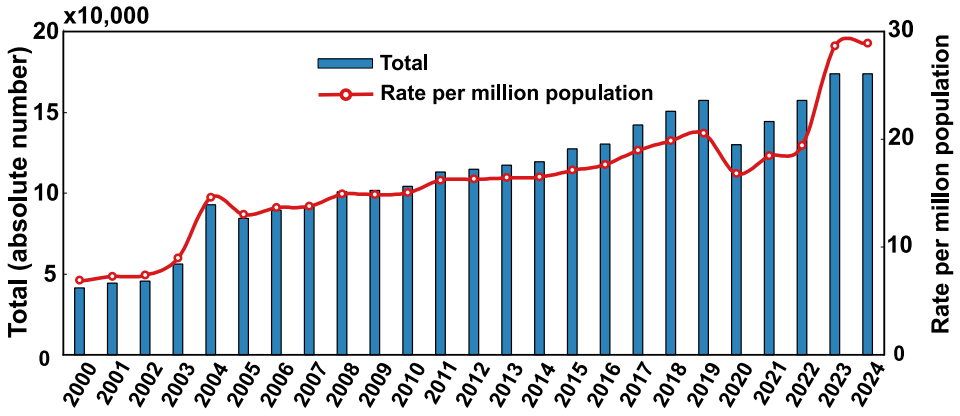


**Figure 1. Global trend of organ transplant [1]**

Bioprinting integrates principles from engineering, chemistry, biology, and materials science to create biomimetic structures. It can be broadly classified into three major classes: extrusion-based, droplet-based, and light-based bioprinting [6]. Extrusion-based bioprinting works on pressure-driven technology in the presence of pneumatic or mechanical pressure [7]. Jetting-based bioprinting involves deposition of discrete volumes of bioink through mechanisms such as inkjet, acoustic, microvalve, etc. [8]. Vat photopolymerization (VP)-based bioprinting involves using a light-based approach to crosslink photosensitive bioink, enabling rapid fabrication with high spatial resolution [9]. Following the notable early success of implanting a bioprinted bladder [10], demonstrating the feasibility of constructing functional organs using patient-derived cells, bioprinted heart [11] and ear [12, 13] have also been successfully transplanted into humans. Bioprinting, beyond its applications for organ transplantation, has been applied in diverse fields, including vaccines and drug testing [14], tissue engineering and wound healing [15], cancer research, and disease modeling [16–18]. These applications demonstrate their broad versatility in advancing both therapeutic and research objectives. This multidisciplinary and rapidly

advancing field holds significant potential for tissue engineering, drug delivery, and regenerative medicine, offering a pathway to create functional tissue constructs from patient-specific cells that could alleviate the organ shortage [19, 20]. On the other hand, the clinical translation of bioprinted constructs remains hindered by the challenges in process reproducibility and structural integrity, where variations in bioink properties and printing conditions may introduce critical defects that compromise the functionality of the bioconstructs. Addressing these challenges demands robust in-line monitoring strategies and closed-loop quality control systems. This review examines defect formation mechanisms, current identification strategies, and the growing role of AI in advancing reliable bioprinting toward clinical practice.

### 1.2. Importance of process monitoring and defect detection in bioprinting

Bioprinted constructs must meet stringent criteria for clinical applications, particularly in organ transplantation. Along with critical factors including biocompatibility and functional performance, the structural integrity–including the architecture, mechanical strength, stiffness, and both micro- and macro-scale composition of the target tissues or organs [21]–is critical to the successful clinical application of 3D bioprinted constructs. Defects in the printing process–such as geometrical inaccuracies (e.g., layer misalignment), inconsistent material deposition (e.g., nozzle clogging), or compromised cell viability due to shear stress–can severely undermine the quality and functionality of the final construct [22]. These challenges are particularly important for hydrogel-based bioinks, whose limited mechanical strength can lead to failures in maintaining structural integrity [23]. Moreover, small initial defects can cascade into catastrophic failures, resulting in the loss of valuable bioinks, cells, and bioactive molecules [24]. In addition to the outer shape fidelity, internal features such as interconnectivity and porosity significantly influence structural stability, cell behavior, and tissue functionality [25, 26].

Process monitoring and defect detection in bioprinting are therefore essential to identify anomalies during fabrication and evaluate resulting constructs [27]. This is particularly critical given the high cost of biomaterials [28], making early defect detection not only technically necessary but also economically imperative. By implementing robust monitoring systems, researchers can enhance printing efficiency, reduce material and cellular waste, and improve the reliability and quality of bioprinted constructs. Furthermore, beyond detection alone, implementing closed-loop feedback control is necessary to autonomously mitigate subtle, early-stage defects and maintain print continuity without disruption. Ultimately, these approaches not only strengthen the structural integrity of the bio-constructs but also advance their readiness for clinical and industrial deployment.

### 1.3. Objective and scope of the review

The increasing demand for bioprinting, driven by its potential to transform organ transplantation and regenerative medicine, has fueled extensive research into its technologies, bioinks, and applications. Previous reviews have broadly explored bioprinting techniques [29–31], bioink development [32, 33], applications to specific tissues such as skin [34, 35], cornea [36, 37], and orthopedic structures [38, 39], ethical considerations [40], and the integration of artificial intelligence (AI) [41–43]. Recent studies have also increasingly focused on the critical role of process monitoring and defect detection [44, 45]. Building on these advances, this review aims to provide a focused synthesis of defect formation and identification in bioprinting, linking defect characteristics to their underlying mechanisms and to both in-situ and post-process detection methods, including AI-driven approaches. The review focuses on literature mainly from 2014 to 2026 with an emphasis on the extrusion-based bioprinting method, which is widely utilized for its versatility, precision, and capacity to create complex tissue constructs. Although cellular responses and tissue- and application-specific requirement are important determinants of the overall quality of bioprinted constructs, the biological and cellular assessment is beyond the scope of this review.

In the following sections, this review organizes the research into defect characteristics, structural health monitoring methodologies, and recent detection strategies utilizing artificial intelligence. Following an overview of the key factors and failure modes governing defect formation, filament-level defects and consequences are systematically examined (Section 2). In Section 3, the most employed structural health monitoring (SHM) techniques are surveyed, and their sensitivity, feasibility, and defect detection compatibility are evaluated. The growing role of artificial intelligence and machine learning in defect detection and process monitoring is then explored in depth in Section 4. Finally, the prevailing challenges, limitations, and research gaps in the bioprinting field are summarized for advancing reliable monitoring frameworks.

## 2. Overview of defects in extrusion-based 3D bioprinting

Defects in 3D bioprinting primarily originate from multiple interdependent sources, including bioink material properties, hardware configurations, process parameters, and construct design. To understand the origins of defects in bioprinting, it is useful to examine them at two hierarchical scales: the global construct level and the local internal structural level. Defects manifest as macroscopic geometric inaccuracies at the global level [44], which are typically the cumulative outcome of instabilities occurring within the local internal structure. At the local internal level, defects typically originate at the filament scale before propagating through the structure. The most prevalent filament-level defects include inconsistent strand width and diameter, filament fusion, filament delamination, filament collapse, and reduced cell viability. These defects primarily occur due to imbalances between the material's rheological properties, printing conditions, and construct design [4, 46].

Understanding the defects requires a systematic examination of how each root-cause category results in observable print defects. Bioink material behavior, particularly rheological stability, is one of the major factors behind most of these defects. Bioink with low viscosity tends to spread upon deposition, reducing shape fidelity [47], while viscoelastic materials are prone to filament sagging and fusion [48]. Gelation kinetics further compound these issues: premature gelation weakens the interlayer adhesion, resulting in layer delamination [49], while the subsequent crosslinking process may alter the material properties of bioink, which may decrease the cell viability [46]. At the hardware and process level, nozzle geometry governs shear-induced reductions in cell viability and clogging [50, 51], nozzle misalignment introduces dimensional errors, and instabilities in extrusion pressure produce inconsistent filament dimensions. Moreover, design choices that ignore bioink rheology introduce geometric deposition errors, such as filament overlaps at sharp corners and insufficient filament gaps at high infill densities, which ultimately produce non-uniform layer heights and filament collapse. Cumulatively, these filament-level inconsistencies compromise the reproducibility of the microarchitecture, which presents a particularly critical challenge in extrusion-based bioprinting.

Collectively, these interdependent structural defects and deviations in geometrical fidelity underscore the necessity for real-time structural health monitoring. The following subsections systematically trace this causal chain along the process flow, as illustrated in Figure 3. Section 2.1 identifies the four major root-cause categories, highlighting the failure mechanisms associated with each. Section 2.2 focuses on the nozzle as the physical site where the mismatch between bioink rheology and process parameters and/or hardware configuration first manifests as failure in extrusion-based bioprinting. Section 2.3 describes the resulting filament-level defect types and explains how their accumulation compromises the integrity of the

global construct. Table 1 summarizes the cause-to-defect pathways across all four categories, while Figure 3 illustrates the relationship among different factors, failure mechanisms, and resulting defects.

**Table 1. Relation between the cause and effect of major defects in 3D bioprinting**

| Root-cause category | Contributing factors | Failure mechanism | Nozzle-level failure | Filament-level defect | Reference |
|---|---|---|---|---|---|
| Material properties | Viscosity | Filament spreading, air bubble trap | Nozzle clogging, filament curling at nozzle-tip | Filament size inconsistency/ filament breakage | [52–62] |
| | Viscoelasticity, low elastic modulus | Excessive material accumulation | – | Filament fusion, sagging, and collapse | [52, 59, 60, 63–67] |
| | Heterogeneity, improper mixing | High shear stress, fluctuating extrusion | Nozzle clogging | Low cell viability, rough surface | [56, 68–74] |
| | Premature gelation, insufficient crosslinking | Weak adhesion and bonding | – | Filament delamination, fusion, collapse, and low cell viability | [48, 65, 75–77] |
| Process parameter | Pressure/velocity mismatch | Over- and under-extrusion | – | Filament diameter/size inconsistency | [22, 27, 53, 58, 59, 66, 78–82] |
| | Nozzle tip-substrate gap | Unsupported filament deformation | Filament curling at nozzle-tip | Filament delamination | [66, 76, 83–86] |
| | Temperature | Temperature induced viscosity, inadequate thermal stabilization | Unstable extrusion | Filament size inconsistency, collapse | [87–91] |
| Hardware configuration | Nozzle shape/size | High shear stress | Nozzle clogging | Reduced cell viability | [46, 53, 66, 84, 92–96] |
| | Nozzle misalignment | Displacement error | – | Dimensional error | [97–99] |

| | | | | | |
|---|---|---|---|---|---|
| Design | Sharp corners | Excessive material accumulation | – | Filament fusion | [63, 64, 66, 97] |
| | Infill density | Large filament gap | – | Filament collapse | [64–66, 83, 100] |

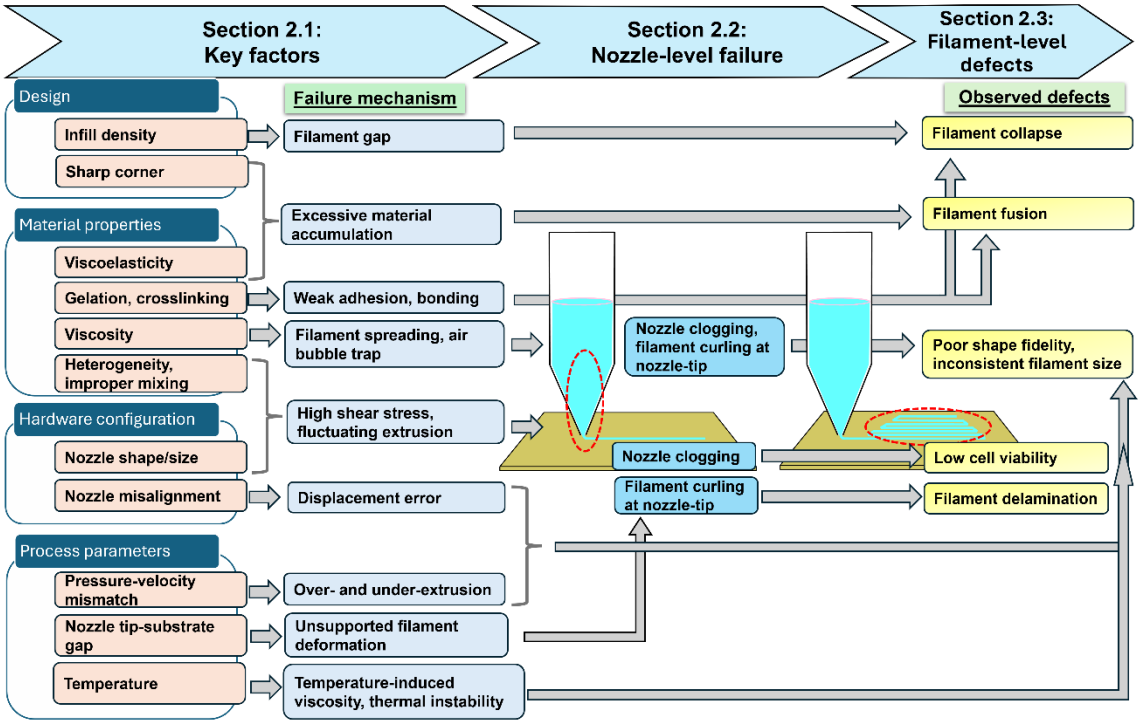


**Figure 2. Defect propagation and failure analysis across the 3D bioprinting workflow**

## 2.1. Key factors causing defects

Defect formation in 3D bioprinting is governed by the interplay of bioink rheology, printing parameters, hardware configurations, and design parameters [75], all of which shape how reliably a filament is deposited and how well the construct retains its intended geometry. Bioink rheology, particularly viscosity and viscoelasticity, governs the material's ability to flow through the nozzle and maintain its shape after deposition. Printing parameters such as extrusion pressure, flow velocity, and layer height determine the consistency and continuity of the extruded filament. Hardware characteristics, including nozzle geometry and alignment, influence flow uniformity and deposition accuracy. Design parameters such as infill density and corner geometry further affect local support and filament deposition. Depending on how these factors interact, defects may emerge immediately after bioink deposition or manifest after a certain printing process

completion. The core factors and the types of defects that arise from them are discussed in the following subsections.

### 2.1.1. Bioink material properties

Material rheological properties are pivotal contributors to defects in extrusion-based bioprinting [45]. Viscosity, viscoelasticity, gelation kinetics, and gel-like elasticity each govern a distinct failure pathway; the water content, polymer concentration, and crosslinker composition of the bioink collectively set these properties and therefore determine which failure modes are most likely. Viscosity remains the most impactful property of bioink in determining the printing quality and shape fidelity [55]. For instance, the water content in bioink influences filament spreading, which poses challenges for maintaining the shape fidelity [101]. Recent studies further emphasize the importance of bioink rheological properties in preventing nozzle clogging in extrusion-based bioprinting [60, 75, 102]. While highly viscous bioink may trap air bubbles, resulting in filament discontinuity [54], low viscosity may decrease the homogeneity in bioink, a cause for premature filament spreading and poor shape fidelity [60, 61]. Thus, applying constant extrusion pressure to such non-homogeneous bioink often results in increased strut diameter [53] and broken filament [56]. While bioinks with a gel-like consistency exhibit improved shape fidelity, they often suffer from reduced cell viability [68].

Beyond the rheological properties, mechanical properties also contribute to printing defects; for example, a low elastic modulus often results in filament sagging [65] and fusion [60]. Moreover, the gelation process [48, 75] and cross-linking density [65, 77] are critical in balancing the shape fidelity and cell viability. A recent study indicates that increasing alginate concentration in cell-laden scaffolds can improve the shape fidelity and mechanical integrity and reduce swelling, yet this improvement may occur at the cost of cell viability [69].

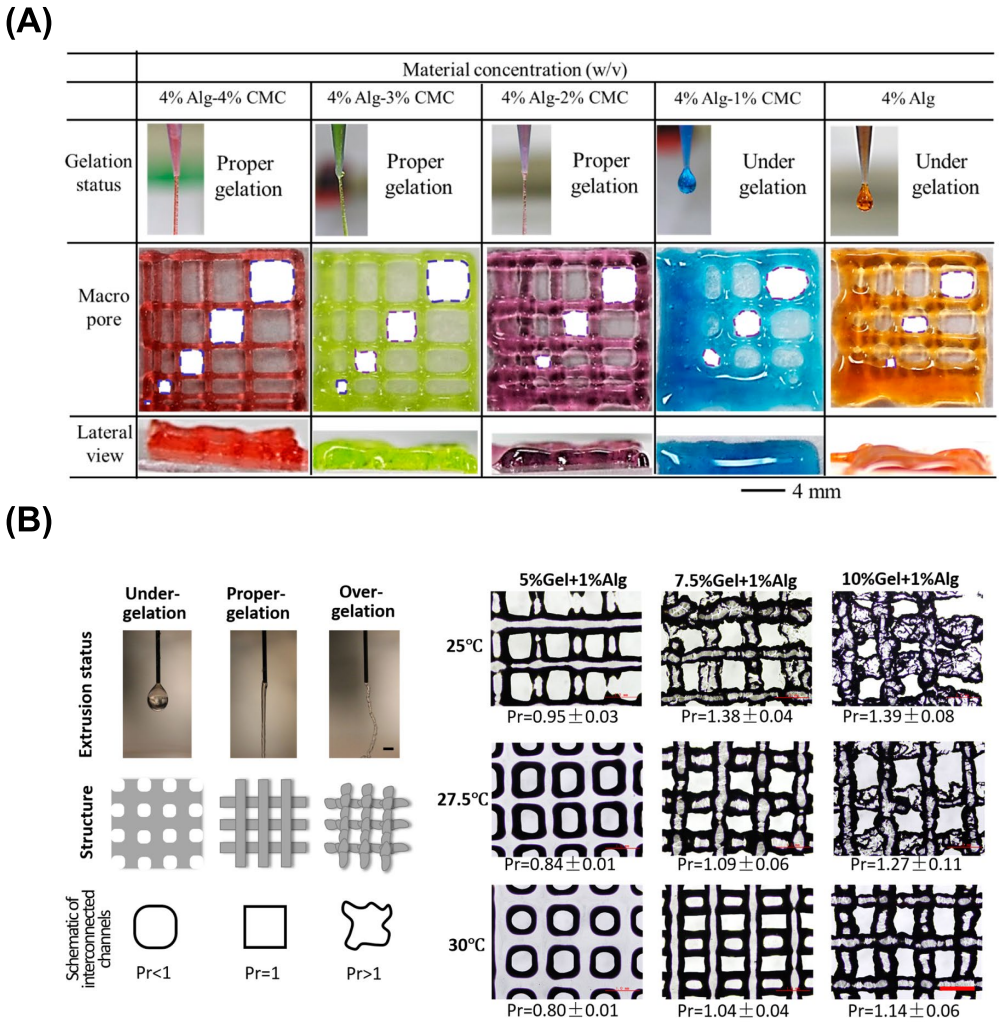


**Figure 3. (A) Effect of carboxymethyl cellulose and alginate concentration on gelation conditions, which contributes to different pore conditions [67]. (B) Determination of printability (Pr) under different gelation conditions and corresponding optical microscopic images [48].**

### 2.1.2. Process parameters

Process parameters, such as extrusion pressure, print speed, tip-substrate gap, and printbed temperature, directly control the volumetric flow rate of bioink, the spatial accuracy of deposition, and the thermal environment in which crosslinking occurs. Mismatches among these parameters, or between any parameter and the rheological properties of the bioink, may produce a characteristic set of extrusion instabilities that resolve into filament-level defects [103].

Flow rate and printing speed represent a tightly coupled parameter pair: velocity and shear stress profiling inside the extrusion needle has shown that any mismatch between flow rate and print speed causes over- or under-extrusion, which subsequently leads to deviations of the strand diameter from its target value

[79, 80, 82]. Related work has also identified filament size and layer thickness deviations arising from pressure-velocity mismatches, with material deposition errors being especially pronounced at the start and stop points of each layer due to pressure hysteresis [22].

The gap between the nozzle tip and the substrate surface during deposition governs how the extruded filament contacts and adheres to the layer below. When this gap is too large, the filament is deposited without adequate mechanical constraint from the substrate, allowing it to deform under its own weight and warp. This nozzle warping deforms the filament away from its intended path and, if severe, pulls the filament away from the previous layer, initiating deformation [84]. Conversely, a gap that is too small compresses the filament excessively, causing lateral spreading and an increase in strand width. The tip-substrate gap, therefore, directly controls whether the nozzle warping failure mode occurs, while the resulting filament delamination is described further in Section 2.2.

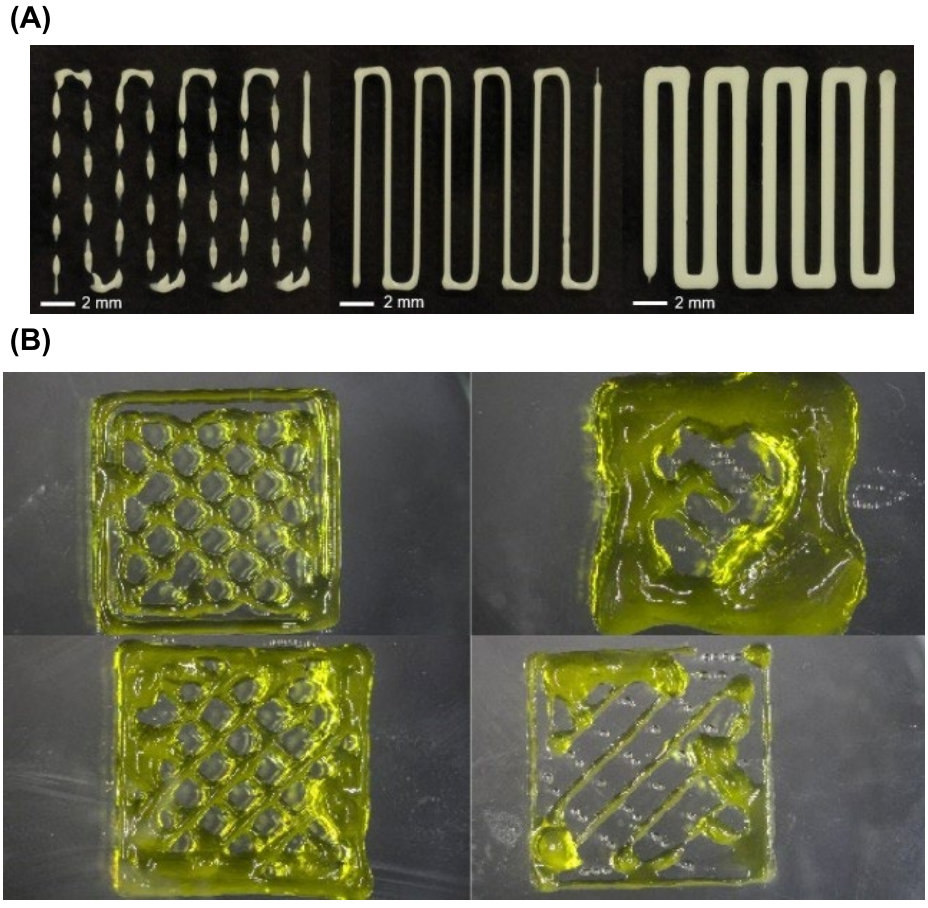


**Figure 4. (A) Effect of air pressure on the extrusion through a conical nozzle. The images range from under- (left) to over-extrusion (right) with an air pressure of 58, 62, and 80 kPa respectively [81]. (B) 3D bio-printed hydrogel scaffold with very good printability (top left), over-extruded (top right), and good printability (bottom left) and under-extruded (bottom right) [104].**

Temperature influences the crosslinking stability of thermally responsive bioinks. For alginate-based formulations, lower printbed temperatures were found to stabilize crosslinking, yielding constructs with more consistent filament geometry [80]. Temperature also affects viscosity: as temperature increases, most hydrogel bioinks become less viscous, which shifts the system toward the low-viscosity failure mode of filament spreading and diameter inconsistency. In multi-material printing, differential thermal responses of co-extruded materials can introduce differential shrinkage or mismatched gelation timing, contributing to delamination at material interfaces [105].

### 2.1.3. Hardware configuration

Defects in bioprinting also emerge from hardware configuration. Hardware configuration, principally nozzle geometry and nozzle alignment, govern two distinct failure pathways: one related to the shear stress field inside the nozzle, and the other related to the positional accuracy of the extruded filament. A central challenge in extrusion-based bioprinting is the shear stress generated as bioink is forced through the narrow nozzle cross-section. Excessive shear stress not only damages the cell viability but can also develop unexpected extrusion behavior [94]. Early research examining the influence of pressure, temperature, and nozzle geometry on strand diameter found that conical needles produce the highest shear stress compared to cylindrical counterparts [53]. However, conical needles offer superior cell viability at low pressure [53, 92]. Subsequent simulation models corroborated this finding and further revealed that increasing nozzle length can improve cell viability, albeit at the cost of reduced printing accuracy [106].

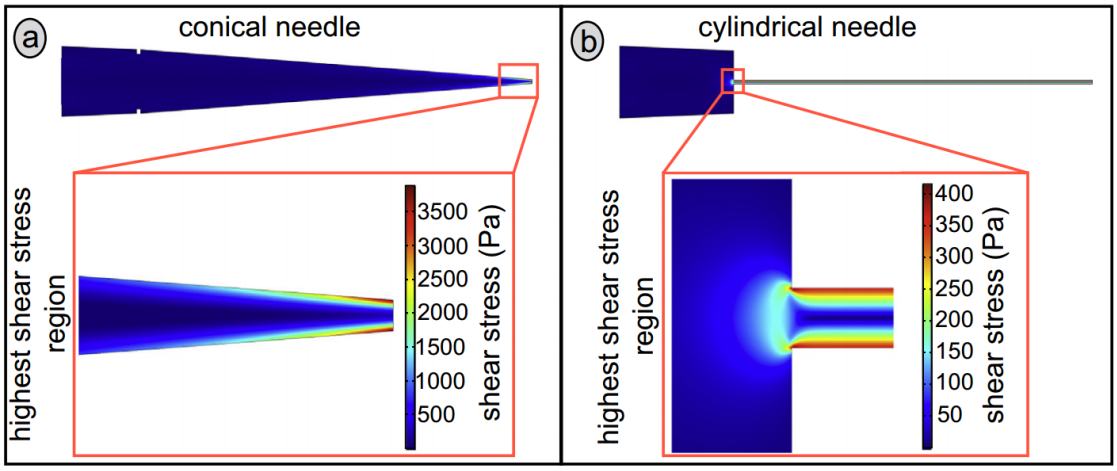


**Figure 5. Finite element simulations of shear stress development in (a) conical and (b) cylindrical nozzle, showing higher shear stress in the conical needle [53].**

Beyond nozzle geometry, hardware limitations such as nozzle misalignment and tip displacement errors introduce dimensional inaccuracies, particularly at tight corners and small radii of curvature, where

fine motion control of the printer axes becomes critical [97, 98]. Compounding this, the material model developed to predict extrusion rate has struggled to achieve sufficient accuracy, further contributing to dimensional errors in the final construct. Moreover, the arrangement of the extrusion system and process selection also affects the material deposition in the case of multi-material extrusion [107]. This study showed the challenges in single-nozzle and multi-nozzle extrusion processes and how they may lead to extrusion-related defects such as discontinuity, misalignment, or unwanted material mixing. Additionally, the resolution of bioprinter defines the deviation between the actual printing trajectory and the reference trajectory, which results in dimensional error in printing samples with complex shape [99].

### 2.1.4. Design parameters

Construct design determines the spatial demands placed on the deposited filament: the angles at which the nozzle must change direction, the gap distance across which each strand must self-support, and the proximity of adjacent strands within a given infill pattern. When these requirements are not matched to the rheological capability of the bioink, geometric deposition errors are the immediate result.

In extrusion-based bioprinting, sharp corners in the print path require the extrusion head to decelerate sharply and reverse direction. At corners where the angle is inconsistent with the bioink viscosity and the printing speed, the nozzle continues to extrude material. As a result, sharp corners in the design often face overlapping issues, which may also damage the uniformity of the layer height [66]. Furthermore, this study notes that the infill density and pattern may lead to strand fusion at the sharp corners if the filament distance is significantly lower than the optimal threshold. In addition, when the angle of corner and printing parameters are not optimized for the bioink viscosity, filament fusion and merging may take place [64].

Scaffold design also determines the unsupported span length across which filaments must bridge. When the design prescribes long gaps between support points, the deposited filament must sustain its own weight without underlying support. Previous studies demonstrated that filament sagging increases with the gap length [64]. A systematic experimental analysis of the structural behavior of filaments was presented in [65], investigating their collapse when spanning long gaps between supports due to specific scaffold designs or printing paths. In line with this, it was further demonstrated that increasing fiber spacing may compromise the mechanical strength of the sample [100].

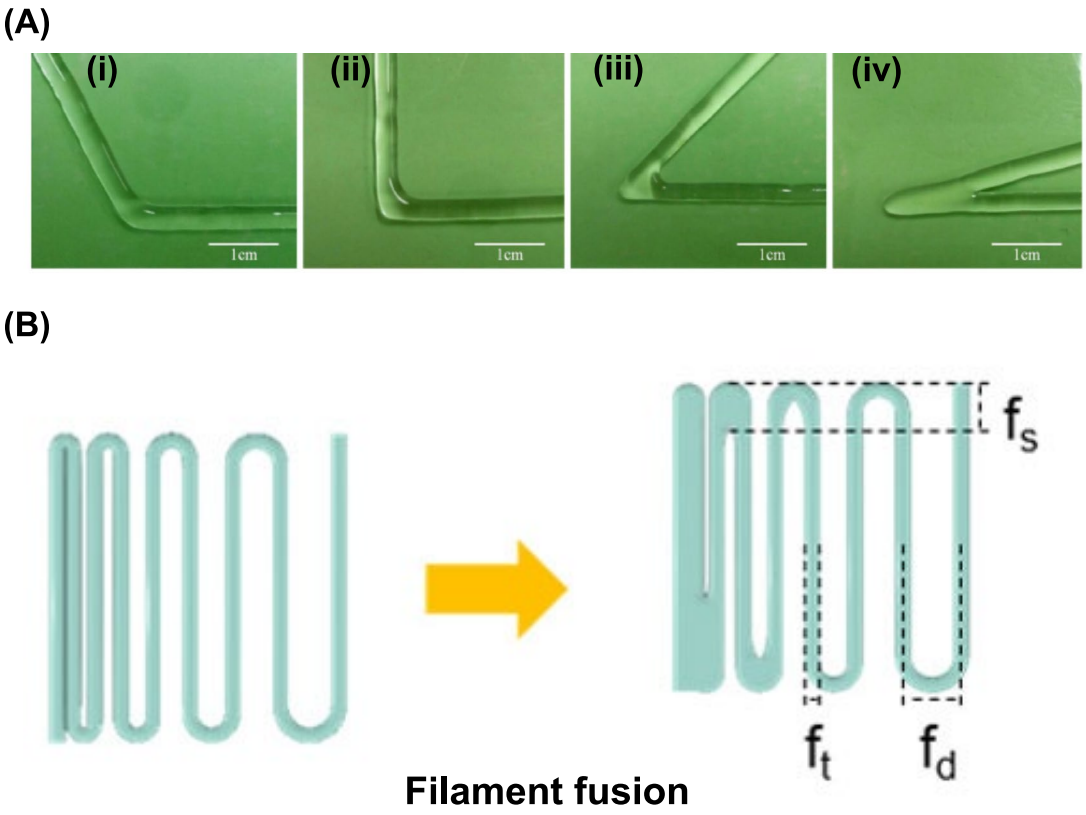


**Figure 6. (A) Visual representation of filament overlap in corner printing: (i) obtuse angle, (ii) right angle, (iii) acute angle, and (iv) sharp angle printing [66]. (B) Adjacent filament fusion at filament fusion test [65]. Bioinks with lower yield stress tend to have longer fused segment length ($f_s$) at higher filament distances ($f_d$)**

### 2.2. Failure modes in the nozzle

The nozzle is a critical physical site at which the combined influence of material properties, hardware geometry, and process parameters first resolves into observable failure in extrusion-based bioprinting. Upstream mismatches among these root-cause factors, identified in Section 2.1, manifest at the nozzle as two primary failure modes: clogging, which disrupts the continuity of extrusion, and filament curling, which disrupts the positional accuracy of deposition. Both failure modes propagate downstream to produce the filament-level defects described in Section 2.3.

#### 2.2.1. Nozzle clogging

Nozzle clogging is one of the most common types of defects for the nozzle-based bioprinting process, which can be triggered by multiple mechanisms. As the bioink is extruded through the nozzle outlet, the bioink material properties and applied pressure are responsible for the smooth flow of bioink. Clogging occurs when the resistance to flow through the nozzle tip exceeds the available extrusion pressure: the

bioink cannot be driven forward at the commanded rate, and the filament output ceases or becomes intermittent. A small nozzle tip may restrict bioink flow and generate excessive shear stress along the nozzle wall, simultaneously risking clogging and compromising cell viability [93]. Similarly, highly viscous bioink needs a higher extrusion force, and the absence of this required force, too small nozzle diameter, or material stiffness increase due to temperature change may trigger nozzle clogging at the outlet.

Material composition further contributes to this challenge. A study identified cell-sedimentation as one of the reasons behind the nozzle clogging [95]. When cells settle within the reservoir or barrel, the local concentration of solids near the nozzle tip rises, increasing effective viscosity and promoting clogging. While the circulation of bioink was proposed in another study to mitigate cell sedimentation, excessively high circulation flow rates can generate bubbles that enlarge and block the nozzle tip [57]. Another research attempted coaxial extrusion for multi-material bioprinting, which also encountered with the nozzle clogging [86].

The consequences of clogging extend beyond a simple interruption of extrusion. Partial clogging where flow is restricted but not fully blocked produces intermittent under-extrusion, which manifests as filament breakage or inconsistent strand width along the print path (Section 2.3.1). Full clogging terminates the print, requiring mechanical cleaning or nozzle replacement. In cell-laden bioprinting, the shear stress generated at the point of partial clogging, especially when the bioink is forced through an effectively narrowed orifice, can exceed the threshold for cell membrane damage, reducing cell viability (Section 5.1).

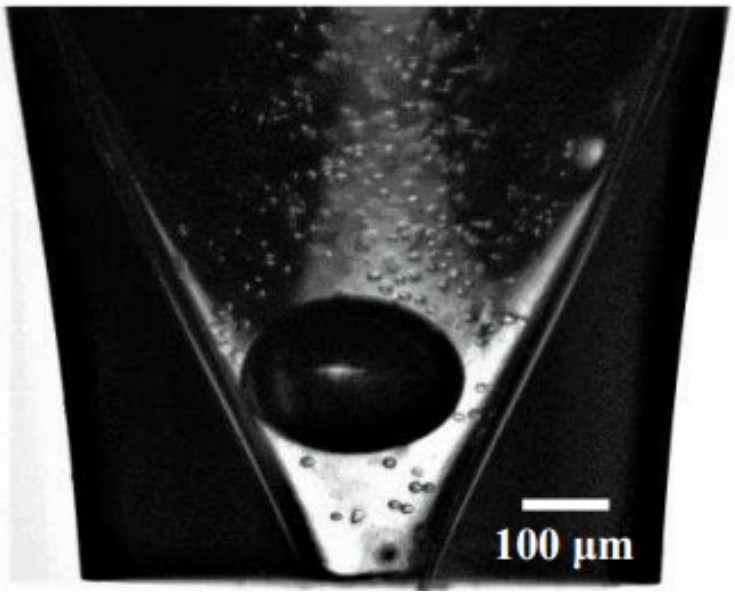


**Figure 7. Nozzle clogging due to the presence of air bubble trapped inside [57]**

### 2.2.2. Filament curling at nozzle-tip

Filament curling at the nozzle tip refers to the deformation of the extruded filament that occurs between the nozzle tip and the substrate, before the material contacts and is constrained by the layer below, often causing the filament to curl into a pig-tail-like shape. It has been reported for soft material 3D printing, including bioprinting [44, 108]. Notably, bioink viscosity has been identified as a critical factor behind lateral buckling of bioink at the nozzle tip, resulting in filament curling [109]. The authors demonstrate how the shear-thickening increases the instantaneous viscosity of the bioink and causes extrusion instability at the nozzle exit. Another study reports that excessive viscosity with higher concentrations of methacrylate mucin (MuMA) results in filament curling for composite bioink [62]. In addition, high concentrations of fibroin and gelatin methacryloyl may increase bioink viscosity to an extent that promotes wrinkle formation at the nozzle tip [95]. A similar phenomenon has also been reported in [56], where bioink warping at the nozzle tip was attributed to the non-uniform rheological behavior of the bioink material.

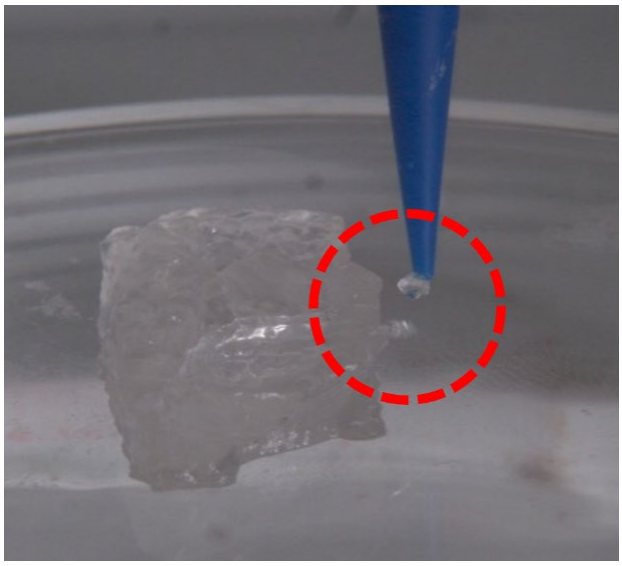

**Figure 8. Filament curling at the nozzle-tip after extrusion**

## 2.3. Filament-level defects

The root-cause factors of extrusion-based bioprinting defects described in Section 2.1, acting through the nozzle-level failures discussed in Section 2.2, ultimately produce structural deviations at the filament scale. These filament-level defects represent the most direct and observable consequence of the underlying imbalances. Their significance extends beyond individual strands. The accumulation of such deviations across consecutive layers can propagate and lead to global structural inaccuracies in the final construct. The following sections describe common defects that are observed at the filament level.

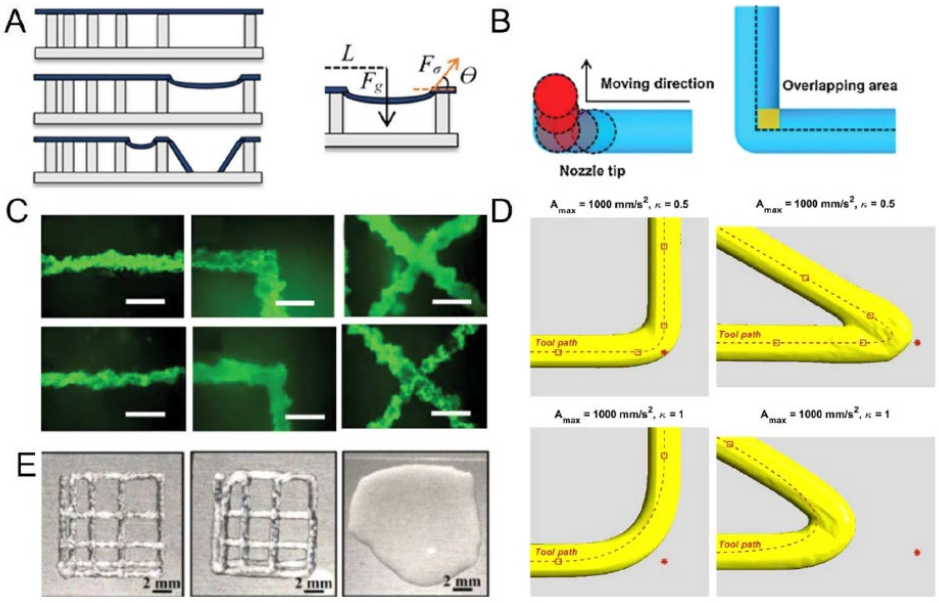


**Figure 9. Visual representation of different types of defects at the filament level: (A) Filament sagging resulting from gravitational force over time (B) Effect of over-extrusion at corner location (C) Effect of over- and under-extrusion on the strand size: left side shows blobs caused by over-extrusion, right side shows disconnected lines due to under-extrusion (D) Optimized toolpaths with adjusted corner acceleration reduce material overshoot, and (E) Variable distances between hydrogel collapsing due to filament fusion [85]**

### 2.3.1. Inconsistent filament diameter

Filament diameter, represented by strand diameter and line width, is highly sensitive to the rheological properties of the bioink and the selected printing parameters. Due to the excessive extrusion force, the viscosity may decrease rapidly after extrusion as a result of shear-thinning response. This reduction in viscosity lowers the material's resistance to spreading, leading to lateral spreading and an increase in the strut diameter [53]. This underscores the need to select appropriate printing speed and dispensing pressure depending on the rheological properties of the bioink [64], as any mismatch may lead to an erroneous strand size compared to the target values [79].

Time-dependent viscosity changes further compound this problem. A study on alginate-gelatin (AG) bioink identified time-dependent viscosity change, temperature, pressure, and mismatch from printing speed as factors contributing to filament diameter variation [58]. The authors reported that the viscosity of the AG bioink decreased initially, leading to an increased flowrate and consequently a larger filament diameter. In addition, the viscoelastic properties of the bioinks have also been shown to promote lateral filament spreading after extrusion, further contributing to diameter variation along the printed line [59].

Collectively, these findings highlight that filament diameter consistency is not governed by a single parameter, but the dynamic interplay between bioink rheology and process conditions.

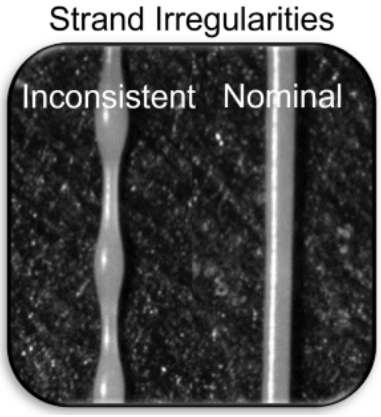


**Figure 10. Visual representation of inconsistent filament size, resulting from a mismatch between the material flow rate and print speed [27]**

Diameter inconsistency is not merely a geometric imprecision. Excessively wide filaments can merge with adjacent strands, closing intended pores and producing strand interaction errors, as described in Section 2.3.2. Conversely, filaments that are narrower than the target width may create gaps in the bioconstructs, thereby compromising mechanical integrity. Filament diameter, therefore, serves as a key indicator of the overall print quality and a sensitive diagnostic variable for detecting mismatches in printing conditions.

### 2.3.2. Filament fusion

Filament fusion is one of the major filament-level defects in 3D bioprinting that results from deposition errors or strand-to-strand interactions. It is defined as the pore closure between two filaments [65], is strongly influenced by both bioink composition and geometric design. An early study analyzed the effect of hydroxyapatite (HA) concentration in alginate-gelatin bioink on filament fusion [63]. The results showed that increasing HA concentration raised the hydrogel's viscosity, and filament fusion occurred at sharp corners where the filament spacing was minimal. Over-deposition, another key factor contributing to filament merging [56], occurs when excess material is extruded, causing adjacent strands to merge and compromising the printability of the bioink. In contrast to unintended filament merging, strategically modulating the strand-to-strand interaction can be exploited constructively. A recent study systematically varied gelatin methacryloyl (GelMA) concentration and printing parameters to identify conditions in which neighboring filaments fuse in a controlled manner to form a continuous membrane [110]. This demonstrates

that the same filament interaction mechanism that constitutes a defect in scaffold printing can be an asset in membrane fabrication, provided that the governing parameters are accurately controlled.

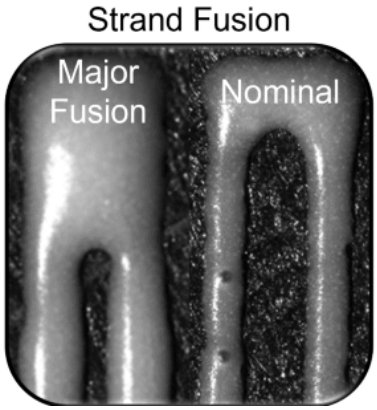


**Figure 11. Demonstration of filament fusion during the extrusion-based bioprinting process [27]**

### 2.3.3. Filament delamination

Filament fusion errors arise from excessive interaction between strands, whereas filament delamination represents the opposite– insufficient bonding between adjacent layers. This defect typically originates from inadequate deposition of material, excessive layer height, and insufficient fusion between successive layers [83]. Material properties play a central role in governing interlayer adhesion. Premature gelation or insufficient crosslinking density may prevent proper bonding during layer-by-layer deposition. This results in structurally weak interfaces that are prone to separation. Several crosslinking strategies have been investigated to address this issue. Post-crosslinking has been proposed as a means of enhancing shape fidelity, retaining the imparted shape without any separation in the filament [65]. Another study demonstrates that application of partial cross-linking after each layer strengthens interlayer bonds throughout the build process [76]. Process continuity and hardware-related factors further compound the risk of filament delamination. As discussed in Section 2.1.3, filament curling at the nozzle tip can introduce discontinuities in extrusion, leading directly to filament delamination within the printed layer. Collectively, these findings suggest that mitigating filament delamination requires simultaneous consideration of crosslinking behavior, deposition consistency, and hardware reliability.

### 2.3.4. Filament collapse and breakage

Filament collapse and breakage represent structural failure at the filament level, arising when the deposited strand cannot sustain its own weight or withstand the mechanical demands of the printing process. These phenomena are governed by gravitational, mechanical, or rheological constraints, and are particularly pronounced in extrusion-based bioprinting, where unsupported spans are unavoidable.

An early study emphasizes that the viscoelastic properties of bioink play a critical role in filament rupture [52]. This study compared the filament structure and its collapse with beam mechanics to characterize structural failure. Soft bioink material goes into deformation after deposition, and filament sagging may occur due to the viscoelastic nature of the bioink, which results in filament collapse. In another study, a model was developed to connect yield stress with filament collapse [64]. This study showed that the severity of filament collapse increased as the filament gap widened. Additionally, this study revealed that higher yield stress in bioink leads to lower filament sagging after deposition, preventing filament collapse. Building on this, a recent study also showed yield stress as an indicator of bioink's resistance to sagging, and the findings from this study demonstrated that bioink with a low elastic modulus may face filament collapse after deposition [65].

Gelation conditions introduce another dimension to this failure mode [48]. Rapid gelation of bioink may provide sufficient stiffness to resist filament collapse, yet bioink may fail to adhere to the previous layer, producing delamination. Slow gelation may enable bioink to support its own weight initially, but it can gradually sag as the viscous component relaxes. This will result in filament collapse if the gelation fails to progress rapidly enough to halt the deformation. The crosslinking rate must therefore be tuned to provide structural support during the time window between deposition and the arrival of the next layer, while remaining sufficiently fluid at the moment of layer contact to enable interlayer bonding.

Filament breakage is a related but mechanistically distinct failure. It occurs when the tensile stress in the elongating filament caused by the motion of the nozzle away from a fixed contact point exceeds the tensile strength of the extruded material [59]. This failure is most common during rapid print movements, when the nozzle accelerates away before the filament has been cleanly separated from the deposition point. Low viscosity bioinks and incompletely gelled formulations are particularly susceptible [111], as their tensile strength is insufficient to withstand the stretching imposed by rapid nozzle movement.

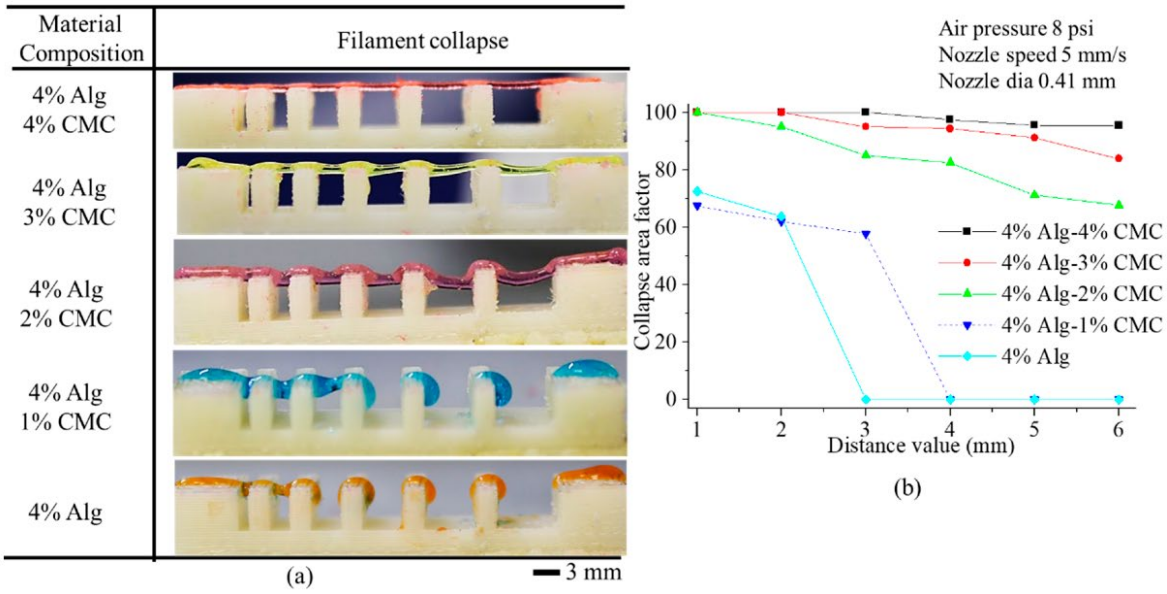


**Figure 12. Effect of carboxymethyl cellulose (CMC) on the deflection of suspended filament in filament collapse test [67]**

## 3. Structural health monitoring techniques

Ensuring the structural integrity of 3D bioprinted constructs requires monitoring techniques capable of detecting the diverse range of defects and process anomalies discussed in the preceding sections. Structural health monitoring in 3D bioprinting encompasses techniques that operate across different stages of printing process, either in situ to capture defects as they form or post-process to evaluate the final construct after printing is completed. Because of the unique principle of the printing workflow of extrusion-based 3D bioprinting and different bio-ink properties, a variety of SHM techniques have been utilized. These techniques are commonly categorized based on their working principles and sensing modalities, ranging from optical and volumetric imaging to ultrasonic sensing, impedance measurements, and flow-based monitoring. The following subsections describe each of these major approaches, highlighting their working principles, the types of defects they address, and the key parameters associated with defect detection.

### 3.1. Vision-based monitoring and surface optical profilometry

Vision- and optical-based methods are among the most widely adopted SHM approaches in 3D bioprinting, owing to their non-contact and non-destructive nature and compatibility with a wide range of soft bioink materials. These methods utilize imaging and light-based sensing to assess the shape fidelity, surface quality, and geometric integrity either during or after the printing process. The visual data obtained by these methods enable the detection of defects such as filament misalignment, dimensional inaccuracies, and deviations in shape fidelity at the surface level of the bioconstructs. The availability of high-resolution

sensors and advanced image processing algorithms has further expanded their capability for real-time, in situ monitoring of 3D bioprinting. Within this broad category, several distinct sensing modalities have been explored, including optical imaging and machine vision analysis, microscopic visualization, thermographic and infrared imaging, video-based methods, and laser-based dimensional approaches, which are discussed in the following subsections.

### 3.1.1. Optical imaging and machine vision analysis

Optical imaging and machine vision-based monitoring have traditionally been, and remain, among the most widely used methods for defect detection in 3D bioprinting. These approaches provide insights into critical aspects of the printed constructs, such as shape fidelity, irregularities, precise layer alignment, and anomalies during material deposition. These techniques harness camera systems to capture high-resolution images of the printing process, which enables defect detection at both micro- and macro-scales. When combined with sophisticated computational image analysis, they allow for a non-invasive assessment of printing quality. By continuously monitoring the printing process, computer vision systems can identify deviations from the intended design and detect geometric inaccuracies at the surface level.

Early efforts focused on quantifying the geometry of extruded strand as a practical indicator for print quality, recognizing that shape accuracy of the printed sample and filament formation is directly governed by bioink rheology [112–114]. An image-based approach was developed to measure the strand size and area in pneumatic extrusion-based bioprinting using a microplate reader [115]. While effective for opaque bioink materials that are commercially available, this method faced limitations in detecting the line width accurately when transparent bioinks with higher water content were used. This limitation immediately revealed the sensitivity of optical approaches to material properties. Recognizing this limitation, subsequent work introduced a coaxial camera system that is mounted close to the printhead to capture axial images at in situ conditions, extending the extruded line monitoring to detect defects due to over-extrusion in systems using commercially available bioinks [116]. A high-definition camera was installed near the printhead, which moves over the construct after each layer is printed and captures coaxial images of the sample. This method compared binarized images of a printed square lattice pattern with the corresponding binarized image from the model, from which the ‘over-extrusion’ metric was developed to quantify defects. Notably, layer drifting phenomena were also detected in this approach, enabling layer-by-layer defect detection. Furthermore, another image-based approach introduced the pore index as a parameter to identify the effect of uneven extrusion based on the pore sizes of the printed layers [117]. Despite this advancement, the cameras remained sensitive to ambient lighting conditions and bioink transparency.

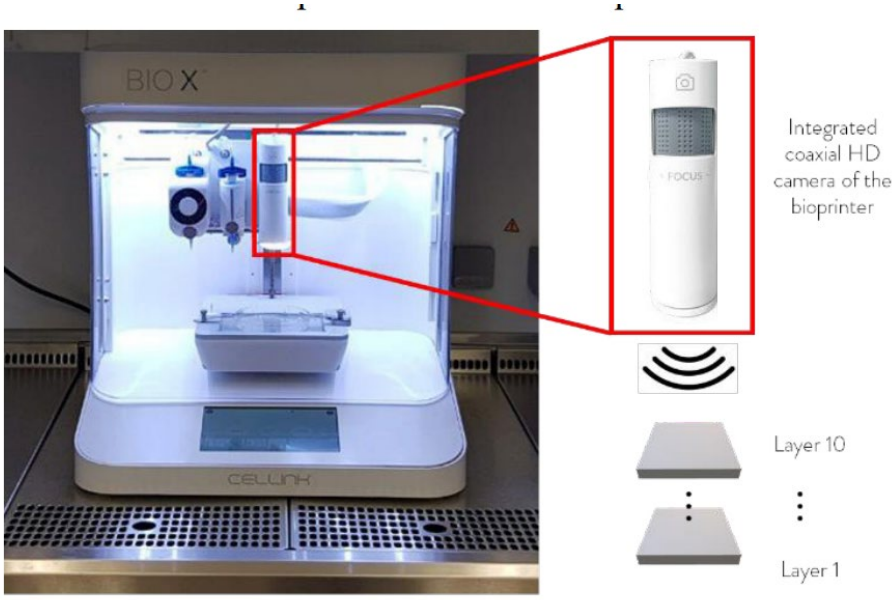


**Figure 13. Experimental setup of an integrated high-definition camera with printhead capturing coaxial images [116]. The camera moves automatically with the printhead and captures axial images of the bioprinted layer.**

Printing correction was also identified as a necessity in extrusion-based bioprinting in addition to the real-time process monitoring, given that the low resolution of bioprinting process [61] could further compromise the printing quality. Therefore, researchers progressively shifted toward more sophisticated strategies to enable the printing correction. An early implementation used a camera to capture the path of the printed helix, detect edge deviations from the reference trajectory, and correct errors exceeding 1 mm [118, 119]. This computer vision-based strategy utilized an algorithm that converted the image data into quantitative error vectors and applied a vector compensation algorithm to enable printing path correction. Building on this, computer-vision was also implemented in robotic 3D bioprinting that pushed resolution further, reducing detectable layer width deviations to 0.15 mm [120]. An industrial camera was used in this process to capture images and send them to the supervisory computer, where deviations were measured and the robotic printing path was adjusted to compensate for errors. This method encountered challenges for closely stacked layers and fluctuating lighting conditions. Most recently, computer vision-based approach was implemented with an integrated camera to capture the images of extrusion outputs at in situ conditions to quantify area and spatial fidelity in embedded bioprinting [121]. A bioprinting system was developed in this study, which included a high-resolution camera installed beneath the extrusion nozzle, enabling the real-time monitoring of the outputs from the nozzle. This integrated approach offers reconstruction of high-resolution images and real-time tracking of nozzle flow, unlike the traditional camera-based approach [116, 122], where the camera is installed at an angular position and relatively larger distances.

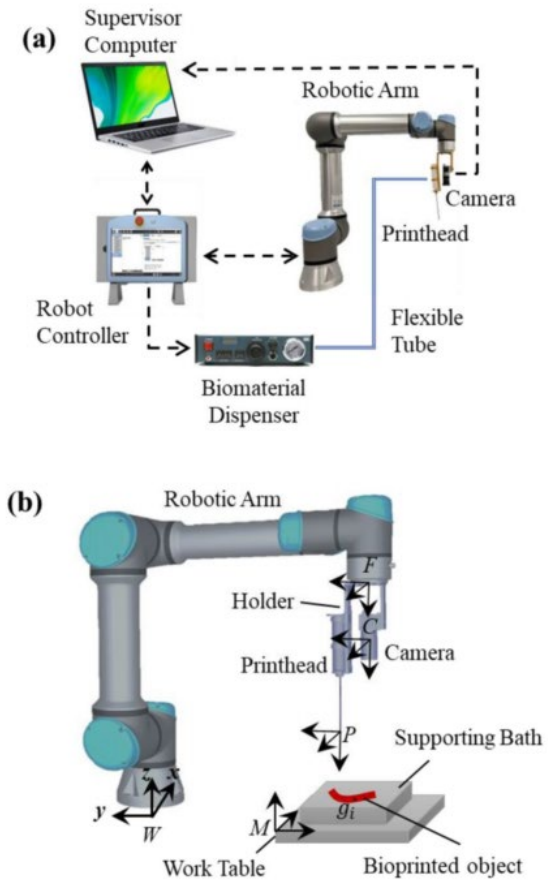


**Figure 14. Schematic diagram for robotic bioprinting process [120]**

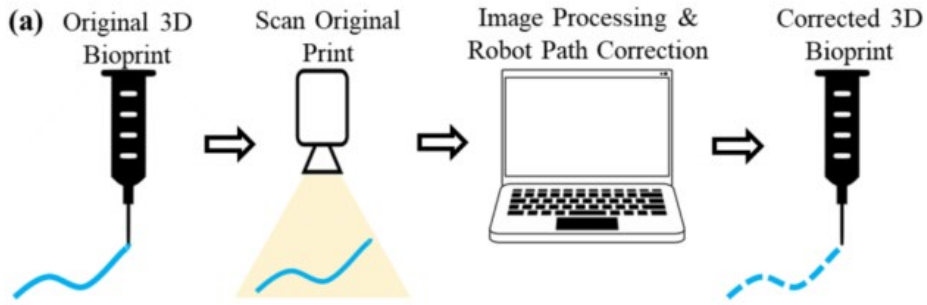


**Figure 15. Workflow of image capturing and printing correction in robotic bioprinting [120]**

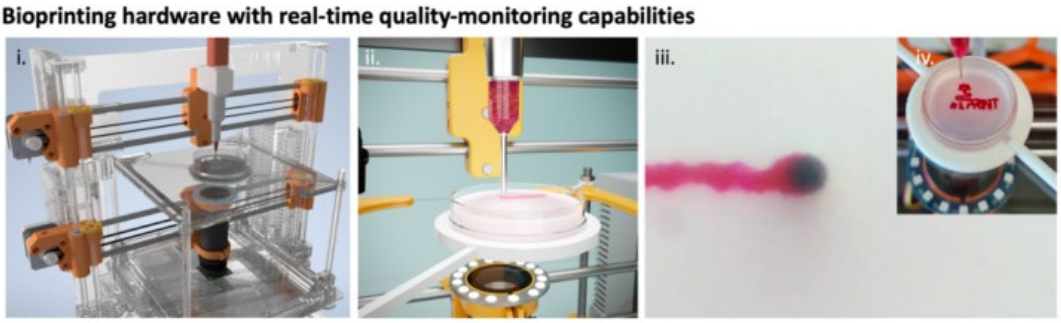


**Figure 16. Visual representation of embedded bioprinting and an example of the camera's field of view during the printing process [121]**

Collectively, optical imaging and machine vision methods have evolved from simple geometric measurements toward sophisticated real-time monitoring systems [123–128]. On the other hand, the effectiveness of these methods remains tied to the experimental conditions, particularly lighting consistency and bioink transparency, underscoring the need for complementary sensing modalities when optical access is limited or material properties compromise image quality.

### 3.1.2. Microscopic visualization

While machine vision methods excel at capturing surface-level geometric deviations, they are limited in their ability to resolve finer structural details. Microscopic visualization helps address this limitation by providing high-resolution, contactless imaging of morphology and geometric deviations at scales that are inaccessible to standard cameras. Two different kinds of microscopic imaging have been utilized in 3D bioprinting: (i) optical microscopy, including fluorescence, confocal, and stereomicroscopy, and (ii) electron microscopy. These methods differ in resolution, depth of field, and magnification.

Optical microscopy has been applied across a range of bioprinting processes to monitor the printing outcomes. The electrohydrodynamic bioprinting process involves extrusion of bioink containing living cells in the presence of high-voltage application [129, 130]. Digital microscopy was used to extract jet centroid and diameter from the captured images, enabling categorization of different jet modes responsible for anomalies in the printed constructs [131]. Similar to the jet monitoring approach, another study used fluorescence microscopy for real-time monitoring of hydrogel flow in extrusion-based bioprinting [132]. This approach offers fluid flow profiles after extrusion from the nozzle, and the findings were used to adjust printing conditions. Additionally, bioink printability was assessed in extrusion-based bioprinting by comparing the images obtained from a laser confocal microscope [48]. This research revealed how gelation rate influences extrusion behavior at the nozzle tip and the integrity of the final structure. Stereomicroscopy has similarly been used to assess the printability by imaging fiber formation and detecting defects such as

fiber detachment, merging, and blending across stacked layers [78]. Building on these findings, a systematic study used optical microscopy to relate nozzle pressure, printing speed, and bioink dilution to extrusion width, providing a practical framework for detecting over- and under-extrusion through parameter optimization [133]. In line with this, microscopic images have also been used to assess extruded filament based on geometry of the filament [134].

The effectiveness of optical microscopy is limited when imaging hydrogel with opaque microparticle due to light scattering [135]. As a result, scanning electron microscopy (SEM) has been introduced for the morphological [136] and sub-surface analysis at both macro- and micro-scale for different hydrogel conditions [137]. Printing defects such as strand shrinkage, surface roughness, and crack formation have been detected under *ex situ* conditions using this technique. Cryo-SEM, a variant of SEM in which samples are rapidly frozen, has been applied to polysaccharide hydrogels to capture surface cracking after sublimation and analyze porosity distribution [138]. In addition, a recent study clarified that microstructural metrics, especially pore size, can be influenced by dehydration and freezing artifacts and may therefore not represent the native state of bioprinted hydrogel scaffold [139].

Collectively, microscopic visualization methods complement machine vision approaches by enabling structural defect detection at finer length scales. On the other hand, the need for extensive sample preparation in electron microscopy and the requirement to interrupt printing for in situ optical imaging remain practical constraints that motivate the development of more seamlessly integrated monitoring solutions.

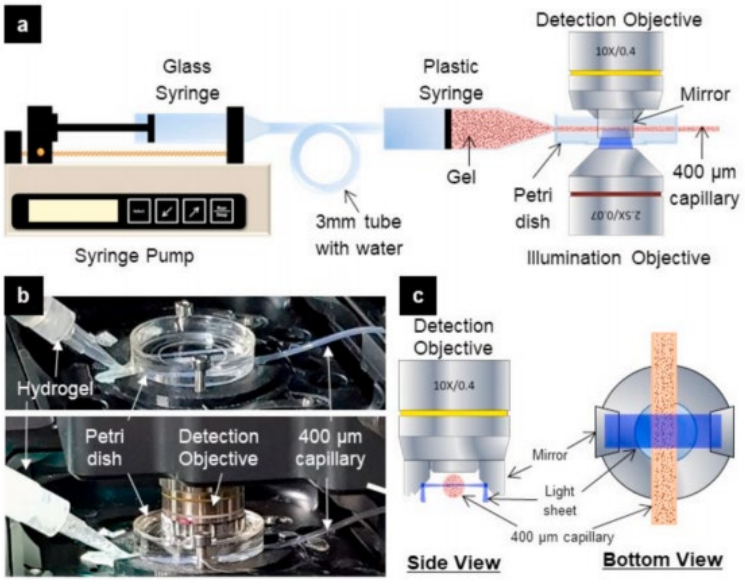


**Figure 17. Experimental setup of light sheet fluorescence microscopy and extrusion to perform real-time imaging of hydrogel extrusion [132]**

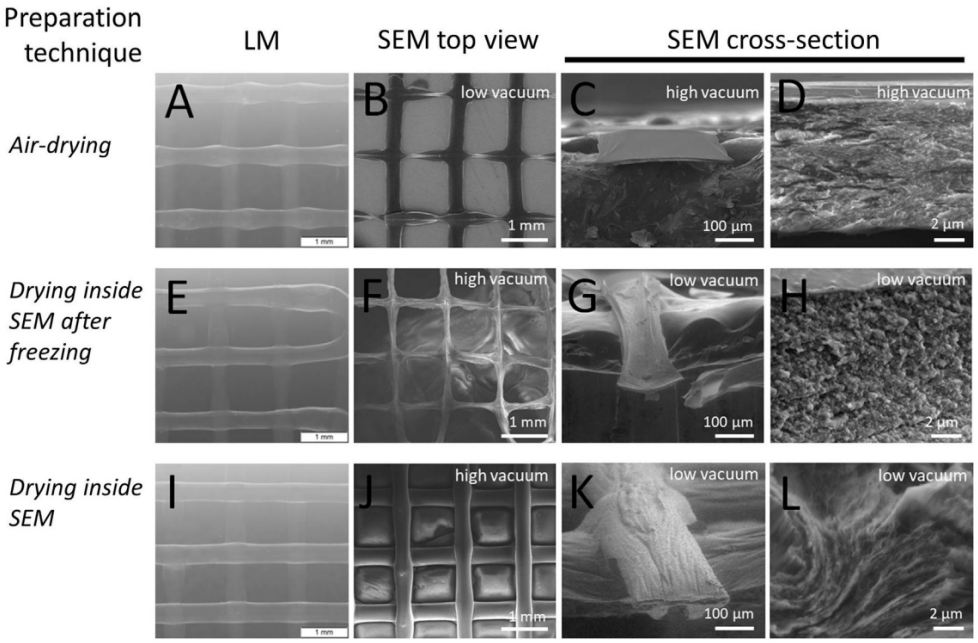


**Figure 18. Conventional SEM investigation of alginate-based hydrogel with different drying conditions. Light microscopic (LM) images of 3D printed scaffolds are shown (A, E, I). SEM images of top views (B, F, J) and cross-sectional views (D, H, L) after sample preparation in different conditions [137]**

### 3.1.3. Thermographic imaging

Thermographic imaging has emerged as a powerful non-contact, non-destructive approach for structural health monitoring in bioprinting. This method exploits the thermal signature of deposited materials to enable defect detection, particularly when printing transparent bioinks where conventional optical contrast is limited. An early study utilized thermal imaging as a process monitoring approach in thermally controlled extrusion bioprinting process, where the infrared thermography was used to optimize and validate the printing parameters [140]. Thermal images were captured using a thermal camera to analyze the selected region of interest of the thermally controlled bioprinting unit. Notably, the thermal signature at the nozzle tip indicated the presence of nozzle clogging in this setup, demonstrating that thermal data can provide process information beyond temperature measurement alone. Building on this work, a recent study has implemented thermal imaging for in situ inspection and monitoring of multi-layered bioprinted constructs [141]. This method analyzed temperature gradients from thermal signatures to determine the deviations in the shape of the most recently printed layer, thereby addressing limitations of visible-range imaging. Additionally, this method enabled the detection of layer geometry variations resulting from non-uniform material extrusion during printing. More recently, the approach has been

extended toward fully in-line monitoring by integrating G-code trajectory information into the thermal analysis pipeline. This integration enabled real-time frame-by-frame segmentation of the extruded biomaterial and direct comparison against the nominal geometry [142]. As a result, color-coded maps were generated to identify correct depositions, under-extrusion, and over-extrusion along the printing path, establishing a foundation for future closed-loop feedback control.

Thermal imaging provides a real-time, non-contact representation of the temperature field of the bioprinting process, which enables continuous process monitoring. Existing studies demonstrate that this method can detect under-extrusion, improper distribution of material, and deviations in shape fidelity of the printed samples. As thermal imaging hardware continues to improve and G-code integration enables tighter coupling between sensing and control, this approach is well-positioned to support the next generation of closed-loop bioprinting systems.

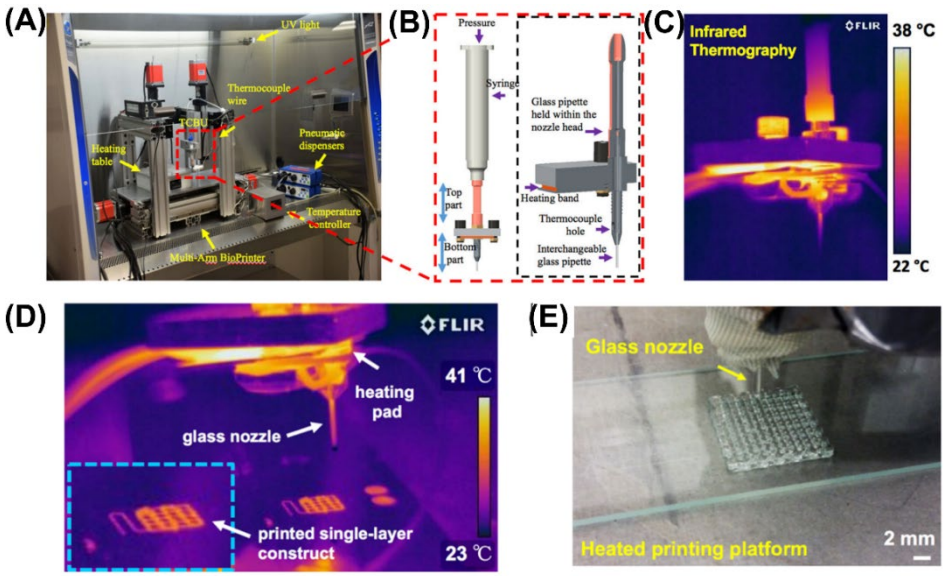


**Figure 19. (A) Experimental setup of the thermally controlled bioprinting unit. (B) Extrusion toolbox where the top part contains the bioink and the bottom part contains the heating system. (C) Thermal image of the extrusion toolbox was taken using an FLIR thermal camera. (D) Infrared image captured by thermal camera showing temperature map of the extrusion unit and extruded single-layer construct on the heated printbed platform, and (E) Bioprinting process [140]**

### 3.1.4. Video-based method

Video-based approaches offer the extraction of motion, deformation, and geometric features [143, 144] in a non-contact manner by analyzing consecutive frames from videos of an object, which contain subtle information related to shape evolution, material distribution, and dynamic response of the printed sample.

The information obtained from these recordings can be utilized to detect the anomalies both at the surface and within the printed constructs.

An early application of this approach focused on a persistent geometric challenge in extrusion-based bioprinting [145], namely achieving accurate material distribution at the corner regions, where bioink rheology makes precise control of strand diameter difficult [146]. By recording the extrusion process through a glass substrate using an industrial camera, three distinct types of corner defects were identified through frame-by-frame analysis of a hexagonal print pattern. These defects include smoothing, swelling, and ringing features. Building on this, another study used the recorded videos of bioprinting process to generate a datasets, enabling the determination of extrusion condition of the process [147].

The utility of video-based monitoring extends beyond geometric assessment to the characterization of embedded internal defects. The vibration signal signature of a bioprinted construct provides a holistic response of its structural state, capturing the complex interplay between material properties and geometry configurations. Defects in a bioprinted construct can introduce deviations in its modal properties. Thus, identifying these modal property changes can provide an effective diagnostic window into the inherent structural health and fidelity of the printed sample. High-speed video recordings contain rich dynamic response information of the sample, which can be used to estimate its modal properties using a phase-based motion estimation approach [148–150]. This concept has been implemented on 3D bioprinted constructs to determine the dynamic properties and monitor the structural integrity of the samples by detecting internal void [151], nozzle clogging effect [152] and embedded defect [153]. These findings demonstrate that dynamic video analysis can reveal internal structural anomalies.

Video-based methods can extract the inherent material properties by analyzing consecutive frames recorded over a very short period, representing any deviations from the baseline design. This technique offers a simple, contactless, and non-destructive structural health monitoring approach. At the same time, the defect detection resolution of this method needs to be investigated further for its broader implementation in the fabrication process.

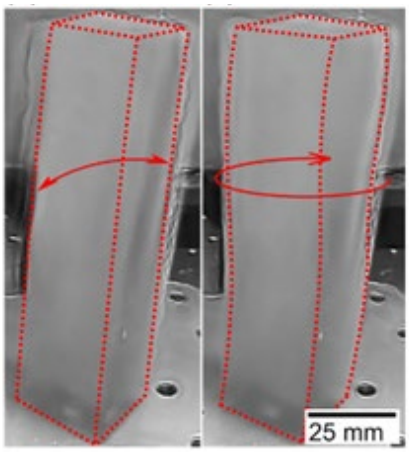


**Figure 20. Visual representation of phase-based motion magnification has been applied on the recorded video of 3D bio-printed column. Magnification was applied on the resonant frequencies of the construct to obtain flexural and torsional operational deflection shape of the bio-printed sample [150]**

### 3.1.5. Laser-based dimensional approach

Laser-based dimensional measurement operates by emitting a focused beam onto the object's surface and analyzing the reflected signal to generate a high-resolution displacement profile. This technique provides a precise, non-contact means for detecting dimensional deviations. In addition to defect detection, laser-based approaches have also been used for bioprinting processes [154], which eliminate defects associated with nozzle clogging [155].

The potential of laser scanning for dimensional error correction was first demonstrated in direct-write bioprinting, which shares the same extrusion principle as extrusion-based bioprinting. This method offers relatively simple printing conditions [156], but suffers from limited spatial resolution [157]. A non-contact laser scanner was used to measure material deposition errors at the single-layer level, and the measured error was fed back to modify the reference trajectory for subsequent prints [97]. This closed-loop correction was then verified through repeated laser scanning, providing a direct link between in situ measurement and print quality improvement. The approach was subsequently extended to multi-layer printing, where extrusion width was measured and corrected simultaneously with deposition location, achieving a 2D normalized error below 15% [98]. This approach was further advanced by deriving cross-sectional area and volumetric flow rate from laser scanner data, enabling active extrusion pressure control to compensate for over- and under-extrusions in real time [158].

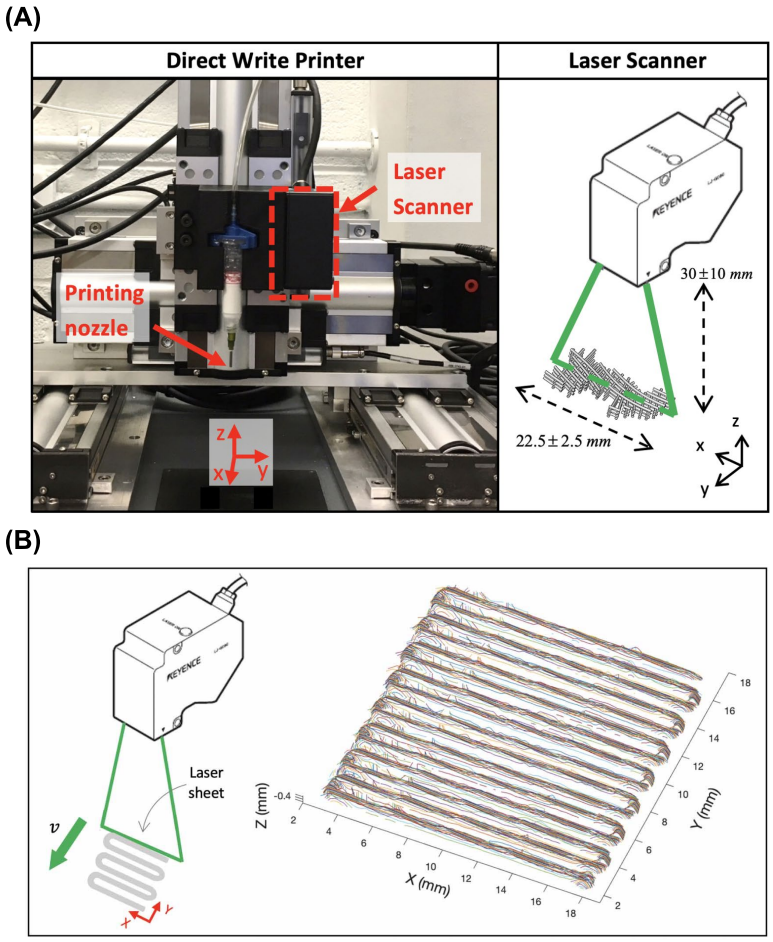


**Figure 21. (A) Experimental setup for laser scanner in a pneumatic extrusion-based bioprinting process. A laser scanner is attached with the printhead to enable direct process feedback. [97] (B) A non-contact 2D laser displacement scanner projects a laser sheet on the fabricated part (left) to generate 3D point cloud (right) [98]**

Collectively, laser-based approaches have evolved from single-layer dimensional error measurement into a versatile platform for closed-loop dimensional control. Their high spatial resolution and compatibility with feedback control make them well suited for applications where precise geometric fidelity is required.

### 3.2. Volumetric and subsurface imaging

Ensuring the internal fidelity of 3D bioprinted constructs requires advanced SHM approaches that can inherently capture volumetric and subsurface information within the printed sample. Conventional surface-level inspection methods often fail to detect subsurface structures, particularly due to the opacity of many bioink materials. Optical coherence tomography and magnetic resonance imaging are among the most

widely adopted volumetric imaging approaches, enabling non-destructive analysis of the internal structural integrity of 3D bioprinted samples.

### 3.2.1. Optical coherence tomography

Optical coherence tomography (OCT) is a non-invasive imaging technique that utilizes low-coherence interferometry with near-infrared light to generate high-resolution cross-sectional and volumetric images by measuring the time delay and intensity of backscattered or reflected lights [159]. Originally developed for ophthalmology and subsequently adopted in cardiology, dermatology, and industrial inspections [160, 161], OCT provides micrometer-scale resolution at imaging depths of 1-3 mm, making it well suited for probing the internal structure of hydrogel-based bioprinted constructs. In recent years, OCT has emerged as one of the powerful modalities in bioprinting, particularly for monitoring the process and evaluating the structural integrity of printed bioconstructs. It enables the detection of internal defects such as voids, delamination, and pore irregularities, which are not visible through conventional imaging techniques.

Early application of OCT in bioprinting focused on morphological characterization of printed scaffolds. Swept-source optical coherence tomography (SS-OCT) was used to capture global and local morphological features of 3D bioprinted scaffolds [162]. By addressing the limitations of digital microscopy, this research enabled the detection of pore fusion, undefined micropores, and closed pores within the hydrogel scaffolds. Expanding on this research, a subsequent study mounted an SS-OCT probe with the extrusion nozzle, enabling full-depth, wide-field imaging in real-time [163]. Material volume, volume porosity, and pore connectivity were measured in this study to determine layer-to-layer thickness, filament size, and pore size. This integration of OCT with the print head marked a significant step toward in-line volumetric monitoring during bioprinting. The approach was further extended to freeform reversible embedding of suspended hydrogels (FRESH) type bioprinting, leveraging the advantage of SS-OCT over camera based imaging approach in real-time [164]. A transparent gelatin support bath was developed in this study, enabling in-process volumetric monitoring and detection of internal defects caused by air bubbles and channel occlusion from over-extrusion, with quantitative 3D gauging achieving average surface deviations below 50 μm.

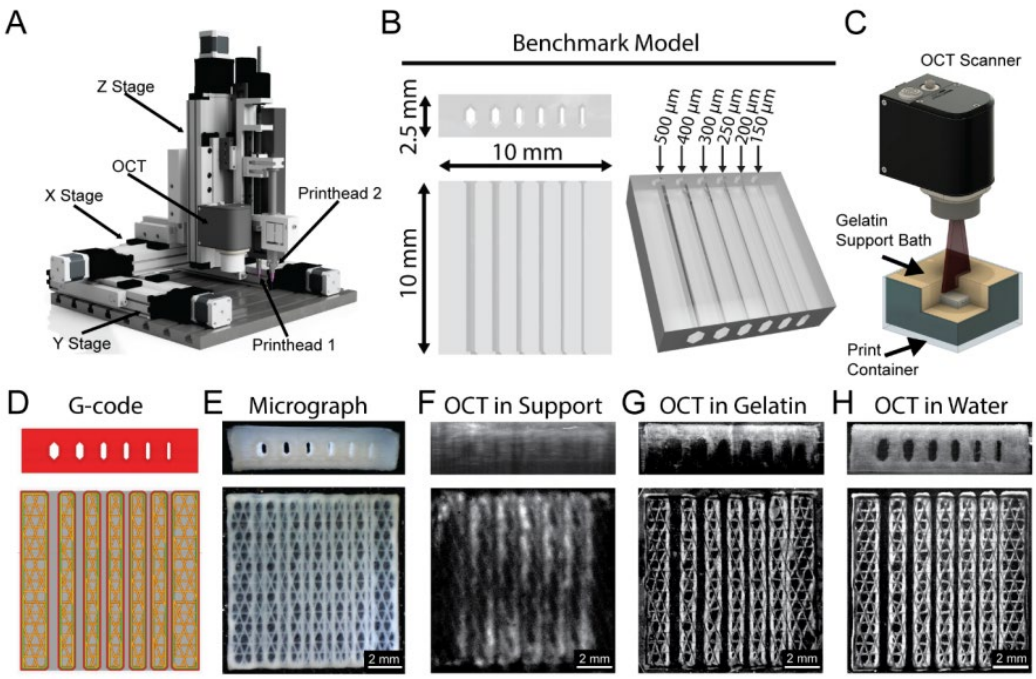


**Figure 22. (A) 3D bioprinter with OCT scan head. (B) Benchmark model with varying internal channel widths to test printer performance and imaging quality. (C) Example rendering of OCT imaging of a FRESH printed construct with support bath. (D) G-code of the benchmark model. (E) Photomicrograph of benchmark model showing end on and top-down views. (F-H) OCT imaging of the benchmark model in gelatin microparticle support bath, melted and resolidified gelatin, or water respectively [164]**

The progression from characterization to active defect detection and correction represents the next logical step in OCT-enabled monitoring. Optical coherence tomography has been combined with a feedback control system in extrusion-based bioprinting, enabling in situ detection of layer thickness, filament size, pore size, and filament breakage. These defects were corrected by adjusting the printing path, extrusion pressure, and printing speed [22]. Similarly, building on the previous work [163], defect detection mapping was developed by the same research group using an OCT system [165]. This study provided a visualization of defect mapping through the structural similarity index, enabling the identification of broken filaments and under-extrusion, which were subsequently corrected through feedback control mechanism. More recently, OCT has been used as an offline quality control tool for FRESH-printed scaffolds, where it verified whether the internal fluidic channels remained open and matched the intended design [166]. 3D image-based comparison with the intended design enabled the detection of geometric defects, such as layer straightness, filament diameter, and material deposition defects, including over- and under-printing and channel shape deformation, with deviations below 20 µm. In addition, OCT has also been employed in multi-material extrusion bioprinting to monitor the dynamic deformation of hydrogel structures in real-time

[167]. Metrics such as filament fusion, lateral pore ratio, and scaffold porosity were used to characterize the structural evolution of the sample during printing.

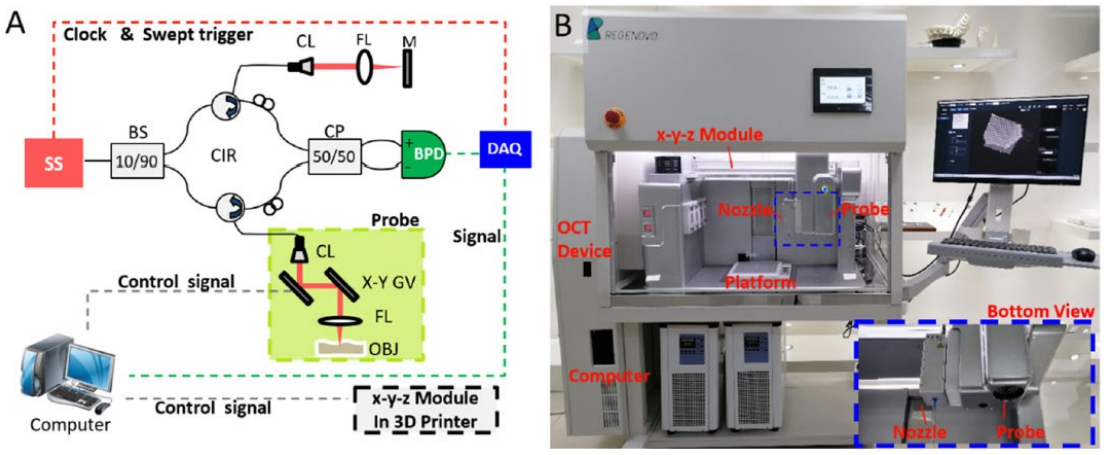


**Figure 23. Schematic diagram of 3D bioprinter-associated OCT system [163]**

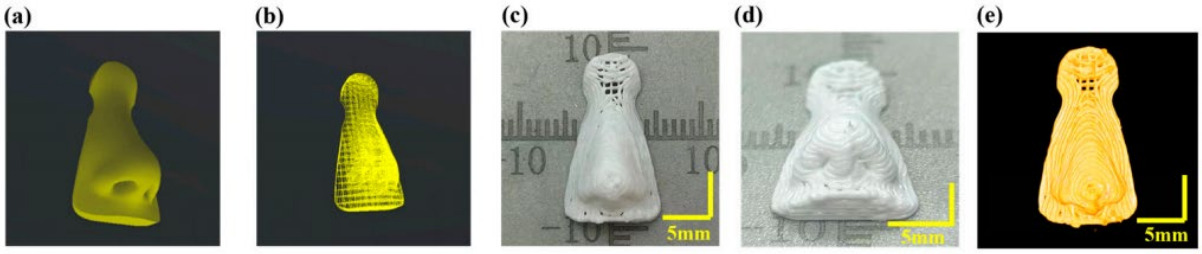


**Figure 24. Defect detection in multilayer nose structure using 3D P-OCT imaging. (a) Designed nose model. (b) Printing path of the designed model. (c, d) Actual images of the printed nose model. (e) 3D P-OCT image data of the nose sample [165]**

Maintaining the internal fidelity of 3D bioprinted structures is one of the major requirements in 3D bioprinting, as internal architecture governs the transportation of nutrients and oxygen to embedded cells [167, 168]. In recent years, OCT has been increasingly integrated into 3D bioprinting for real-time in situ process monitoring and quality control, addressing limitations of traditional camera-based visualization approaches. This technique provides high-resolution volumetric and sub-surface imaging, which offers a precise assessment of the internal structure of bioprinted constructs.

### 3.2.2. X-ray computed tomography, micro-CT

X-ray-based imaging methods enable non-destructive evaluation of bioprinted hydrogels and scaffolds by exploiting the differences in X-ray attenuation or phase shift as the beam passes through the material. Because hydrogels exhibit relatively low density and weak attenuation, the imaging contrast is primarily

derived from other factors such as crystalline domains, embedded particles, or phase-contrast effects. Early studies addressed this by using X-ray diffraction profiles to characterize free water and crystalline aggregates within polymeric hydrogel networks [169]. Similarly, another study employed small-angle X-ray scattering synchrotron radiation to characterize polymeric hydrogels by analyzing their nano- and micro-structure [170]. Building on these findings, synchrotron X-ray radiation was further applied to bioglass-enriched hydrogel material to determine particle size and distribution in wet state condition, motivated by the potential of inorganic particle enrichment to improve scaffold suitability for bone regeneration [171].

As bioprinting advanced, computed tomography (CT) and micro-computed tomography (micro-CT) techniques were introduced to analyze the three-dimensional architecture of printed constructs [172, 173], enabling quantification of pore distribution, pore size, and surface area [174]. Notably, micro-CT was used to analyze the degradation behavior of bioprinted radiopaque constructs fabricated by an extrusion-based bioprinter, where porosity, strut dimension, and local mass density were determined [175]. The findings from this study revealed spatially non-uniform degradation rates across the scaffold. Expanding this further, another group developed synchrotron propagation-based imaging with CT to assess scaffold fidelity, diameter deformation, and pore size from the captured images [176]. This process differs from conventional CT by using X-ray refraction-based phase contrast rather than attenuation alone, enabling high-SNR visualization of soft, low-density materials like hydrogel [177]. Moreover, compressive loading was applied to identify structural properties, and the images during this process were analyzed to identify structural deformation from strand size, porous spacing, and layer position.

Micro-CT often suffers from insufficient resolution and contrast in hydrogel applications [178]. While various contrast agents have been applied to address this issue [179], recent work has focused on incorporating gold nanoparticles (Au-NPs) into bioinks [180]. The findings from this study show that the introduction of Au-NPs enhanced the imaging resolution, enabling enhanced visualization of the bioprinted scaffold's internal microstructure.

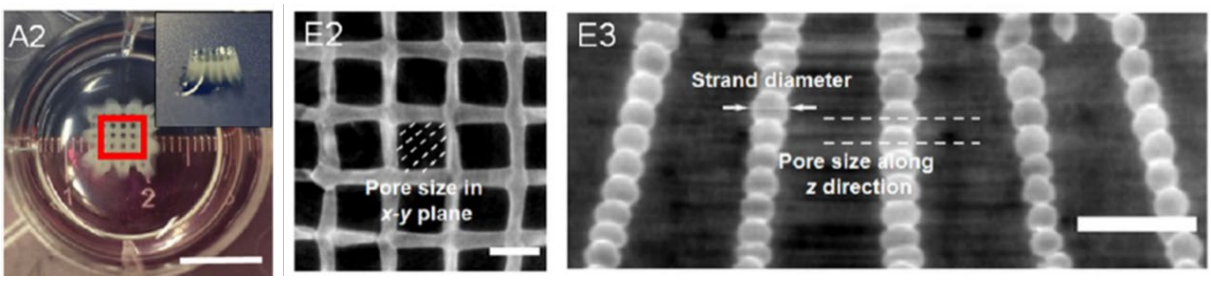


**Figure 25. Hydrogel scaffolds (A2) after printing and (E2) top view, (E3) side view visualized by SR-PBI-CT [176]**

Collectively, X-ray-based imaging methods provide a powerful non-destructive pathway for structural health monitoring of bioprinted constructs across multiple length scales–from nanoscale network characterization to scaffold-level geometric and degradation analysis. However, the inherently low attenuation of soft hydrogels necessitates either specialized synchrotron infrastructure or the introduction of contrast agents, both of which add experimental complexity and limit broader accessibility. These practical constraints motivate the continued development of contrast strategies and imaging configurations that are more seamlessly compatible with standard bioprinting workflows.

### 3.2.3. Magnetic resonance imaging

Magnetic resonance imaging (MRI) has emerged as a powerful non-destructive imaging technique that enables visualization of internal features of 3D bioprinted samples with high contrast. Beyond its use in evaluating patient-specific implant designs [181] and internal cavity structures of scaffolds for brain tissue engineering [182], MRI has also been employed as a powerful tool for structural health monitoring. MRI offers volumetric imaging by exploiting the response of hydrogen nuclei in bioink materials to strong magnetic fields. As the hydrogen nuclei return to equilibrium, radiofrequency signals emitted by the nuclei are detected and used to reconstruct high-resolution volumetric images. This makes the MRI method particularly well-suited for cell-laden hydrogels, which are inherently hydrogen-rich.

Early works focused on utilizing MRI primarily as a structural analysis tool. The movement of water during the extrusion of microcrystalline cellulose pastes was first investigated using MRI [183], establishing the feasibility of MRI-based monitoring in bioprinting context. This was followed by a study that implemented MRI in extrusion-based bioprinting to determine geometric deviations in a 3D printed cubic scaffold composed of alginate, GelMA, and calcium phosphate-based bioinks [184]. Cross-sectional slices were analyzed in this study along the height of each scaffold to assess the geometric and structural fidelity. This method enabled quantitative slice-by-slice evaluation of scaffold geometry by detecting defects such as swelling, strand merging, porosity associated with air bubbles, and layer collapse. Beyond structural fidelity, MRI has also been used to monitor hydrogel degradation and cartilage regeneration over time [185]. In this study, hydrogels were labeled with ultrasmall superparamagnetic iron oxide particles, which gradually disappeared or redistributed over time. MRI was then employed to monitor the signal changes over time, enabling non-destructive monitoring of scaffold degradation and cartilage regeneration.

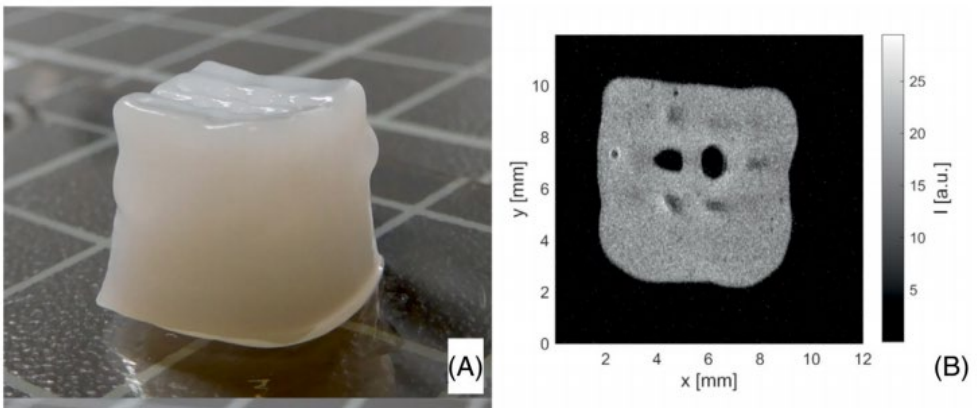


**Figure 26. (A) Actual image of alginate GelMA scaffolds on a grid of 10×10 mm$^2$ and (B) representative slice from pseudo 3D (2.5D) MRI measurements [184]**

Recognizing the high spatial resolution of MRI technique, subsequent work integrated MRI coil with a non-magnetic bioreactor system, enabling real-time monitoring of tissue growth with a planar resolution of 75 μm [186]. To further enhance imaging contrast and measurement precision, GelMA-based bioinks were incorporated with superparamagnetic iron oxide nanoparticles, which enhanced the MR imaging contrast and enabled more accurate fidelity assessment of the printed scaffolds [187]. Such contrast enhancement may further enable precise fidelity measurements of the bioprinted constructs.

Magnetic resonance imaging offers volumetric and sub-surface visualization, enabling detection of internal features that are otherwise challenging to observe, such as voids, material degradation, and air bubbles. This functional capability establishes the MRI method as a reliable tool for structural health monitoring and quality control of 3D bioprinted constructs.

### 3.3. Ultrasound and acoustic sensing approaches

Ultrasound has emerged as a versatile, non-contact modality for structural health monitoring of bioprinted constructs, offering deep penetration and sensitivity to both mechanical and compositional changes in soft, optically opaque materials [188–190]. It operates by transmitting acoustic waves in the kHz to MHz range into the construct and interpreting the reflected and transmitted signals to infer internal structure, stiffness, and, in some cases, biological state. In a typical configuration, a piezoelectric transducer emits short acoustic pulses into the hydrogel or tissue-engineered scaffold and records the returning radio frequency (RF) echoes after interaction with cells, polymer networks, and fluid-filled pores. By measuring time-of-flight and analyzing the RF amplitude and spectrum, depth-resolved or volumetric maps of acoustic impedance can be reconstructed, which relate to effective stiffness and microstructure [189, 191]. As a non-destructive method that can be integrated with printing platforms, ultrasound enables repeated

measurements on the same sample, supporting in-process monitoring, in vitro maturation studies, and, in some cases, post-implantation assessment [188, 190, 192].

Early work on ultrasound for engineered hydrogels focused on non-destructive estimation of mechanical properties. One of the studies investigated agarose hydrogels and demonstrated that the speed of sound measured ultrasonically correlates with compressive modulus obtained from mechanical testing, establishing an early quantitative framework for stiffness estimation in hydrated polymer networks [191]. Importantly, this study highlighted that accurate interpretation requires poroelastic modeling rather than purely elastic assumptions, because fluid–solid interactions strongly influence wave propagation in hydrogels. Subsequent reviews synthesized these findings and confirmed that quantitative ultrasound can reliably estimate elastic and viscoelastic properties across a wide range of engineered biomaterials [188, 189].

Building on this foundation, high-frequency ultrasound transducers extended the technique from bulk property estimation to microstructural characterization. An ultrasound system (up to 38 MHz) computed the integrated backscatter coefficient in three-dimensional collagen hydrogels, revealing that backscatter strength increases with collagen fiber density and diameter, while also revealing spatial heterogeneities in microstructure [193]. High-resolution spectral ultrasound further demonstrated the ability to track mineralization in collagen hydrogels over multi-week culture, with spectral parameters correlating with mineral content over time [194]. Collectively, these studies demonstrate that high-frequency and spectral ultrasound can resolve micro-textural and compositional features that are critical to scaffold function.

These characterization capabilities were subsequently translated toward in situ process monitoring in bioprinting systems. An early study reported that ultrasound can be implemented in low cost monitoring process of bioprinted samples, offering internal visualization and quality assessment [190]. Another study developed a real-time in situ ultrasound monitoring system for soft hydrogel 3D printing with subwavelength resolution, integrating an ultrasound probe with the printing stage to monitor interlayer bonding, effective elastic properties, surface profile, and defects such as nozzle-induced scratches and non-uniform layers during extrusion [192]. This progression from off-line characterization to in-process monitoring mirrors the development trajectory observed in optical and laser-based approaches discussed earlier.

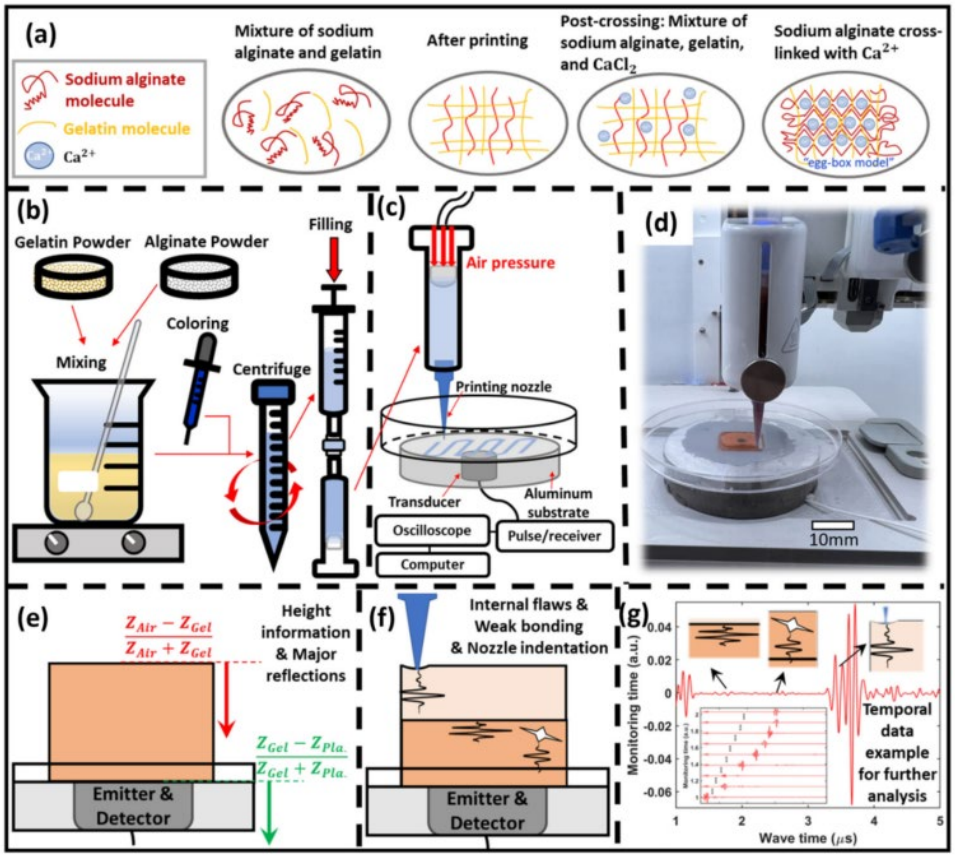


**Figure 27. (a) Polymer chains illustration of gelatin-alginate hydrogel before and after printing, and before and after crosslinking. (b) Hydrogel preparation steps include mixing, heating, centrifugation and syringe loading. (c) Schematic diagram of ultrasound monitoring experimental setup and (d) Raw image of ultrasound monitoring setup during printing. (e) Illustration of the two primary reflections from the lower and upper hydrogel surfaces. (f) Detection of internal flaws and nozzle scratching. (g) Representative temporal data captured during continuous ultrasound monitoring indicating internal flaws. [192]**

### 3.4. Dielectric impedance spectroscopy

Dielectric impedance spectroscopy (DIS) is an impedance-based approach that has emerged as a sensitive, label-free approach for monitoring the electrical and biological state of bioprinted constructs. This method offers a non-destructive, real-time assessment of internal features including porosity and material distribution. In DIS, the complex electrical impedance of a construct is measured over a frequency sweep, exploiting the fact that intact cell membranes behave as insulating capacitors. This gives rise to characteristic frequency-dependent dispersion behavior that reflects morphology and concentration, yielding quantitative signatures of cellular and matrix states within cell-laden hydrogels.

An early study established a detailed framework for applying DIS to process monitoring in bioprinted constructs, focusing on the β-dispersion region where the capacitive properties of cell membranes dominate the dielectric response [195]. Parameters such as permittivity change and the Cole-Cole dispersion parameter were shown to correlate with critical quality attributes, including cell viability, metabolic activity, and spatial distribution within alginate constructs. Decreases in these parameters were linked to process-induced damage from excessive extrusion pressure or unfavorable thermal conditions, establishing DIS as an early-warning indicator of compromised quality during fabrication. Building on this, subsequent work generalized this approach into a broader manufacturability framework for biofabrication, combining DIS with failure mode analysis and process modeling to enable layer-by-layer assessment of construct quality during printing rather than only post-fabrication inspection [196].

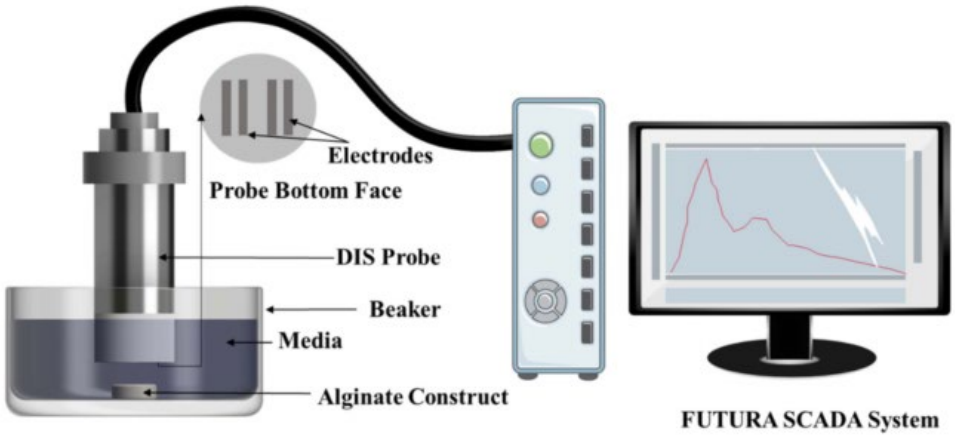


**Figure 28. Experimental setup for measurement of relative permittivity of bioprinted sample [195]**

These foundational studies motivated efforts to embed impedimetric sensing directly within the printing hardware. A hollow multifunctional fiber was introduced that acts simultaneously as an extrusion nozzle and an impedimetric sensor, enabling continuous monitoring of bioink properties inside the nozzle during printing [197]. By measuring impedance across a broad frequency range, the system distinguished between various cell types and detected in real time whether a stem cell remained undifferentiated or had differentiated into a target cell type. This capability enables continuous monitoring between stable and defective cell populations during extrusion, providing a robust mechanism for bioprinting quality control. In a complementary approach, interdigitated electrode sensors were used as “smart substrates” for monitoring epithelial cell cultures post-fabrication [198]. Impedance variations were shown to correlate with cell coverage and density over time, providing a non-invasive means of tracking cell attachment, migration, and proliferation.

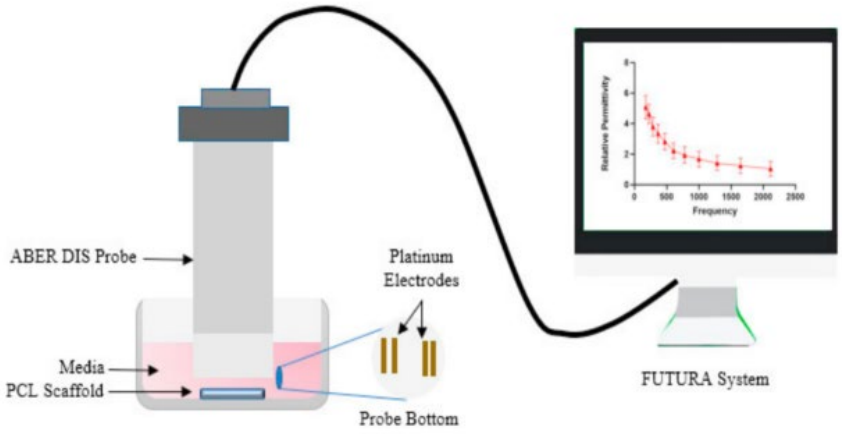


**Figure 29. Schematic diagram of the DIS system for analyzing NaOH-treated polycaprolactone (PCL) scaffolds [199]**

Given that DIS systems generate high-dimensional frequency spectra, the research focus has transitioned from measurement hardware toward automated data interpretation. DIS systems have been combined with supervised machine learning to classify dielectric spectra from polycaprolactone scaffolds seeded with multiple cell types, with the k-nearest neighbors algorithm achieving classification accuracies approaching 99% in distinguishing both cell type and culture duration [199]. This demonstrated that properly processed DIS data can serve as a robust input for intelligent, automated quality control of tissue constructs. Recent developments have extended DIS-based monitoring further in the bioprinting workflow by integrating impedance measurement capabilities directly into the syringe for pre-extrusion assessment [200]. Impedance and phase angle recorded within the syringe reservoir prior to the onset of nozzle-induced shear during extrusion demonstrated a strong linear relationship with viable cell count and concentration. This enables non-conforming or compromised bioinks to be identified before the printing begins, adding a preventive quality control step at the earliest stage of the fabrication process.

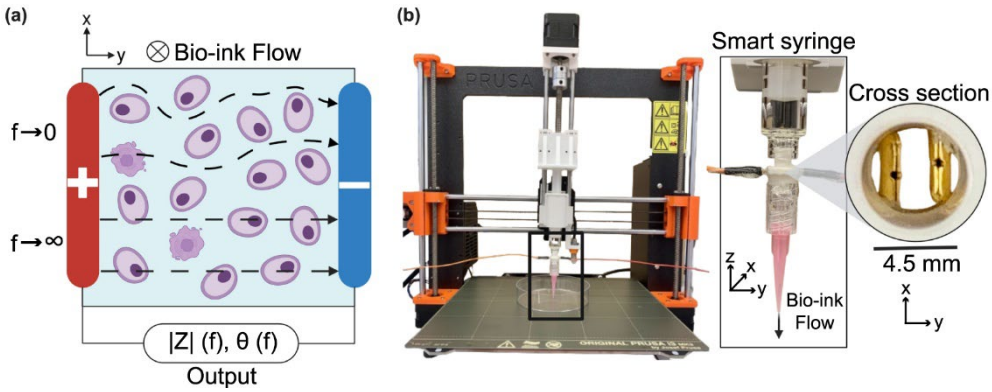


**Figure 30. Experimental setup of DIS integrated into syringe for in-line monitoring of bioink [200]**

Collectively, DIS-based monitoring has progressed from post-fabrication construct assessment to inline nozzle sensing and pre-extrusion syringe monitoring, covering the full bioprinting workflow and positioning impedance spectroscopy as a uniquely comprehensive tool for biological quality control in bioprinting.

### 3.5. Flow sensing approaches

Flow sensor-based monitoring has been introduced to overcome the limitations of conventional open-loop pneumatic control in extrusion-based bioprinting. In standard setups, a fixed air pressure is assumed to produce a consistent material flow rate. However, changes in cartridge fill level, temperature, and bioink viscosity often result in variations in strand diameter and deposited volume. Flow sensing shifts the control objective from constant pressure to constant volumetric flow, enabling more reproducible deposition across varying process conditions. In this approach, a microfluidic liquid flow meter is often placed between the syringe and the nozzle to measure the actual volumetric flow rate in real time. The measured flow is then fed into a feedback controller that continuously adjusts the applied pneumatic pressure to track a specified target flow rate. An early study demonstrating this strategy showed that identical pressure setpoints can produce markedly different flow rates across devices or as the fill level decreases [201]. Switching from pressure control to flow-rate control substantially reduced variability in printed alginate strand dimensions, with the coefficient of variation decreasing by an order of magnitude. Consequently, the inline flow sensing has emerged as a key process-analytical tool for aligning biofabrication outcomes across platforms and laboratories. Building on this concept, a subsequent study implemented a Python-based proportional-integral-derivative controller that uses flow-sensor feedback for active error correction [202]. The system detected transient flow reductions caused by bioink inhomogeneities or viscosity changes and responded by briefly increasing pressure to restore the desired flow. The same control framework also reduced the trial-and-error associated with changing nozzle diameters, as the controller automatically identified the pressure required to achieve the desired flow rate for each nozzle geometry. Collectively, these studies illustrate how flow sensing transforms extrusion bioprinting from an open-loop pressure-driven process into a closed-loop, flow-regulated system, directly addressing one of the most fundamental sources of deposition variability in bioprinting.

### 3.6. Integrated Perspective on SHM Methods in 3D Bioprinting

Structural health monitoring in 3D bioprinting encompasses a diverse suite of defect-detection and process-monitoring techniques designed to identify and assess process-induced defects, structural inconsistencies, and functional impairments during or after fabrication. The methods discussed in Sections 3.1 through 3.5 operate across complementary sensing physical principles and length scales, collectively

addressing the broad spectrum of defect types encountered in bioprinted constructs. Structural health monitoring of bioprinted constructs is most commonly centered at the surface level, where optical imaging serves as the predominant approach that leverages its ability to detect surface-level anomalies, such as filament size inconsistency and dimensional error. Microscopic visualization extends this capability to a finer spatial scale, enabling detection of filament fusion, filament delamination, surface roughness, and crack formation. Moving inward, non-destructive techniques–including thermographic and infrared imaging, optical coherence tomography, computed tomography, and magnetic resonance imaging–characterize subsurface and internal features such as porosity, filament collapse, layer delamination, and strand fusion. Acoustic methods such as ultrasound further expand this capability by providing information on mechanical properties and internal structural integrity. Complementing these approaches, in-process monitoring techniques such as flow sensing and dielectric impedance spectroscopy provide real-time information on deposition consistency, internal void formation, and deviation in filament line width, detecting defects as they form. More recently, data-driven approaches using machine learning have been integrated with several of these sensing modalities, enabling automated defect classification, prediction, and diagnosis. This integration elevates SHM from passive observation toward intelligent process control and is discussed in further detail in Section 4. Each SHM method targets different objects of analysis, ranging from cellular components and extruded filaments to printed scaffolds and overall geometry, while quantifying distinct physical and biological parameters. Table 2 summarizes different defect types detectable by SHM approaches, while Table 3 organizes the relationships between sensing modalities, monitored targets, and measured parameters across all reviewed techniques. These integrated perspectives illustrate how the SHM approaches complement one another in capturing the multiscale complexity of bioprinted constructs, which is essential for guiding future research toward integrated characterization protocols tailored to specific objectives, including printing parameter optimization, structural fidelity validation, and assessment of biological functionality. Based on the target objects of different structural health monitoring approaches, the following table correlates different target objects with the structural health monitoring methods. While the methods reviewed here represent the current state of the art, the field of SHM is broad and continues to evolve. Several well-established monitoring techniques from adjacent engineering disciplines, such as acoustic emission, electrical impedance tomography, and fiber Bragg grating sensors, have yet to be systematically explored in the context of bioprinting and may offer promising avenues for future investigation.

**Table 2. Overview of different structural health monitoring methods and types of defects detected**

| Defect type / Method | Under extrusion | Over extrusion | Filament collapse/breakage | Irregularities | Strand fusion/merging | Improper material distribution | Deviation in line width | Deviation in shape fidelity | Swelling/shrinkage | Internal Layer delamination | Internal void Porosity | Surface roughness | Microstructure heterogeneity | Improper crosslinking | Mechanical Deformation | Mechanical stiffness change | Cell aggregation/dispersion | Cell viability | Vascularization, perfusion | Cell density change |
|---|---|---|---|---|---|---|---|---|---|---|---|---|---|---|---|---|---|---|---|---|
| **Optical imaging & machine vision** | ✓ | ✓ | | | | | ✓ | ✓ | | | ✓ | | | | ✓ | ✓ | | | | |
| **Microscopic visualization** | | | ✓ | | ✓ | | ✓ | | ✓ | | | ✓ | | | | | ✓ | ✓ | | |
| **Thermographic and infrared imaging** | | | | | | ✓ | | ✓ | | | | | | | | | | ✓ | | |
| **Video-based** | ✓ | ✓ | | | | | | ✓ | ✓ | | ✓ | | | | | | | | | |

| Defect type / Method | Under extrusion | Over extrusion | Filament collapse/breakage | Irregularities | Strand fusion/merging | Improper material distribution | Deviation in line width | Deviation in shape fidelity | Swelling/shrinkage | Internal Layer delamination | Internal void Porosity | Surface roughness | Microstructure heterogeneity | Improper crosslinking | Mechanical Deformation | Mechanical stiffness change | Cell aggregation/dispersion | Cell viability | Vascularization, perfusion | Cell density change |
|---|---|---|---|---|---|---|---|---|---|---|---|---|---|---|---|---|---|---|---|---|
| **Laser-based** | ✓ | ✓ | | ✓ | | | ✓ | ✓ | | | | | | | | | ✓ | | | |
| **OCT** | ✓ | ✓ | ✓ | ✓ | ✓ | ✓ | | ✓ | | | ✓ | | | | | | | | | |
| **X-ray CT, micro-CT** | | | | | | ✓ | ✓ | ✓ | | | ✓ | | | | | | | ✓ | | |
| **MRI** | ✓ | | | | ✓ | | | ✓ | ✓ | | ✓ | | | | | | | | | |
| **Ultrasound** | | | | | | ✓ | | | | ✓ | | ✓ | ✓ | | | ✓ | ✓ | ✓ | ✓ | ✓ |
| **DIS** | | | | | | | | ✓ | | | ✓ | | | | | | | ✓ | | ✓ |
| **Flow sensing** | ✓ | | | | | | ✓ | | | | | | | | | | | | | |
| **ML** | ✓ | ✓ | | ✓ | | | ✓ | ✓ | | | | | | | | ✓ | | ✓ | | ✓ |

**Table 3. Overview of structural health monitoring methods in bioprinting and their corresponding target objects and analysis parameters**

| Method | Target object | Analyzing parameters | Reference |
|---|---|---|---|
| Optical imaging and machine vision | Cellular components | Droplet velocity, cell count in droplet | [203] |
| | Extruded filament/jet | Filament width, effect of printing temperature | [120, 121, 204] |
| | Printed Geometry-macro scale | Line geometry, over- and under-extrusion metric, trajectory deviation, printability, cell-viability, laser power, scan speed, pore index | [114–119, 123, 205–207] |
| Microscopic visualization | Cellular components | Droplet velocity, cell count | [69, 208] |
| | Extruded filament/jet | Bioink rheology, printability, dead/live cell ratio | [131] |
| | Hydrogel/biomaterial matrix | Extrusion pressure, speed, and line width | [69, 137] |
| | Layer & process dynamics | Yield stress, shear-thinning, recovery behavior, fiber formation, layer stacking, rheology, pore size, swelling rate, and live/dead cells observation | [48, 78, 208] |
| | Microstructure/pore network | Pore size, and distribution, quantitative and qualitative parameters, pore size, pore morphology | [138, 209] |
| | Printed geometry-macro scale | Filament width, height, viscosity, etc. | [124, 133, 134] |
| Thermographic and infrared imaging | Cellular components | Cellular behavior, printability | [210] |
| | Extruded filament/jet | Filament width, position, area | [141] |
| | Hydrogel/biomaterial matrix | Printing parameters, rheological parameters, structural parameters | [140] |

| Method | Target object | Analyzing parameters | Reference |
|---|---|---|---|
| Video-based | Printed geometry-macro scale | Deviation in position, width, vibration characteristics | [151–153] |
| | Front view of printing process | Layer height, extrusion flow, infill density | [128, 147] |
| Laser-based | Extruded filament/jet | Geometric error, process parameter, pressure, speed, nozzle size | [98, 158] |
| | Layer & process dynamics | Deviation in path | [97] |
| | Tissue constructs | Spheroid geometry & growth, cell viability | [17] |
| Optical coherence tomography | Hydrogel/biomaterial matrix | Pore size, shape, strut size | [162] |
| | Layer & process dynamics | Filament size, layer thickness | [22] |
| | Microstructure/pore network | Porosity, pore ratio, dynamic deformation | [167] |
| | Printed geometry-macro scale | Layer-to-layer thickness, filament size, pore size, OCT image quality, geometric fidelity, deviation from the model | [163–165] |
| X-ray CT, micro-CT | Nano- and micro-structure of the hydrogel network | Free water and crystalline aggregates, crystalline size, and spectral intensity | [169] |
| | Gellan gun-bioglass hydrogel composites | Particle size, distribution | [171] |
| | Bioprinted scaffold | Porosity, strut dimension, local mass density, diameter deformation, and pore size | [175, 176] |
| | Extruded filament/jet | Water intensity using varying parameters | [183] |

| Method | Target object | Analyzing parameters | Reference |
|---|---|---|---|
| Magnetic resonance imaging | Hydrogel/biomaterial matrix | MRI-based, histological, and in-vitro parameters, the strand's geometrical feature | [185] |
| | Microstructure/pore network | Porous size, hole area, and scaffold height | [184] |
| | Tissue constructs | Electromagnetic field & simulation parameters, MRI-imaging parameters | [187] |
| Ultrasound and acoustic sensing approaches | Hydrogel/biomaterial matrix | Ultrasound-based, mechanical, statistical parameters, mineral content inside hydrogel, collagen fiber microstructure, ultrasound parameters, bioink properties, frequency domain, thermal parameters, printing parameters, etc. | [191, 194, 211, 212, 79, 192] |
| | Nozzle-material interface | Cell positioning, alignment, and morphology | [93] |
| Dielectric impedance spectroscopy | Cellular components | Dielectric spectrum, Impedimetric parameter, process parameters, biological validation parameters, dielectric, biological & flow-related parameters | [195, 200] |
| | Nozzle-material interface | Impedance-based, morphological parameters | [198] |
| Flow sensing approaches | Layer & process dynamics | Flow, process, feedback control, material parameters | [202] |
| | Nozzle-material interface | Flow, printing-performance, pressure-related, material parameters | [201] |

## 4. Machine learning for structural health monitoring and process control in bioprinting

As discussed in the previous sections, structural health monitoring in bioprinting aims to continuously assess the integrity and fidelity of printed constructs during fabrication. Modern bioprinting platforms generate large volumes of heterogeneous data originating from multiple sensing modalities, including imaging data (images and videos), electrical signals such as impedance spectra, as well as process-level signals including flow rate, extrusion pressure, printing speed, and temperature. Collectively, these datasets describe the evolving state of the printing process and the printed construct. While various classical analytical or physics-based models have been extensively explored to explain specific aspects of the printing process, these traditional approaches often struggle to interpret subtle defect signatures, integrate multimodal sensing signals, and predict failure events before they occur. This limitation is particularly evident in bioprinting, where complex rheological behavior, material heterogeneity, and the layer-by-layer accumulation of errors challenge conventional modeling approaches [44]. Machine learning has therefore emerged as a powerful tool for extracting information from high-dimensional process data, learning defect signatures from labeled datasets, quantifying anomaly severity, and supporting predictive and adaptive control [213]. While ML has already been explored across multiple areas of bioprinting, including parameter optimization [214], printability, print quality prediction [215], and cell viability estimation [216], the focus of this section is specifically on the role of ML in interpreting monitoring data collected during bioprinting, assessment of printing quality and defect detection, and, ultimately, closed-loop and predictive control. The discussion is organized according to sensing modality and then extended toward integrated control frameworks.

### 4.1. Data- driven defect identification across monitoring modalities

#### 4.1.1. Optical image-based monitoring

Optical imaging remains one of the most widely adopted modalities for ML-integrated structural health monitoring in extrusion-based bioprinting. This technique provides high-resolution visual information about filament morphology and scaffold geometry, allowing ML algorithms to detect deviations from the intended printing pattern [125, 128]. By directly integrating camera-acquired images into machine learning workflows, these frameworks enable automated recognition of deviations from the prescribed printing trajectory, thereby mitigating the limitations of manual, error-prone visual inspection [217].

Early deep learning efforts demonstrated that standard convolutional architectures could be effectively tuned for filament-level defect detections. In one such effort, an anomaly detection system was developed for transparent GelMA hydrogels by capturing layer-by-layer images and extracting patches corresponding

to individual filament segments [123]. In this study, a pretrained ResNeXt 50 Convolutional Neural Network (CNN) was applied to classify three types of structural anomalies–discontinuity, irregularity, and non-uniformity–across four infill patterns, achieving an accuracy of over 90% and an F1 score of 0.868. Building on this foundation, subsequent studies explored alternative architectures to further improve the classification reliability. Liquid Neural Networks (LNNs), for instance, achieved near-perfect accuracy in differentiating ideal prints from under- and over-extrusion defects [205]. This performance underscores that architectures capable of modeling temporal dynamics may offer advantages over traditional static convolutional approaches for certain defect categories. Recent studies have further expanded image-based monitoring by incorporating more advanced deep learning architectures and segmentation strategies. As confidence in image-based classification matured, the research focus has transitioned toward more rigorous analytical tasks. Beyond simple print defect labeling, a dual-task framework was developed to compare printed scaffolds directly against their reference models, simultaneously yielding a quality classification and a continuous structural similarity score [217]. This model achieved an overall accuracy of 92.7% across multiple scaffold geometries. Concurrently, the integration of foundation models, such as Segment Anything Model (SAM), has facilitated zero-shot filament segmentation without the need for manual annotation. This approach enables the direct extraction of geometric measurements that align closely with results obtained via standard confocal microscopy [218]. An example of AI-based filament segmentation and subsequent geometric feature extraction from in situ images is shown in Figure 31, illustrating how structural features can be directly quantified from raw imaging data. This model could extract filament diameter and spatial deviation directly from in situ images and showed strong agreement with ex-situ confocal microscopy measurements. These advances indicate that image-based monitoring is evolving beyond defect classification toward segmentation and geometric quantification, enabling more detailed quality assessment of the printed construct.

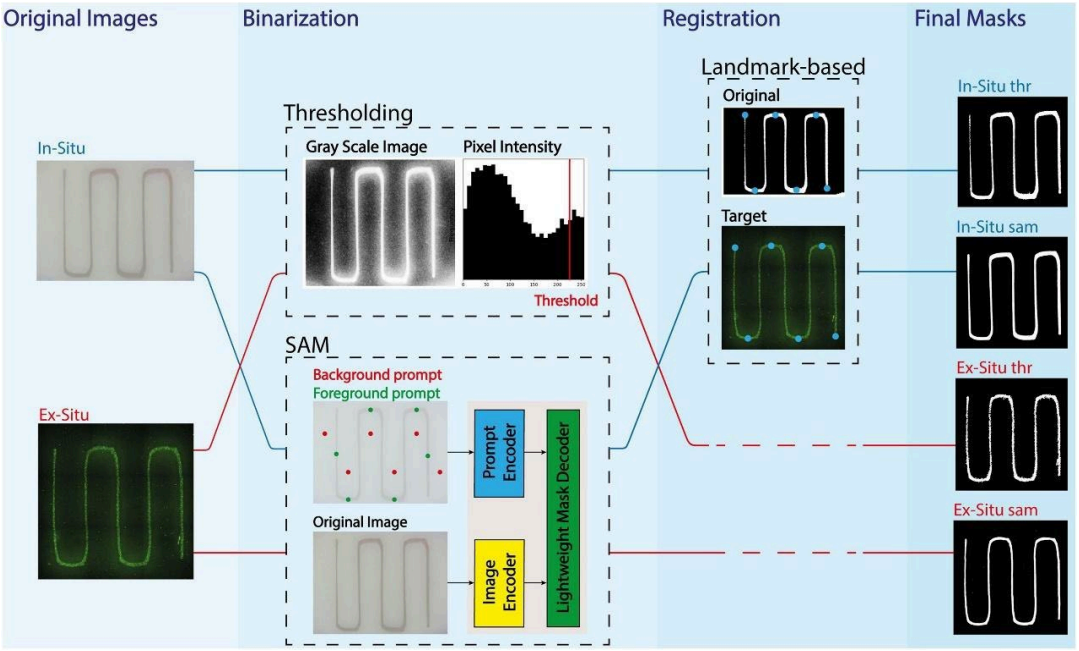


**Figure 31. AI-based filament segmentation and geometric feature extraction from in situ bioprinting images [218]**

More recent work has further expanded the capabilities of image-based monitoring by incorporating advanced architecture and high-resolution imaging strategies. Transformer-based models have been introduced to capture both local and global structural features from in situ images, improving generalization across different materials and printing conditions [204]. In parallel, AI-powered printability evaluation systems integrating segmentation models, support vector regression, multilayer perceptrons, and regression-based CNNs have been used to quantitatively assess shape fidelity and geometric deviation using metrics such as Hausdorff distance between printed structures and reference CAD geometries [206]. High-resolution imaging in specialized processes, such as two-photon polymerization, has also been integrated with deep learning models to predict structural quality from layer-wise grayscale images. These systems incorporate additional uncertainty estimation to identify ambiguous regions, such as incomplete polymerization or bubble formation [207]. Such advancements extend image-based monitoring toward increasingly complex objectives, including cross-material analysis and confidence-aware prediction.

Collectively, these studies illustrate a clear evolutionary trajectory in image-based monitoring utilizing ML techniques. The field has advanced from single-modality defect classification via CNN architectures toward sophisticated multi-task frameworks capable of structural benchmarking, zero-shot segmentation, and precise geometric quantification. These image-based systems are increasingly being integrated into scaffold and bone tissue engineering applications for real-time, in situ quality assessment [125–127]. This

shift reflects a growing consensus that optical ML monitoring is an indispensable component of next-generation bioprinting process monitoring and control [213, 219].

### 4.1.2. Video-based anomaly monitoring

Video-based monitoring extends image-based approaches by incorporating temporal information, enabling the detection of transient instabilities that cannot be captured from static images alone. In extrusion-based bioprinting, defects such as internal void, filament size inconsistencies, and embedded defects, making video data particularly valuable for identifying early-stage process deviations before they manifest as visible geometric defects.

Early studies demonstrated that spatiotemporal deep learning architectures can effectively learn normal printing dynamics from video sequences. A convolutional long short-term memory (ConvLSTM) autoencoder was developed to model stable extrusion behavior using only defect-free video data [147]. The overall architecture of this framework is illustrated in Figure 32(A), where the network learns spatiotemporal patterns of normal extrusion through sequential frame encoding and reconstruction. In this framework, the model reconstructs incoming frame sequences, and deviations from learned patterns are quantified through reconstruction error, which increases in the presence of filament size inconsistencies from under- or over-extrusion. This approach enables continuous anomaly scoring, allowing not only the detection of abnormal events but also the quantification of defect severity. Building on this foundation, subsequent work incorporated supervised learning to directly classify defect states from video streams.

To enable real-time quality assessment, a CNN-based monitoring framework was developed to categorize printing conditions into ‘ok,’ ‘under-extrusion,’ and ‘over-extrusion’ using frontal-view video frames collected under varying process conditions [128]. As shown in Figure 32(B), video frames undergo preprocessing and data augmentation before being used to train CNN, improving robustness across variations in lighting, material appearance, and printing conditions. Integrated within an online monitoring loop, this system enabled early identification of process instabilities and facilitated intervention during printing. Furthermore, by coupling the classifier output with a process model, the framework demonstrated the ability to iteratively adjust extrusion parameters and converge toward optimal printing conditions.

Collectively, these studies highlight the progression of video-based monitoring from unsupervised anomaly detection toward real-time classification and control integration. By capturing the temporal evolution of the printing process, video-based machine learning provides a critical capability for early detection of dynamic instabilities and supports the development of adaptive and automated bioprinting systems.

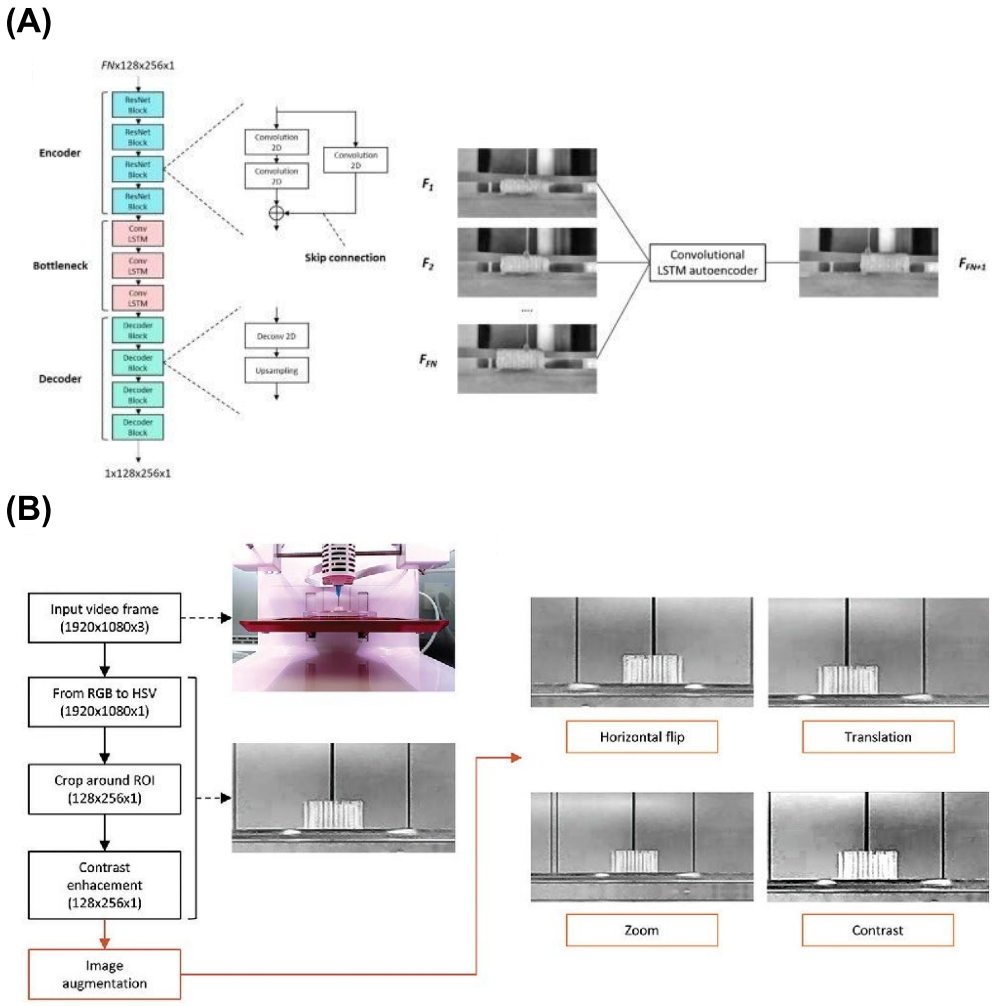


**Figure 32. (A) Spatiotemporal deep learning framework for video-based anomaly detection in bioprinting [147]. (B) Deep learning-based video processing pipeline for real-time defect classification [128]**

### 4.2. From defect detection to closed-loop control and autonomous bioprinting

While machine learning has demonstrated strong capabilities for identifying defects and anomalies in bioprinting processes, defect detection alone does not ensure reliable manufacturing. Traditional structural health monitoring systems typically operate in a passive mode, where sensor data are used to observe the process and identify deviations after they occur, often requiring manual intervention. Early monitoring studies primarily focused on detecting errors and stopping or restarting prints, resulting in reactive and material-intensive workflows [125]. In extrusion-based bioprinting, the layer-by-layer nature of fabrication makes the process particularly sensitive to error accumulation. Small deviations in extrusion conditions,

such as minor fluctuations in material flow or under-extrusion, can progressively alter filament geometry, distort pore architecture, and weaken interlayer bonding. As a result, ensuring structural integrity and functional performance requires SHM systems that move beyond passive observation toward active correction and adaptive control. This integrated monitoring–decision–control framework is schematically illustrated in Figure 43, where sensing, machine learning inference, and process actuation are combined into a unified closed-loop architecture for real-time process stabilization.

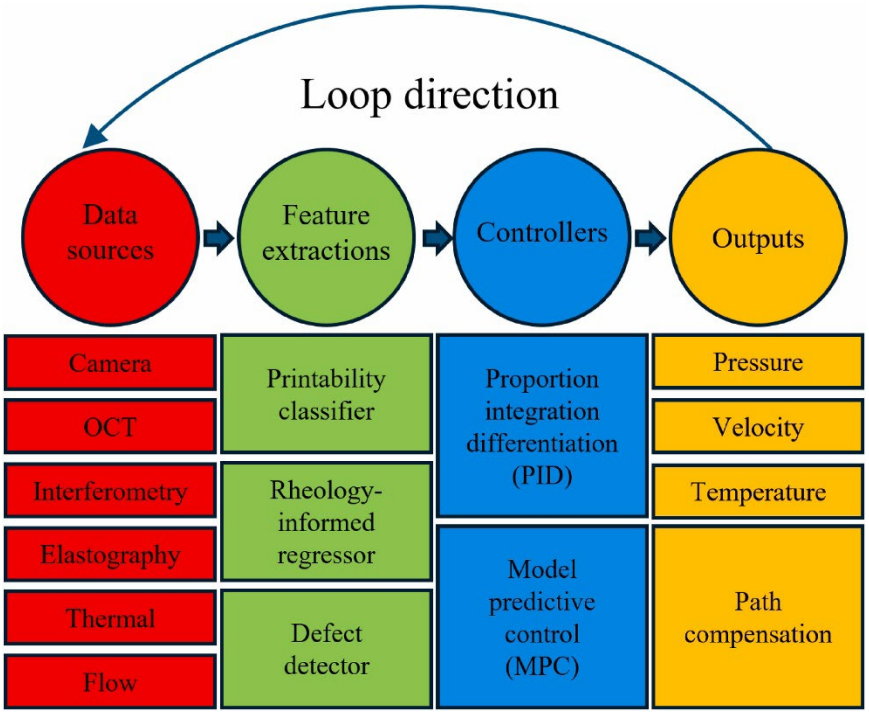


**Figure 33. Closed-loop bioprinting framework integrating sensing, machine learning, and real-time control [220]**

To address this need, recent ML-driven frameworks have adopted a multi-stage pipeline that integrates monitoring, diagnosis, and control. In such systems, sensor data are first analyzed to detect deviations from expected behavior. These deviations are then interpreted to diagnose underlying causes, such as nozzle clogging, unstable flow, or variations in bioink properties. Based on this diagnosis, a decision module determines appropriate corrective actions, and process parameters (e.g., extrusion pressure, print speed, or toolpath) are updated in real time to restore stable conditions. By learning process–defect relationships from data, ML models enable increasingly accurate mapping between sensor inputs, defect severity, and optimal parameter adjustments as more operational data becomes available. This transition from passive monitoring to active control is reflected in recent frameworks that integrate ML-based perception with real-time process regulation, forming the foundation for closed-loop and ultimately autonomous bioprinting systems. The following subsection discusses these developments in detail.

### 4.2.1. Machine learning-based closed-loop and adaptive control

A key advancement beyond passive monitoring is the integration of ML models with real-time sensing to enable closed-loop control. In these systems, monitoring data are continuously analyzed and used to guide parameter adjustments during printing, allowing the process to respond dynamically to evolving conditions.

Vision-based approaches have demonstrated that deep learning models can extract control-relevant information directly from temporal printing data. Both ConvLSTM autoencoder frameworks and CNN-based monitoring systems have utilized frontal-view videos collected under varying process conditions, including layer height, extrusion multiplier (EM), infill density, nozzle geometry, and extrusion configuration, to evaluate extrusion stability and detect process deviations [128, 147]. In these approaches, under- and over-extrusion were identified through either reconstruction-error-based anomaly scoring or direct defect classification. The ConvLSTM autoencoder [147] learned the temporal dynamics of stable extrusion from defect-free video sequences and quantified deviations using reconstruction mean squared error (MSErec), which increased proportionally with defect severity. This enabled continuous monitoring of process instability and provided a quantitative indication of extrusion quality over time. Building on similar video-based monitoring concepts, another study incorporated CNN-derived defect predictions into an explicit adaptive quality-control loop [128]. In this framework, the printing state was classified into "ok," "under-extrusion," and "over-extrusion" categories, and the predicted output was used to iteratively adjust the extrusion multiplier during printing. Detection of under-extrusion increased EM to restore stable filament formation, whereas over-extrusion predictions reduced EM to minimize filament spreading and excessive material accumulation. By integrating the CNN predictions with a printability-window model, the framework progressively converged toward optimized deposition conditions while also enabling early termination of unstable prints to reduce material waste and printing time [128]. Collectively, these studies demonstrate how spatiotemporal video analysis can evolve from passive anomaly monitoring toward adaptive extrusion regulation and real-time quality control

Beyond vision-based approaches, process-aware sensing has also been integrated into ML-driven control frameworks. An early study employed in situ IR thermocouple sensing and layer imaging to monitor process variables associated with extrusion stability, including strand width, strand height, and inter-filament fusion behavior [27]. These thermal and geometric measurements were used to train machine learning models capable of predicting filament morphology and deposition quality under varying printing conditions. The resulting predictions were incorporated into a feedforward control strategy in which printing speed was dynamically adjusted to compensate for deviations in filament geometry and fusion quality, thereby improving geometric consistency and reducing irregular filament spreading during

deposition. Compared with purely vision-based approaches, thermal-process monitoring can provide a more physically grounded basis for intervention during printing. Beyond direct defect detection, recent machine learning frameworks have also explored adaptive quality optimization across varying printing environments and material systems. For instance, CNN-based real-time monitoring system was integrated to progressively improve autonomous extrusion control of flow rate under increasingly complex printing conditions [221].

Taken together, these studies demonstrate that ML-derived outputs, ranging from discrete defect classifications to continuous anomaly scores and predicted geometric features which can be effectively integrated into both feedback and feedforward control strategies. This capability represents a critical step toward adaptive and autonomous bioprinting systems, where process stability is maintained through continuous sensing, learning, and real-time parameter optimization.

### 4.2.2. From reactive monitoring to predictive control

Conventional closed-loop control systems primarily operate in a reactive manner, correcting deviations only after they are detected. In contrast, ML-enhanced SHM enables predictive control by identifying early "pre-defect" signatures in monitoring data, allowing intervention before defects become fully developed in the printed structure.

Early work in this direction demonstrated that image-based deep learning models can capture subtle spatial features associated with emerging process instabilities. Patch-level classification using convolutional neural networks has been shown to identify deviations in filament continuity, regularity, and uniformity at an early stage of formation [123]. Extending this concept to temporal data, spatiotemporal models such as ConvLSTM autoencoders provide continuous anomaly signals that evolve with process conditions, enabling detection of gradual drift rather than discrete failure events [147]. Overall, these approaches establish that both spatial and temporal features extracted from imaging data can serve as early indicators of instability, supporting predictive intervention during printing.

Beyond in situ monitoring, a complementary class of methods uses machine learning as a predictive tool to estimate printability and optimal process conditions prior to fabrication. Rather than relying solely on empirical parameter tuning, physically informed models incorporating rheological and mechanical properties have been developed to predict printing resolution across different bioinks [222]. By embedding material descriptors such as viscosity and storage modulus into the learning framework, these models improve generalizability and enable reliable extrapolation to previously unseen material systems. Predictive control has also been advanced through data-efficient optimization strategies. Bayesian optimization frameworks, for example, have been used to explore high-dimensional process parameter spaces with a

limited number of experiments, identifying near-optimal printing conditions based on morphology-driven objective functions [214]. Similarly, lightweight machine learning models trained on sparse datasets have been shown to generate probabilistic process maps that define stable printing regions and suggest compensatory parameter adjustments under varying conditions [223].

While these studies primarily focused on identifying stable printing regions and optimizing process windows, more recent efforts have expanded predictive control to directly estimate geometric fidelity and scaffold quality from process variables and structural measurements using supervised learning algorithms, including support vector machines, Gaussian process regression, ensemble learning, and transfer learning. For instance, an open-loop extrusion control framework was developed in which logistic regression was first used to eliminate defective parameter combinations associated with discontinuous filaments and unstable extrusion, while a support vector machine model subsequently predicted target filament geometry based on process variables [134]. Similarly, transfer learning frameworks coupled with Gaussian process regression have been employed to reduce the experimental burden associated with retraining models for new bioinks, enabling the prediction of optimal pressure and printing-speed combinations using only limited target-material datasets [117]. More generalized predictive frameworks have also been developed to estimate scaffold printability across diverse biomaterial systems. Large-scale ensemble learning studies incorporating XGBoost, LightGBM, and Extra Trees models have been applied to correlate process parameters such as extrusion pressure, nozzle speed, temperature, and biomaterial composition with scaffold-quality and printability metrics [215]. Unlike localized defect-detection frameworks focused on filament-level anomalies, this approach emphasized global process-quality prediction across various printing conditions, demonstrating the potential of ensemble learning for identifying robust operating windows and stable fabrication conditions. In parallel, ML models have been combined with optimization techniques to directly target biological outcomes, such as maximizing cell viability through inverse prediction of crosslinking and process parameters [216].

At a higher level, these predictive models are increasingly integrated into digital twin frameworks, where virtual representations of the bioprinting process are continuously updated using experimental and in situ data [224]. Within such systems, ML models link process parameters, material properties, and monitoring signals to predicted structural and biological outcomes, enabling silico exploration of process evolution and evaluation of corrective strategies before physical implementation. This predictive simulation integration is conceptually illustrated in Figure 44, where real-time monitoring data, machine learning inference, and virtual process models are coupled within a digital twin framework to enable in silico prediction and optimization prior to physical fabrication.

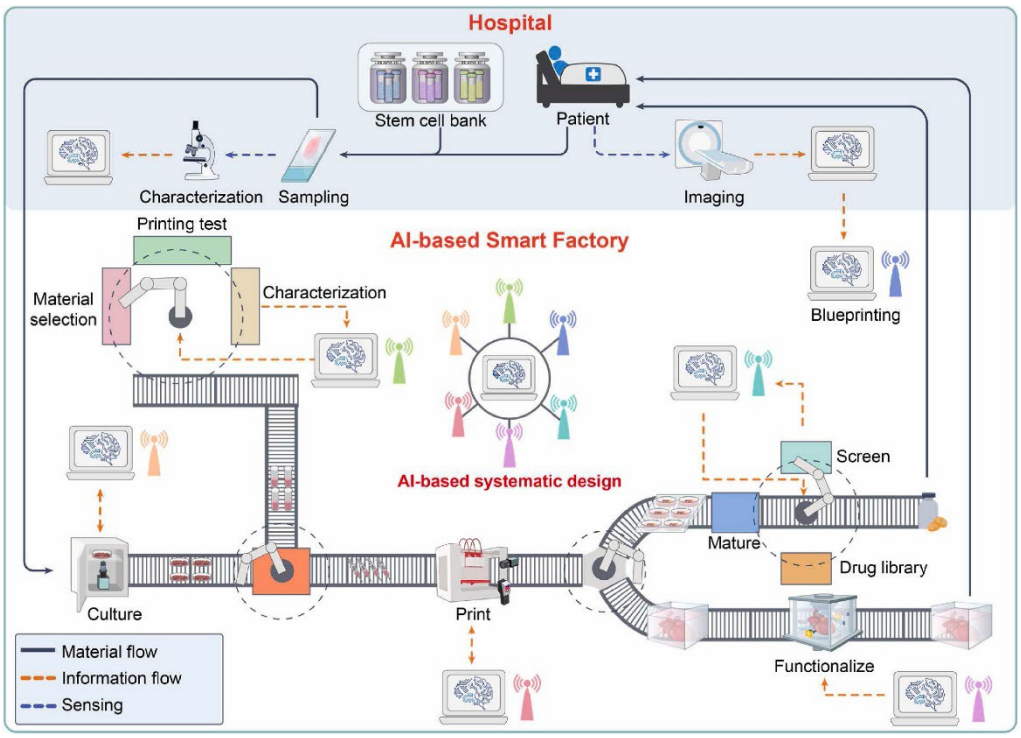


**Figure 34. AI-driven digital twin framework for predictive and autonomous bioprinting [225]**

Collectively, these developments demonstrate a clear transition from reactive monitoring toward predictive process management. By combining early-stage anomaly detection with physics-informed modeling, data-efficient optimization, and digital twin integration, ML enables proactive adjustment of process parameters. This shift reduces defect accumulation, minimizes material waste, and constrains the process space to conditions more likely to yield structurally and biologically viable constructs.

### 4.2.3. Toward autonomous biofabrication systems

The convergence of ML-based monitoring, predictive modeling, adaptive control, and digital twin frameworks is driving the development of fully autonomous biofabrication systems. In conventional bioprinting workflows, process quality depends heavily on operator expertise, manual parameter tuning, and post hoc inspection. AI-driven SHM aims to reduce this dependency by enabling self-correcting systems that learn from data and adapt in real time.

Recent studies have emphasized the integration of machine learning across the entire bioprinting pipeline, spanning pre-print parameter optimization, in situ monitoring, and post-print evaluation of structural and biological outcomes [41]. Within this paradigm, quality control is no longer treated as a single-stage task but as a continuous, data-driven process encompassing pre-process optimization, in-process monitoring, and post-process assessment [226]. To address the persistent challenge of limited

experimental data, these frameworks increasingly incorporate simulation-based datasets, synthetic data augmentation, and knowledge extracted from prior studies.

At the system level, the integration of monitoring and control has enabled the development of closed loop bioprinting platforms capable of autonomous regulation. These systems combine real-time sensor feedback, computer vision, and ML inference to dynamically adjust process parameters [220]. While such approaches demonstrate significant potential for improving print fidelity and consistency, challenges remain in ensuring model generalizability across materials and processes, establishing standardized datasets, and meeting regulatory requirements for clinical translation. Beyond process-level autonomy, broader considerations are emerging as critical for real-world deployment. The need for explainable AI, privacy-preserving learning strategies, and standardized data infrastructures has been highlighted as essential for building trust among clinicians and regulatory bodies [227]. Approaches such as federated learning enable collaborative model development across distributed datasets without requiring direct data sharing, addressing privacy concerns in biomedical applications [228]. In parallel, the adoption of FAIR (Findable, Accessible, Interoperable, and Reusable) data principles is increasingly recognized as important for improving data sharing, interoperability, and reproducibility across biomedical and bioprinting research platforms.

Overall, these advances indicate a gradual transition from parameter-driven, operator-dependent bioprinting toward adaptive and autonomous biofabrication systems. In this emerging paradigm, SHM evolves from a passive quality assurance tool into an active and intelligent component of the manufacturing process. By tightly coupling multimodal sensing, machine learning inference, predictive modeling, and adaptive control, future bioprinting platforms are expected to achieve higher reliability, reduce material waste, and improved reproducibility, ultimately accelerating the clinical translation of biofabricated tissues and organs.

### 4.3. Overview of machine learning approaches in 3D bioprinting

Machine learning-assisted structural health monitoring in bioprinting encompasses a broad range of data-driven frameworks designed to detect defects, quantify print quality, predict process outcomes, and support adaptive process control. The approaches discussed in Sections 4.1 and 4.2 operate across multiple monitoring methods and control strategies. They are directed toward challenges associated with extrusion instability, geometric inconsistency, material heterogeneity, and process variability during bioprinting. Image-based monitoring remains the most extensively explored ML-integrated SHM approach, where convolutional neural networks, liquid neural networks, transformer architectures, and segmentation-based frameworks are utilized to identify filament discontinuities, under- and over-extrusions, geometric

deviations, and structural similarities from in situ images. These systems increasingly extend beyond simple defect classification toward quantitative geometric assessment through segmentation, feature extraction, and shape-fidelity evaluation using metrics such as Hausdorff distance. Complementing image-based methods, video-based monitoring incorporates temporal information to detect dynamic process instabilities and extrusion deviation through spatiotemporal learning architectures such as ConvLSTM autoencoders and CNN-based classification frameworks.

Beyond defect identification, machine learning is increasingly integrated with process monitoring and control frameworks to enable adaptive and predictive bioprinting. Closed-loop systems combine monitoring data with real-time parameter adjustment, allowing process variables such as extrusion multiplier, flow rate, printing speed, and deposition conditions to be dynamically regulated in response to predicted defects. More recent predictive-control frameworks extend this capability by estimating printability, filament geometry, scaffold quality, and biological outcomes prior to fabrication using rheology-informed learning, Bayesian optimization, transfer learning, ensemble learning, and digital twin integration. These predictive approaches utilize process variables including extrusion pressure, nozzle speed, temperature, bioink concentration, viscosity, and storage modulus to identify stable operating windows and optimize printing performance across different biomaterial systems. At a broader level, autonomous biofabrication frameworks further integrate monitoring, prediction, and adaptive control into unified data-driven systems capable of continuous process regulation and decision-making.

Collectively, these developments demonstrate a clear transition of ML-assisted SHM from passive defect observation toward intelligent and autonomous process management in bioprinting. Different ML frameworks target complementary objectives, ranging from local filament-level anomaly detection and geometric fidelity assessment to global process optimization, predictive quality evaluation, and adaptive process regulation. Table 4 summarizes the major monitoring methods and ML algorithms reported for structural health monitoring, defect detection, process assessment, and adaptive control in bioprinting.

**Table 4. Summary of machine learning techniques and associated sensing modalities for structural health monitoring in bioprinting**

| **Monitoring method** | **Machine learning algorithm used** | **Reference** |
|---|---|---|
| Image | CNN, Bayesian regression head | [123, 207, 217, 228, 229] |
| | SVM, Logistic Regression | [134] |
| | Liquid neural network | [205] |

| Monitoring method | Machine learning algorithm used | Reference |
|---|---|---|
| | CNN (VGG-16), transfer learning, Curriculum Learning | [221] |
| | Segment anything model | [218] |
| | SVM, Logistic Regression | [134] |
| | Vision transformer | [204] |
| Process parameter | Bayesian Optimization | [214] |
| | SVM | [223] |
| | Gaussian Process regression, Transfer learning | [117] |
| | Support Vector Regression (SVR), Multi-Layer Perceptron (MLP), Segment Anything Model 2 (SAM2), CNN (regression model) | [206] |
| Video | LSTM autoencoder | [147] |
| | CNN | [128] |
| Thermal data | KNN, Random Forest | [27] |
| Rheology/printing process | Rheology-Informed Hierarchical Machine Learning | [222] |
| Printing parameter | Tree-based ensemble machine learning models specifically XGBoost, LightGBM, and Extra Trees | [230] |

## 5. Beyond structure: The interplay between structural and cellular quality

While this review primarily highlights the structural defects in 3D bioprinting, structural and cellular qualities in 3D bioprinting are inseparable in practice. The parameters that govern geometric fidelity, such as nozzle geometry, extrusion pressure, and bioink rheology, simultaneously determine the limits of cell viability, which is the ultimate outcome of a biofabrication process. This section briefly evaluates cellular-level defects and current monitoring strategies while identifying the research gaps that persist in the field.

### 5.1. Cellular defects in bioprinting

A growing body of evidence demonstrates that printability-related structural parameters, including rheological properties of bioink, scaffold/pore geometry, and process parameters such as nozzle geometry, extrusion pressure, and tip size, directly govern the cellular microenvironment and, consequently, cell fate. The rheological properties that enable stable bioink formation may contribute to the mechanical stress transmitted to the encapsulated cells. For instance, higher alginate concentration improves shape fidelity and mechanical integrity, and on the other hand, it may reduce cell viability due to the stress developed [69]. Furthermore, the relationship between scaffold/pore geometry and cell viability is well-documented, as is the subsequent influence of cells, in turn, on the mechanical properties of the bioconstructs [231, 232]. In addition to that, process parameters may affect structural and cellular outcomes simultaneously. Nozzle geometry, pressure, and tip size are the primary factors of shear stress development within the nozzle [53, 92, 106], which directly correlates with an elevated dead-to-live cell ratio. A relationship between shear exposure and cell damage has been demonstrated, with effects depending on both the magnitude and duration of stress [233, 234], along with additional contributions from thermal and radiative sources [71, 72]. Extrusion pressure has been identified as a more critical determinant of cell damage compared to nozzle diameter [70]. Furthermore, stress at the channel center, often neglected relative to wall shear, was shown to make an independent contribution [235]. Moreover, efforts to improve cell distribution through aggressive mixing damage the very cells being distributed [94], and the small nozzle tips that enhance print resolution simultaneously intensify shear stress and promote clogging [51]. These coupled trade-offs indicate that optimizing structural quality without monitoring cellular outcomes risks producing geometrically accurate but biologically compromised constructs.

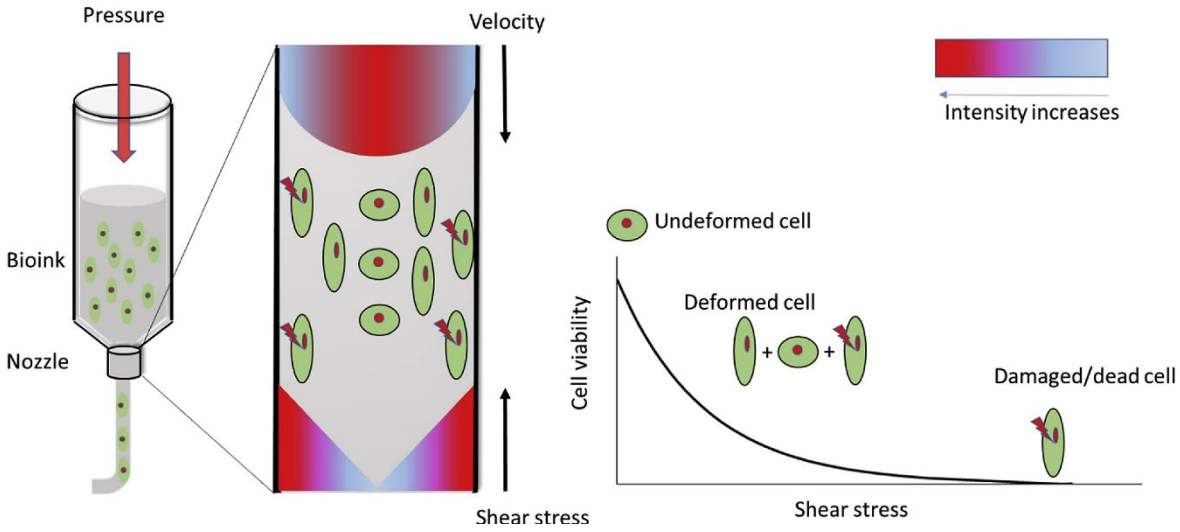


**Figure 35. Effect of shear stress on cell viability [236]**

### 5.2. Monitoring approaches for cellular quality

Efforts to monitor cellular quality have progressed from post-fabrication optical inspection toward inline, multi-physics sensing. An image-based approach was introduced to monitor the cell distribution at in situ condition using high-speed camera [203, 237]. This approach offers determining the number of cells in the droplet, which will enable assessing the performance of the bioprinting process. Fluorescence and confocal microscopy established the baseline–confirming stress-viability relationships in printed constructs [48, 132]. On the other hand, their dependence on optical transparency limited applicability to opaque bioinks. Near-infrared imaging and layer-resolved digital microscopy extended optical monitoring closer to in situ conditions [209, 210, 238], yet still required process interruptions or label preparation. Acoustic and tomographic methods broke through the opacity barrier: OCT tracked hydrogel deformation in real time [167], and spectral ultrasound, combined with machine learning, detected shifts in cellular composition within implanted scaffolds [212]. Acoustic fields also proved useful in the opposite direction, by not just sensing but actively improving cell distribution and reducing clogging during printing [51, 211]. Additionally, dielectric impedance spectroscopy brought these threads together most directly, exploiting the capacitive behavior of cell membranes to produce viability signatures in dense, opaque hydrogels and linking impedance changes to the same pressure- and temperature-induced damage mechanisms identified in process studies [195, 196]. The subsequent integration of DIS into a nozzle-embedded sensor enabled real-time, inline cell monitoring during extrusion [197], representing the closest realization to date of truly in-process cellular quality assurance. For a more detailed discussion, the reader is referred to [231, 239].

## 6. Open challenges and research gaps

Structural and cellular monitoring have advanced substantially, yet several critical bottlenecks remain that hinder the transition of bioprinting from a research tool to a clinically viable manufacturing platform.

At the technical level, structural and biological assessments continue to operate as largely independent domains: no platform yet integrates real-time geometric fidelity monitoring with concurrent cell viability feedback into a unified quality control framework. It is well established that the cell viability of bioprinted constructs is heavily influenced by the mechanical properties and structural fidelity of the bioconstructs [236, 240]. However, current stress-viability models, which describe how mechanical stress affects cell viability to estimate biological damage based on printing process [241] and configuration [242], have been validated only for limited combinations of bioink formulations and cell types, and generalizing them across the diversity of clinical and industrial applications requires physics-informed, adaptive approaches that remain be further developed. Compounding this, the integration of inline sensors without compromising sterility or print fidelity remains an unsolved engineering challenge, and the absence of standardized

performance benchmarks for cellular monitoring–analogous to geometric tolerances in additive manufacturing–prevents meaningful comparison across platforms and slows translation toward reliable and scalable bioprinting quality assurance.

These technical limitations are further amplified by an immature regulatory and standardization landscape. Unlike conventional medical devices or logistics, bioprinted samples contain living cells, which make the standardization and regulatory work challenging [243]. Ethical considerations surrounding data privacy from embedded sensors and machine learning decision-making also warrant regulatory attention. However, the existing regulation framework, which was designed for 3D printed medical devices and non-living samples, struggles to accommodate patient-specific and process-dependent bioprinting technologies, thus creating a regulatory vacuum surrounding 3D bioprinting [244]. Without agreed-upon metrics for acceptable structural or cellular deviation, the role of SHM in regulatory compliance remains ambiguous. Classification ambiguities persist at the global level as well. For example, in the European Union, bioprinted tissues with living cells are regulated as combined advanced therapy medicinal products. On the other hand, the U.S. FDA evaluates bioprinted samples under biologics, devices, or combination product pathways, depending on the mechanism action [245]. Similarly, the existing standards, such as GMP, ISO 13485, and ICH guidelines, were developed for centralized manufacturing and do not fully address decentralized or point-of-care bioprinting contexts [246].

Addressing these gaps will require coordinated progress on multiple fronts. Technically, future efforts should prioritize multimodal sensor fusion that bridges structural and biological monitoring, as well as the development of generalizable, data-efficient models capable of operating across diverse bioink–cell–printer combinations. From a regulatory perspective, the field requires process-centric frameworks that incorporate SHM into formal assessments [243]. These need to be supported by interoperable data formats, validation criteria, and biocompatibility standards tailored for sensor-integrated constructs. Sustained cross-disciplinary collaboration among biologists, engineers, clinicians, and regulators remains essential to establish a quality assurance framework that keeps pace with rapid technical innovation while ensuring safety and accountability.

## 7. Conclusion

3D bioprinting stands at the forefront of regenerative medicine and tissue engineering. It offers the unprecedented ability to fabricate complex, cell-laden structures that can replicate human tissues and organs. However, its successful clinical and commercial translation depends on ensuring structural integrity, mechanical stability, and biological functionality. These objectives are often compromised by printing-related defects and inconsistencies. This review has comprehensively explored the structural health

monitoring landscape for bioprinting, highlighting a range of imaging-based, ultrasound, and simulation-driven techniques that enable defect detection and quality control of bioconstructs. The integration of optical coherence tomography, infrared thermography, and ultrasound imaging provides versatile tools for assessing both surface and internal architecture during or after fabrication. An equally important development is the increasing use of machine learning and artificial intelligence to enhance printing anomaly detection and control, turning it from a passive observation method into an intelligent and autonomous part of the bioprinting process. From supervised classification of defects to deep learning-based quality control loops and reinforcement learning for adaptive printing, AI is rapidly enhancing the precision and scalability of the bioprinting process. Despite these advancements, significant challenges remain. The field must overcome several issues related to the consistency of the bioink, printer reliability, regulatory uncertainties, and lack of standardization. Multimodal SHM systems, which integrate feedback from various sensors, along with real-time biological modeling and simulation, will be crucial in pushing bioprinting toward clinical maturity. The development of autonomous, feedback-controlled bioprinting systems that can detect and correct errors in real time will represent a major advancement in tissue engineering. Achieving this goal will require interdisciplinary collaboration among experts in materials science, bioengineering, computer science, and regulatory fields. In conclusion, integrating intelligent monitoring systems with advanced fabrication strategies, the future of bioprinting promises not only enhanced quality of the bioconstructs but also improved reproducibility, safety, and viability. This will bring us closer to the goal of producing functional, implantable tissues and organs on demand.

## 8. Conflict of Interest

The authors declare no competing interests.

## 9. Acknowledgements

This research is supported by the National Science Foundation under Award No. 2301948 and by the faculty research seed grant from the College of Engineering and Computing at Georgia Southern University.

## 10. References


[1] World Health Organization, “Global Observatory on Donation and Transplantation.”

[2] “National Data - Organ Procurement and Transplantation Network.”

[3] Health Resources & Services Administration, “Organ Donation Statistics.”

[4] Derby, B., 2012, “Printing and Prototyping of Tissues and Scaffolds,” Science, **338**(6109), pp. 921–926.

[5] Ng, W. L., and Bartolo, P., 2026, “3D Bioprinting of Tissues and Organs for Systemic Diseases and Localized Injuries,” Military Medical Research, **13**(1), p. 100006.

[6] Chameettachal, S., Yeleswarapu, S., Sasikumar, S., Shukla, P., Hibare, P., Bera, A. K., Bojedla, S. S. R., and Pati, F., 2019, “3D Bioprinting: Recent Trends and Challenges,” J Indian Inst Sci, **99**(3), pp. 375–403.

[7] Jergitsch, M., and Mateos-Timoneda, M. A., 2026, “3D Extrusion Bioprinting: Rational Bioink Design and Advanced Fabrication Techniques,” Trends in Biotechnology, **44**(2), pp. 378–388.

[8] Ng, W. L., and Shkolnikov, V., 2024, “Jetting-Based Bioprinting: Process, Dispense Physics, and Applications,” Bio-design and manufacturing, **7**(5), pp. 771–799.

[9] Ng, W. L., Paula, C. T., Serra, A. C., Coelho, J. F., and Bartolo, P., 2026, “Vat Photopolymerization-based Bioprinting: Shaping Next-generation Tissues with Light,” Interdisciplinary Medicine, **4**(1), p. e70078.

[10] Atala, A., Bauer, S. B., Soker, S., Yoo, J. J., and Retik, A. B., 2006, “Tissue-Engineered Autologous Bladders for Patients Needing Cystoplasty,” The Lancet, **367**(9518), pp. 1241–1246.

[11] Mirdamadi, E., Tashman, J. W., Shiwarski, D. J., Palchesko, R. N., and Feinberg, A. W., 2020, “FRESH 3D Bioprinting a Full-Size Model of the Human Heart,” ACS Biomater. Sci. Eng., **6**(11), pp. 6453–6459.

[12] Kim, M., Kim, Y. J., Kim, Y. S., Roh, T. S., Lee, E.-J., Shim, J.-H., Kang, E. H., Kim, M. J., and Yun, I. S., 2024, “One-Year Results of Ear Reconstruction with 3D Printed Implants,” Yonsei Med J, **65**(8), p. 456.

[13] Mannoor, M. S., Jiang, Z., James, T., Kong, Y. L., Malatesta, K. A., Soboyejo, W. O., Verma, N., Gracias, D. H., and McAlpine, M. C., 2013, “3D Printed Bionic Ears,” Nano Lett., **13**(6), pp. 2634–2639.

[14] Nguyen, D. G., Funk, J., Robbins, J. B., Crogan-Grundy, C., Presnell, S. C., Singer, T., and Roth, A. B., 2016, “Bioprinted 3D Primary Liver Tissues Allow Assessment of Organ-Level Response to Clinical Drug Induced Toxicity In Vitro,” PLOS ONE, **11**(7), p. e0158674.

[15] Weng, T., Zhang, W., Xia, Y., Wu, P., Yang, M., Jin, R., Xia, S., Wang, J., You, C., Han, C., and Wang, X., 2021, “3D Bioprinting for Skin Tissue Engineering: Current Status and Perspectives,” J Tissue Eng, **12**, p. 20417314211028574.

[16] Wang, X., Zhang, X., Dai, X., Wang, X., Li, X., Diao, J., and Xu, T., 2018, “Tumor-like Lung Cancer Model Based on 3D Bioprinting,” 3 Biotech, **8**(12), p. 501.

[17] Hakobyan, D., Médina, C., Dusserre, N., Stachowicz, M.-L., Handschin, C., Fricain, J.-C., Guillermet-Guibert, J., and Oliveira, H., 2020, “Laser-Assisted 3D Bioprinting of Exocrine Pancreas Spheroid Models for Cancer Initiation Study,” Biofabrication, **12**(3), p. 035001.

[18] Arjoca, S., Robu, A., Neagu, M., and Neagu, A., 2023, "Mathematical and Computational Models in Spheroid-Based Biofabrication," Acta Biomaterialia, **165**, pp. 125–139.

[19] Welman, T., Michel, S., Segaren, N., and Shanmugarajah, K., 2015, "Bioengineering for Organ Transplantation: Progress and Challenges," Bioengineered, **6**(5), pp. 257–261.

[20] Zoghi, S., 2024, "Advancements in Tissue Engineering: A Review of Bioprinting Techniques, Scaffolds, and Bioinks," Biomed Eng Comput Biol, **15**, p. 11795972241288099.

[21] Arslan-Yildiz, A., Assal, R. E., Chen, P., Guven, S., Inci, F., and Demirci, U., 2016, "Towards Artificial Tissue Models: Past, Present, and Future of 3D Bioprinting," Biofabrication, **8**(1), p. 014103.

[22] Yang, S., Chen, Q., Wang, L., and Xu, M., 2022, "In Situ Defect Detection and Feedback Control with Three-Dimensional Extrusion-Based Bioprinter-Associated Optical Coherence Tomography," IJB, **9**(1), p. 624.

[23] Ricci, G., Gibelli, F., and Sirignano, A., 2023, "Three-Dimensional Bioprinting of Human Organs and Tissues: Bioethical and Medico-Legal Implications Examined through a Scoping Review," Bioengineering, **10**(9), p. 1052.

[24] Gillispie, G. J., Han, A., Uzun-Per, M., Fisher, J., Mikos, A. G., Niazi, M. K. K., Yoo, J. J., Lee, S. J., and Atala, A., 2020, "The Influence of Printing Parameters and Cell Density on Bioink Printing Outcomes," Tissue Engineering Part A, **26**(23–24), pp. 1349–1358.

[25] Melchels, F. P. W., Barradas, A. M. C., van Blitterswijk, C. A., de Boer, J., Feijen, J., and Grijpma, D. W., 2010, "Effects of the Architecture of Tissue Engineering Scaffolds on Cell Seeding and Culturing," Acta Biomaterialia, **6**(11), pp. 4208–4217.

[26] Van Bael, S., Chai, Y. C., Truscello, S., Moesen, M., Kerckhofs, G., Van Oosterwyck, H., Kruth, J.-P., and Schrooten, J., 2012, "The Effect of Pore Geometry on the in Vitro Biological Behavior of Human Periosteum-Derived Cells Seeded on Selective Laser-Melted Ti6Al4V Bone Scaffolds," Acta Biomaterialia, **8**(7), pp. 2824–2834.

[27] Gerdes, S., Gaikwad, A., Ramesh, S., Rivero, I. V., Tamayol, A., and Rao, P., 2024, "Monitoring and Control of Biological Additive Manufacturing Using Machine Learning," J Intell Manuf, **35**(3), pp. 1055–1077.

[28] Gomes Gama, J. F., Dias, E. A., Aguiar Coelho, R. M. G., Chagas, A. M., Aguiar Coelho Nt, J., and Alves, L. A., 2023, "Development and Implementation of a Significantly Low-Cost 3D Bioprinter Using Recycled Scrap Material," Front. Bioeng. Biotechnol., **11**, p. 1108396.

[29] Zhang, X., and Zhang, Y., 2015, "Tissue Engineering Applications of Three-Dimensional Bioprinting," Cell Biochem Biophys, **72**(3), pp. 777–782.

[30] Sun, W., Starly, B., Daly, A. C., Burdick, J. A., Groll, J., Skeldon, G., Shu, W., Sakai, Y., Shinohara, M., Nishikawa, M., Jang, J., Cho, D.-W., Nie, M., Takeuchi, S., Ostrovidov, S., Khademhosseini, A., Kamm, R. D., Mironov, V., Moroni, L., and Ozbolat, I. T., 2020, "The Bioprinting Roadmap," Biofabrication, **12**(2), p. 022002.

[31] Zoghi, S., 2024, "Advancements in Tissue Engineering: A Review of Bioprinting Techniques, Scaffolds, and Bioinks," Biomed Eng Comput Biol, **15**, p. 11795972241288099.

[32] Gogoi, D., Kumar, M., and Singh, J., 2024, "A Comprehensive Review on Hydrogel-Based Bio-Ink Development for Tissue Engineering Scaffolds Using 3D Printing," Annals of 3D Printed Medicine, **15**, p. 100159.

[33] Gungor-Ozkerim, P. S., Inci, I., Zhang, Y. S., Khademhosseini, A., and Dokmeci, M. R., 2018, "Bioinks for 3D Bioprinting: An Overview," Biomater. Sci., **6**(5), pp. 915–946.

[34] Lee, V., Singh, G., Trasatti, J. P., Bjornsson, C., Xu, X., Tran, T. N., Yoo, S.-S., Dai, G., and Karande, P., 2014, "Design and Fabrication of Human Skin by Three-Dimensional Bioprinting," Tissue Engineering Part C: Methods, **20**(6), pp. 473–484.

[35] Weng, T., Zhang, W., Xia, Y., Wu, P., Yang, M., Jin, R., Xia, S., Wang, J., You, C., Han, C., and Wang, X., 2021, "3D Bioprinting for Skin Tissue Engineering: Current Status and Perspectives," J Tissue Eng, **12**, p. 20417314211028574.

[36] Isaacson, A., Swioklo, S., and Connon, C. J., 2018, "3D Bioprinting of a Corneal Stroma Equivalent," Experimental Eye Research, **173**, pp. 188–193.

[37] Jia, S., Bu, Y., Lau, D.-S. A., Lin, Z., Sun, T., Lu, W. W., Lu, S., Ruan, C., and Chan, C.-H. J., 2023, "Advances in 3D Bioprinting Technology for Functional Corneal Reconstruction and Regeneration," Front. Bioeng. Biotechnol., **10**.

[38] Zheng, X., Huang, J., Lin, J., Yang, D., Xu, T., Chen, D., Zan, X., and Wu, A., 2019, "3D Bioprinting in Orthopedics Translational Research," Journal of Biomaterials Science, Polymer Edition, **30**(13), pp. 1172–1187.

[39] Chae, S., and Cho, D.-W., 2023, "Biomaterial-Based 3D Bioprinting Strategy for Orthopedic Tissue Engineering," Acta Biomaterialia, **156**, pp. 4–20.

[40] Ricci, G., Gibelli, F., and Sirignano, A., 2023, "Three-Dimensional Bioprinting of Human Organs and Tissues: Bioethical and Medico-Legal Implications Examined through a Scoping Review," Bioengineering (Basel), **10**(9), p. 1052.

[41] Ramesh, S., Deep, A., Tamayol, A., Kamaraj, A., Mahajan, C., and Madihally, S., 2024, "Advancing 3D Bioprinting through Machine Learning and Artificial Intelligence," Bioprinting, **38**, p. e00331.

[42] Chen, H., Zhang, B., and Huang, J., 2024, "Recent Advances and Applications of Artificial Intelligence in 3D Bioprinting," Biophysics Rev., **5**(3), p. 031301.

[43] Robazzi, J. V. S., Derman, I. D., Gupta, D., Haugh, L., Singh, Y. P., Pal, V., Yilmaz, Y. O., Liu, S., Dias, A. L., and Flauzino, R. A., 2026, "The Synergy of Artificial Intelligence and 3D Bioprinting: Unlocking New Frontiers in Precision and Tissue Fabrication," Advanced Functional Materials, **36**(1), p. e09530.

[44] Yu, K., Yao, Y., Zhang, W., Lu, L., Gao, Q., Zhang, P., and Sing, S. L., 2025, "Defects, Monitoring, and AI-Enabled Control in Soft Material Additive Manufacturing: A Review," Virtual and Physical Prototyping, **20**(1), p. e2588456.

[45] Matavosian, A. A., and Bonassar, L. J., 2025, "Reimagining Bioprinters: Real-Time Monitoring for Quality Control of Bioprinted Constructs and Future Vision," Biofabrication, **17**(4), p. 042008.

[46] Murphy, S. V., and Atala, A., 2014, "3D Bioprinting of Tissues and Organs," Nature biotechnology, **32**(8), pp. 773–785.

[47] Hölzl, K., Lin, S., Tytgat, L., Van Vlierberghe, S., Gu, L., and Ovsianikov, A., 2016, "Bioink Properties before, during and after 3D Bioprinting," Biofabrication, **8**(3), p. 032002.

[48] Ouyang, L., Yao, R., Zhao, Y., and Sun, W., 2016, "Effect of Bioink Properties on Printability and Cell Viability for 3D Bioplotting of Embryonic Stem Cells," Biofabrication, **8**(3), p. 035020.

[49] Wenger, L., Radtke, C. P., Gerisch, E., Kollmann, M., Niemeyer, C. M., Rabe, K. S., and Hubbuch, J., 2022, "Systematic Evaluation of Agarose-and Agar-Based Bioinks for Extrusion-Based Bioprinting of Enzymatically Active Hydrogels," Frontiers in Bioengineering and Biotechnology, **10**, p. 928878.

[50] Manzoli, S., Merotto, E., Piccoli, M., Gobbo, P., Todros, S., and Pavan, P. G., 2025, "An Overview of 3D Bioprinting Impact on Cell Viability: From Damage Assessment to Protection Solutions," Journal of Functional Biomaterials, **16**(12), p. 436.

[51] Sriphutkiat, Y., Kasetsirikul, S., Ketpun, D., and Zhou, Y., 2019, "Cell Alignment and Accumulation Using Acoustic Nozzle for Bioprinting," Scientific Reports, **9**(1), p. 17774.

[52] Therriault, D., White, S. R., and Lewis, J. A., 2007, "Rheological Behavior of Fugitive Organic Inks for Direct-Write Assembly," Applied Rheology, **17**(1), pp. 10112–10121.

[53] Billiet, T., Gevaert, E., De Schryver, T., Cornelissen, M., and Dubruel, P., 2014, "The 3D Printing of Gelatin Methacrylamide Cell-Laden Tissue-Engineered Constructs with High Cell Viability," Biomaterials, **35**(1), pp. 49–62.

[54] Mouser, V. H., Melchels, F. P., Visser, J., Dhert, W. J., Gawlitta, D., and Malda, J., 2016, "Yield Stress Determines Bioprintability of Hydrogels Based on Gelatin-Methacryloyl and Gellan Gum for Cartilage Bioprinting," Biofabrication, **8**(3), p. 035003.

[55] Gao, T., Gillispie, G. J., Copus, J. S., Pr, A. K., Seol, Y.-J., Atala, A., Yoo, J. J., and Lee, S. J., 2018, "Optimization of Gelatin–Alginate Composite Bioink Printability Using Rheological Parameters: A Systematic Approach," Biofabrication, **10**(3), p. 034106.

[56] Gillispie, G., Prim, P., Copus, J., Fisher, J., Mikos, A. G., Yoo, J. J., Atala, A., and Lee, S. J., 2020, "Assessment Methodologies for Extrusion-Based Bioink Printability," Biofabrication, **12**(2), p. 022003.

[57] Liu, J., Shahriar, M., Xu, H., and Xu, C., 2022, "Cell-Laden Bioink Circulation-Assisted Inkjet-Based Bioprinting to Mitigate Cell Sedimentation and Aggregation," Biofabrication, **14**(4), p. 045020.

[58] Ahmadi Soufivand, A., Faber, J., Hinrichsen, J., and Budday, S., 2023, "Multilayer 3D Bioprinting and Complex Mechanical Properties of Alginate-Gelatin Mesostructures," Scientific Reports, **13**(1), p. 11253.

[59] Lamberger, Z., Schubert, D. W., Buechner, M., Cabezas, N. C., Schrüfer, S., Murenu, N., Schaefer, N., and Lang, G., 2024, "Advanced Optical Assessment and Modeling of Extrusion Bioprinting," Scientific Reports, **14**(1), p. 13972.

[60] Elango, J., and Zamora-Ledezma, C., 2025, "Rheological, Structural, and Biological Trade-Offs in Bioink Design for 3d Bioprinting," Gels, **11**(8), p. 659.

[61] Holland, I., 2025, "Extrusion Bioprinting: Meeting the Promise of Human Tissue Biofabrication?," Prog. Biomed. Eng., **7**(2), p. 023001.

[62] Sasikumar, S. C., Goswami, U., and Raichur, A. M., 2024, "3D Bioprinting with Visible Light Cross-Linkable Mucin-Hyaluronic Acid Composite Bioink for Lung Tissue Engineering," ACS Applied Bio Materials, **7**(8), pp. 5411–5422.

[63] Wüst, S., Godla, M. E., Müller, R., and Hofmann, S., 2014, "Tunable Hydrogel Composite with Two-Step Processing in Combination with Innovative Hardware Upgrade for Cell-Based Three-Dimensional Bioprinting," Acta biomaterialia, **10**(2), pp. 630–640.

[64] Ribeiro, A., Blokzijl, M. M., Levato, R., Visser, C. W., Castilho, M., Hennink, W. E., Vermonden, T., and Malda, J., 2017, "Assessing Bioink Shape Fidelity to Aid Material Development in 3D Bioprinting," Biofabrication, **10**(1), p. 014102.

[65] Schwab, A., Levato, R., D'este, M., Piluso, S., Eglin, D., and Malda, J., 2020, "Printability and Shape Fidelity of Bioinks in 3D Bioprinting," Chemical reviews, **120**(19), pp. 11028–11055.

[66] Malekpour, A., and Chen, X., 2022, "Printability and Cell Viability in Extrusion-Based Bioprinting from Experimental, Computational, and Machine Learning Views," Journal of Functional Biomaterials, **13**(2), p. 40.

[67] Habib, A., Sathish, V., Mallik, S., Khoda, B., Habib, A., Sathish, V., Mallik, S., and Khoda, B., 2018, "3D Printability of Alginate-Carboxymethyl Cellulose Hydrogel," Materials, **11**(3).

[68] Cooke, M. E., and Rosenzweig, D. H., 2021, "The Rheology of Direct and Suspended Extrusion Bioprinting," APL bioengineering, **5**(1).

[69] Zhang, J., Wehrle, E., Vetsch, J. R., Paul, G. R., Rubert, M., and Müller, R., 2019, "Alginate Dependent Changes of Physical Properties in 3D Bioprinted Cell-Laden Porous Scaffolds Affect Cell Viability and Cell Morphology," Biomed. Mater., **14**(6), p. 065009.

[70] Nair, K., Gandhi, M., Khalil, S., Yan, K. C., Marcolongo, M., Barbee, K., and Sun, W., 2009, "Characterization of Cell Viability during Bioprinting Processes," Biotechnology Journal: Healthcare Nutrition Technology, **4**(8), pp. 1168–1177.

[71] Xu, H.-Q., Liu, J.-C., Zhang, Z.-Y., and Xu, C.-X., 2022, "A Review on Cell Damage, Viability, and Functionality during 3D Bioprinting," Military Medical Research, **9**(1), p. 70.

[72] Manzoli, S., Merotto, E., Piccoli, M., Gobbo, P., Todros, S., and Pavan, P. G., 2025, "An Overview of 3D Bioprinting Impact on Cell Viability: From Damage Assessment to Protection Solutions," Journal of Functional Biomaterials, **16**(12), p. 436.

[73] Huang, G., Zhao, Y., Chen, D., Wei, L., Hu, Z., Li, J., Zhou, X., Yang, B., and Chen, Z., 2024, "Applications, Advancements, and Challenges of 3D Bioprinting in Organ Transplantation."

[74] Cohen, D. L., Lo, W., Tsavaris, A., Peng, D., Lipson, H., and Bonassar, L. J., 2011, "Increased Mixing Improves Hydrogel Homogeneity and Quality of Three-Dimensional Printed Constructs," Tissue Engineering Part C: Methods, **17**(2), pp. 239–248.

[75] Derakhshanfar, S., Mbeleck, R., Xu, K., Zhang, X., Zhong, W., and Xing, M., 2018, "3D Bioprinting for Biomedical Devices and Tissue Engineering: A Review of Recent Trends and Advances," Bioactive materials, **3**(2), pp. 144–156.

[76] Placone, J. K., and Engler, A. J., 2018, "Recent Advances in Extrusion-based 3D Printing for Biomedical Applications," Advanced healthcare materials, **7**(8), p. 1701161.

[77] GhavamiNejad, A., Ashammakhi, N., Wu, X. Y., and Khademhosseini, A., 2020, "Crosslinking Strategies for 3D Bioprinting of Polymeric Hydrogels," Small, **16**(35), p. 2002931.

[78] Paxton, N., Smolan, W., Böck, T., Melchels, F., Groll, J., and Jungst, T., 2017, "Proposal to Assess Printability of Bioinks for Extrusion-Based Bioprinting and Evaluation of Rheological Properties Governing Bioprintability," Biofabrication, **9**(4), p. 044107.

[79] Aliabouzar, M., Ley, A. W. Y., Meurs, S., Putnam, A. J., Baker, B. M., Kripfgans, O. D., Fowlkes, J. B., and Fabiilli, M. L., 2022, "Micropatterning of Acoustic Droplet Vaporization in Acoustically-Responsive Scaffolds Using Extrusion-Based Bioprinting," Bioprinting, **25**, p. e00188.

[80] Rossi, A., Pescara, T., Gambelli, A. M., Gaggia, F., Asthana, A., Perrier, Q., Basta, G., Moretti, M., Senin, N., and Rossi, F., 2024, "Biomaterials for Extrusion-Based Bioprinting and Biomedical Applications," Frontiers in Bioengineering and Biotechnology, **12**, p. 1393641.

[81] Tansell, A. V., Mahmoodi, N., Crolla, J. P., Dyson, R. J., Luo, G. J., and Thomas-Seale, L. E. J., 2025, "Exploiting Nozzle Geometry to Predict Resolution in Extrusion-Based Bioprinting: Mathematical Modelling of a Power-Law Fluid," Royal Society Open Science, **12**(11).

[82] Rastin, H., Ormsby, R. T., Atkins, G. J., and Losic, D., 2020, "3D Bioprinting of Methylcellulose/Gelatin-Methacryloyl (MC/GelMA) Bioink with High Shape Integrity," ACS Applied Bio Materials, **3**(3), pp. 1815–1826.

[83] Hinton, T. J., Jallerat, Q., Palchesko, R. N., Park, J. H., Grodzicki, M. S., Shue, H.-J., Ramadan, M. H., Hudson, A. R., and Feinberg, A. W., 2015, "Three-Dimensional Printing of Complex Biological Structures by Freeform Reversible Embedding of Suspended Hydrogels," Science advances, **1**(9), p. e1500758.

[84] Ma, J., Qi, C., Liu, Z., Meng, S., and Kong, T., 2024, "Instability-Driven 3D Bioprinting for Engineering Composite Bio-Inks," Engineered Regeneration, **5**(3), pp. 350–360.

[85] van der Valk, P. C., and Mirzaali, M. J., 2025, "Non-Planar Additive Manufacturing with Hydrogels: A Review of Flow Control and Toolpath Strategies," npj Soft Matter, **1**(1), p. 5.

[86] Xu, Y., Wang, C., Yang, Y., Liu, H., Xiong, Z., Zhang, T., and Sun, W., 2022, "A Multifunctional 3D Bioprinting System for Construction of Complex Tissue Structure Scaffolds: Design and Application," International Journal of Bioprinting, **8**(4), p. 617.

[87] Iberite, F., Badiola-Mateos, M., Loggini, S., Paci, C., Ruspi, J., Iachetta, D., Mannini, A., Gruppioni, E., and Ricotti, L., 2024, "3D Bioprinting of Thermosensitive Inks Based on Gelatin, Hyaluronic Acid, and Fibrinogen: Reproducibility and Role of Printing Parameters," Bioprinting, **39**, p. e00338.

[88] Abdollahi, A., Malek-Khatabi, A., Razavi, M. S., Sheikhi, M., Abbaspour, K., Rezagholi, Z., Atashi, A., Rahimzadegan, M., Sadeghi, M., and Javar, H. A., 2023, "The Recent Advancement in the Chitosan-Based Thermosensitive Hydrogel for Tissue Regeneration," Journal of Drug Delivery Science and Technology, **86**, p. 104627.

[89] Yu, K., Gao, Q., Lin, Z., Wang, F., Zhang, P., Liu, Y., and Lu, L., 2024, "Investigation of the Temperature Gradient Control in the Printing Space for the Material Extrusion of Medical Biodegradable Hydrogel," Computers in Biology and Medicine, **168**, p. 107722.

[90] Gómez-Blanco, J. C., Mancha-Sánchez, E., Marcos, A. C., Matamoros, M., Díaz-Parralejo, A., and Pagador, J. B., 2020, "Bioink Temperature Influence on Shear Stress, Pressure and Velocity Using Computational Simulation," Processes, **8**(7), p. 865.

[91] Li, Q., Zhang, B., Xue, Q., Zhao, C., Luo, Y., Zhou, H., Ma, L., Yang, H., and Bai, D., 2021, "A Systematic Thermal Analysis for Accurately Predicting the Extrusion Printability of Alginate–Gelatin-Based Hydrogel Bioinks," International Journal of Bioprinting, **7**(3), p. 394.

[92] Townsend, J. M., Beck, E. C., Gehrke, S. H., Berkland, C. J., and Detamore, M. S., 2019, "Flow Behavior Prior to Crosslinking: The Need for Precursor Rheology for Placement of Hydrogels in Medical Applications and for 3D Bioprinting," Progress in polymer science, **91**, pp. 126–140.

[93] Sriphutkiat, Y., Kasetsirikul, S., Ketpun, D., and Zhou, Y., 2019, "Cell Alignment and Accumulation Using Acoustic Nozzle for Bioprinting," Sci Rep, **9**(1), p. 17774.

[94] Kuzucu, M., Vera, G., Beaumont, M., Fischer, S., Wei, P., Shastri, V. P., and Forget, A., 2021, "Extrusion-Based 3D Bioprinting of Gradients of Stiffness, Cell Density, and Immobilized Peptide Using Thermogelling Hydrogels," ACS Biomaterials Science & Engineering, **7**(6), pp. 2192–2197.

[95] Chen, N., Zhu, K., Zhang, Y. S., Yan, S., Pan, T., Abudupataer, M., Yu, G., Alam, M. F., Wang, L., and Sun, X., 2019, "Hydrogel Bioink with Multilayered Interfaces Improves Dispersibility of Encapsulated Cells in Extrusion Bioprinting," ACS applied materials & interfaces, **11**(34), pp. 30585–30595.

[96] Magalhães, I. P., Oliveira, P. M. de, Dernowsek, J., Casas, E. B. L., and Casas, M. S. L., 2019, "Investigation of the Effect of Nozzle Design on Rheological Bioprinting Properties Using Computational Fluid Dynamics," Matéria (Rio de Janeiro), **24**(3), p. e12401.

[97] Armstrong, A. A., Norato, J., Alleyne, A. G., and Wagoner Johnson, A. J., 2019, "Direct Process Feedback in Extrusion-Based 3D Bioprinting," Biofabrication, **12**(1), p. 015017.

[98] Armstrong, A. A., Alleyne, A. G., and Wagoner Johnson, A. J., 2020, "1D and 2D Error Assessment and Correction for Extrusion-Based Bioprinting Using Process Sensing and Control Strategies," Biofabrication, **12**(4), p. 045023.

[99] Lee, A., Hudson, A. R., Shiwarski, D. J., Tashman, J. W., Hinton, T. J., Yerneni, S., Bliley, J. M., Campbell, P. G., and Feinberg, A. W., 2019, "3D Bioprinting of Collagen to Rebuild Components of the Human Heart," Science, **365**(6452), pp. 482–487.

[100] Godau, B., Stefanek, E., Gharaie, S. S., Amereh, M., Pagan, E., Marvdashti, Z., Libert-Scott, E., Ahadian, S., and Akbari, M., 2022, "Non-Destructive Mechanical Assessment for Optimization of 3D Bioprinted Soft Tissue Scaffolds," Iscience, **25**(5).

[101] Jungst, T., Smolan, W., Schacht, K., Scheibel, T., and Groll, J., 2016, "Strategies and Molecular Design Criteria for 3D Printable Hydrogels," Chemical reviews, **116**(3), pp. 1496–1539.

[102] Daskalakis, P., Kanakousaki, E., Ntoulias, C., Peponaki, K., Kavatzikidou, P., Manousaki, A., Vlassopoulos, D., Ranella, A., and Stratakis, E., 2025, "3D Bioprinting with High-Viscosity Bioinks: A Custom-Designed Extrusion Head for High-Resolution Cellulose Acetate Scaffolds," International Journal of Bioprinting, **11**(3), pp. 337–357.

[103] Gerdes, S., Mostafavi, A., Ramesh, S., Memic, A., Rivero, I. V., Rao, P., and Tamayol, A., 2020, "Process–Structure–Quality Relationships of Three-Dimensional Printed Poly (Caprolactone)-Hydroxyapatite Scaffolds," Tissue Engineering Part A, **26**(5–6), pp. 279–291.

[104] Balters, L., and Reichl, S., 2025, "A Design of Experiment to Evaluate the Printability for Bioprinting by Using Deep Learning Image Similarity," Journal of Biomedical Materials Research Part A, **113**(7), p. e37961.

[105] Cai, B., Kilian, D., Ramos Mejia, D., Rios, R. J., Ali, A., and Heilshorn, S. C., 2024, "Diffusion-based 3D Bioprinting Strategies," Advanced Science, **11**(8), p. 2306470.

[106] Chand, R., Muhire, B. S., and Vijayavenkataraman, S., 2022, "Computational Fluid Dynamics Assessment of the Effect of Bioprinting Parameters in Extrusion Bioprinting," International Journal of Bioprinting, **8**(2), p. 545.

[107] Liu, W., Zhang, Y. S., Heinrich, M. A., De Ferrari, F., Jang, H. L., Bakht, S. M., Alvarez, M. M., Yang, J., Li, Y., and Trujillo-de Santiago, G., 2017, "Rapid Continuous Multimaterial Extrusion Bioprinting," Advanced materials, **29**(3), p. 1604630.

[108] Xin, S., Deo, K. A., Dai, J., Pandian, N. K. R., Chimene, D., Moebius, R. M., Jain, A., Han, A., Gaharwar, A. K., and Alge, D. L., 2021, "Generalizing Hydrogel Microparticles into a New Class of Bioinks for Extrusion Bioprinting," Science advances, **7**(42), p. eabk3087.

[109] Talluri, D. J., Nguyen, H. T., Avazmohammadi, R., and Miri, A. K., 2022, "Ink Rheology Regulates Stability of Bioprinted Strands," Journal of Biomechanical Engineering, **144**(7), p. 074503.

[110] Luo, Y., Li, D., Lin, C., Zhou, X., Ma, J., and Zhang, B., 2025, "Three-Dimensional Bioprinting of Gelatin Methacryloyl Hydrogel with a Tri-Layered Vascularized Architecture for Full-Thickness Skin Regeneration," International Journal of Bioprinting, **11**(4), pp. 328–349.

[111] Theus, A. S., Ning, L., Hwang, B., Gil, C., Chen, S., Wombwell, A., Mehta, R., and Serpooshan, V., 2020, "Bioprintability: Physiomechanical and Biological Requirements of Materials for 3D Bioprinting Processes," Polymers, **12**(10), p. 2262.

[112] Soltan, N., Ning, L., Mohabatpour, F., Papagerakis, P., and Chen, X., 2019, "Printability and Cell Viability in Bioprinting Alginate Dialdehyde-Gelatin Scaffolds," ACS Biomater. Sci. Eng., **5**(6), pp. 2976–2987.

[113] Gao, Q., Niu, X., Shao, L., Zhou, L., Lin, Z., Sun, A., Fu, J., Chen, Z., Hu, J., Liu, Y., and He, Y., 2019, "3D Printing of Complex GelMA-Based Scaffolds with Nanoclay," Biofabrication, **11**(3), p. 035006.

[114] Dey, M. K., Ikponmwoba, E., John, P., Belgodere, J. A., Semmes, I., Park, D. S., Monroe, W. T., and Devireddy, R., "Ai Driven Dual-Task Deep Learning Framework for Automated Scaffold Quality Assessment in Extrusion Based 3d Bioprinting," Available at SSRN 5374136.

[115] Strauß, S., Meutelet, R., Radosevic, L., Gretzinger, S., and Hubbuch, J., 2021, "Image Analysis as PAT-Tool for Use in Extrusion-Based Bioprinting," Bioprinting, **21**, p. e00112.

[116] Gugliandolo, S. G., Margarita, A., Santoni, S., Moscatelli, D., and Colosimo, B. M., 2022, "In-Situ Monitoring of Defects in Extrusion-Based Bioprinting Processes Using Visible Light Imaging," Procedia CIRP, **110**, pp. 219–224.

[117] Bracco, F., Zanderigo, G., Paynabar, K., and Colosimo, B., 2025, "Leveraging Transfer Learning for Efficient Bioprinting," Biofabrication, **17**(3), p. 035022.

[118] Liu, C., Liu, J., Yang, C., Tang, Y., Lin, Z., Li, L., Liang, H., Lu, W., and Wang, L., 2022, "Computer Vision-Aided 2D Error Assessment and Correction for Helix Bioprinting," Int J Bioprint, **8**(2), p. 547.

[119] Liu, C., Yang, C., Liu, J., Tang, Y., Lin, Z., Li, L., Liang, H., Lu, W., and Wang, L., 2022, "Error Assessment and Correction for Extrusion-Based Bioprinting Using Computer Vision Method," Int J Bioprint, **9**(1), p. 644.

[120] Barjuei, E. S., Shin, J., Kim, K., and Lee, J., 2024, "Precision Improvement of Robotic Bioprinting via Vision-Based Tool Path Compensation," Sci Rep, **14**(1), p. 17764.

[121] Sergis, V., Kelly, D., Pramanick, A., Britchfield, G., Mason, K., and Daly, A. C., 2025, "In-Situ Quality Monitoring during Embedded Bioprinting Using Integrated Microscopy and Classical Computer Vision," Biofabrication, **17**(2), p. 025004.

[122] Prendergast, M. E., and Burdick, J. A., 2022, "Computational Modeling and Experimental Characterization of Extrusion Printing into Suspension Baths," Advanced Healthcare Materials, **11**(7), p. 2101679.

[123] Jin, Z., Zhang, Z., Shao, X., and Gu, G. X., 2023, "Monitoring Anomalies in 3D Bioprinting with Deep Neural Networks," ACS Biomater. Sci. Eng., **9**(7), pp. 3945–3952.

[124] Zanderigo, G., Afghah, F., Colosimo, B. M., and Raman, R., 2025, "Modular and AI-Driven in Situ Monitoring Platform for Real-Time Process Analysis in Embedded Bioprinting," Device, **3**(11).

[125] Bonatti, A. F., Vozzi, G., and De Maria, C., 2024, "Enhancing Quality Control in Bioprinting through Machine Learning," Biofabrication, **16**(2), p. 022001.

[126] Sun, J., Yao, K., Huang, K., and Huang, D., 2022, "Machine Learning Applications in Scaffold Based Bioprinting," Materials Today: Proceedings, **70**, pp. 17–23.

[127] Liu, C., Wang, L., Lu, W., Liu, J., Yang, C., Fan, C., Li, Q., and Tang, Y., 2022, "Computer Vision-Aided Bioprinting for Bone Research," Bone Res, **10**(1), p. 21.

[128] Bonatti, A. F., Vozzi, G., Chua, C. K., and De Maria, C., 2022, "A Deep Learning Quality Control Loop of the Extrusion-Based Bioprinting Process," International Journal of Bioprinting, **8**(4), p. 620.

[129] Gasperini, L., Maniglio, D., Motta, A., and Migliaresi, C., 2015, "An Electrohydrodynamic Bioprinter for Alginate Hydrogels Containing Living Cells," Tissue Engineering Part C: Methods, **21**(2), pp. 123–132.

[130] He, J., Zhang, B., Li, Z., Mao, M., Li, J., Han, K., and Li, D., 2020, "High-Resolution Electrohydrodynamic Bioprinting: A New Biofabrication Strategy for Biomimetic Micro/Nanoscale Architectures and Living Tissue Constructs," Biofabrication, **12**(4), p. 042002.

[131] Sun, J., Jing, L., Fan, X., Gao, X., and Liang, Y. C., 2018, "Electrohydrodynamic Printing Process Monitoring by Microscopic Image Identification," Int J Bioprint, **5**(1), p. 164.

[132] Poologasundarampillai, G., Haweet, A., Jayash, S. N., Morgan, G., Moore, J. E., and Candeo, A., 2021, "Real-Time Imaging and Analysis of Cell-Hydrogel Interplay within an Extrusion-Bioprinting Capillary," Bioprinting, **23**, p. e00144.

[133] Sedigh, A., DiPiero, D., Shine, K. M., and Tomlinson, R. E., 2022, "Enhancing Precision in Bioprinting Utilizing Fuzzy Systems," Bioprinting, **25**, p. e00190.

[134] Arduengo, J., Hascoet, N., Chinesta, F., and Hascoet, J.-Y., 2024, "Open-Loop Control System for High Precision Extrusion-Based Bioprinting through Machine Learning Modeling," Journal of Machine Engineering, **24**(1), pp. 103–117.

[135] Tashman, J. W., Shiwarski, D. J., Coffin, B., Ruesch, A., Lanni, F., Kainerstorfer, J. M., and Feinberg, A. W., 2022, "In Situ Volumetric Imaging and Analysis of FRESH 3D Bioprinted Constructs Using Optical Coherence Tomography," Biofabrication, **15**(1), p. 014102.

[136] Van Der Valk, D. C., Van Der Ven, C. F. T., Blaser, M. C., Grolman, J. M., Wu, P.-J., Fenton, O. S., Lee, L. H., Tibbitt, M. W., Andresen, J. L., Wen, J. R., Ha, A. H., Buffolo, F., Van Mil, A., Bouten, C. V. C., Body, S. C., Mooney, D. J., Sluijter, J. P. G., Aikawa, M., Hjortnaes, J., Langer, R., and Aikawa, E., 2018, "Engineering a 3D-Bioprinted Model of Human Heart Valve Disease Using Nanoindentation-Based Biomechanics," Nanomaterials, **8**(5), p. 296.

[137] Koch, M., and Włodarczyk-Biegun, M. K., 2020, "Faithful Scanning Electron Microscopic (SEM) Visualization of 3D Printed Alginate-Based Scaffolds," Bioprinting, **20**, p. e00098.

[138] Aston, R., Sewell, K., Klein, T., Lawrie, G., and Grøndahl, L., 2016, "Evaluation of the Impact of Freezing Preparation Techniques on the Characterisation of Alginate Hydrogels by Cryo-SEM," European Polymer Journal, **82**, pp. 1–15.

[139] Franco, A., Van Durme, B., Van Vlierberghe, S., and Dupont-Gillain, C., 2024, "Misleading Pore Size Measurements in Gelatin and Alginate Hydrogels Revealed by Confocal Microscopy," Tissue Engineering Part C: Methods, **30**(7), pp. 307–313.

[140] Moncal, K. K., Ozbolat, V., Datta, P., Heo, D. N., and Ozbolat, I. T., 2019, "Thermally-Controlled Extrusion-Based Bioprinting of Collagen," J Mater Sci: Mater Med, **30**(5), p. 55.

[141] Giovanni Gugliandolo, S., Prioglio, E., Moscatelli, D., and Maria Colosimo, B., 2024, "A New Solution for in Situ Monitoring of Shape Fidelity in Extrusion-Based Bioprinting via Thermal Imaging," IJB, **0**(0), p. 2021.

[142] Prioglio, E., Zanderigo, G., and Colosimo, B. M., 2026, "In-Line Process Monitoring of Extrusion-Based Bioprinting Using In-Situ Thermal Imaging," Procedia CIRP, **138**, pp. 1207–1212.

[143] Chen, J. G., Wadhwa, N., Cha, Y.-J., Durand, F., Freeman, W. T., and Buyukozturk, O., 2014, "Structural Modal Identification Through High Speed Camera Video: Motion Magnification,"

*Topics in Modal Analysis I, Volume 7*, J. De Clerck, ed., Springer International Publishing, Cham, pp. 191–197.

[144] Chen, J. G., Davis, A., Wadhwa, N., Durand, F., Freeman, W. T., and Büyüköztürk, O., 2017, "Video Camera–Based Vibration Measurement for Civil Infrastructure Applications," J. Infrastruct. Syst., **23**(3), p. B4016013.

[145] Friedrich, L., and Begley, M., 2020, "Corner Accuracy in Direct Ink Writing with Support Material," Bioprinting, **19**, p. e00086.

[146] Gharraei, R., Bergstrom, D., and Chen, X. (Daniel), 2024, "Extrusion Bioprinting from a Fluid Mechanics Perspective," Int J Bioprint., **10**(6).

[147] Bonatti, A. F., Vozzi, G., Kai Chua, C., and De Maria, C., 2022, "A Deep Learning Approach for Error Detection and Quantification in Extrusion-Based Bioprinting," Materials Today: Proceedings, **70**, pp. 131–135.

[148] Wadhwa, N., Rubinstein, M., Durand, F., and Freeman, W. T., 2013, "Phase-Based Video Motion Processing," ACM Trans. Graph., **32**(4), pp. 1–10.

[149] Sarrafi, A., Mao, Z., Niezrecki, C., and Poozesh, P., 2018, "Vibration-Based Damage Detection in Wind Turbine Blades Using Phase-Based Motion Estimation and Motion Magnification," Journal of Sound and Vibration, **421**, pp. 300–318.

[150] Sands, M., and Kim, J., 2023, "A Low-Cost and Open-Source Measurement System to Determine the Young's and Shear Moduli and Poisson's Ratio of Soft Materials Using a Raspberry Pi Camera Module and 3D Printed Parts," HardwareX, **13**, p. e00386.

[151] Taylor, R., and Kim, J., 2023, "Monitoring Volumetric Defects in 3D Bioprinting Using Video-Based Vibrometry," American Society of Mechanical Engineers Digital Collection.

[152] Rahman, M. A., Khan, M. A. H., and Kim, J., 2024, "Nozzle Pressure Defect Detection in Extrusion-Based Bio 3D Printing Using Video-Based Motion Estimation," *ASME 2024 Conference on Smart Materials, Adaptive Structures and Intelligent Systems*, American Society of Mechanical Engineers, Atlanta, Georgia, USA, p. V001T05A008.

[153] Khan, M. A. H., Rahman, M. A., and Kim, J., 2025, "In-Situ Condition Monitoring of Extrusion-Based 3d Bio-Printing Using Phase-Based Motion Estimation," American Society of Mechanical Engineers Digital Collection.

[154] Barron, J. A., Wu, P., Ladouceur, H. D., and Ringeisen, B. R., 2004, "Biological Laser Printing: A Novel Technique for Creating Heterogeneous 3-Dimensional Cell Patterns," Biomedical Microdevices, **6**(2), pp. 139–147.

[155] Chang, J., and Sun, X., 2023, "Laser-Induced Forward Transfer Based Laser Bioprinting in Biomedical Applications," Front Bioeng Biotechnol, **11**, p. 1255782.

[156] Vijayavenkataraman, S., Yan, W.-C., Lu, W. F., Wang, C.-H., and Fuh, J. Y. H., 2018, "3D Bioprinting of Tissues and Organs for Regenerative Medicine," Advanced Drug Delivery Reviews, **132**, pp. 296–332.

[157] Dababneh, A. B., and Ozbolat, I. T., 2014, "Bioprinting Technology: A Current State-of-the-Art Review," J. Manuf. Sci. Eng, **136**(061016).

[158] Armstrong, A. A., Pfeil, A., Alleyne, A. G., and Wagoner Johnson, A. J., 2021, "Process Monitoring and Control Strategies in Extrusion-Based Bioprinting to Fabricate Spatially Graded Structures," Bioprinting, **21**, p. e00126.

[159] Huang, D., Swanson, E. A., Lin, C. P., Schuman, J. S., Stinson, W. G., Chang, W., Hee, M. R., Flotte, T., Gregory, K., Puliafito, C. A., and Fujimoto, J. G., 1991, "Optical Coherence Tomography," Science, **254**(5035), pp. 1178–1181.

[160] Swanson, E. A., and Fujimoto, J. G., 2017, "The Ecosystem That Powered the Translation of OCT from Fundamental Research to Clinical and Commercial Impact [Invited]," Biomed. Opt. Express, BOE, **8**(3), pp. 1638–1664.

[161] Fu, M.-Y., Yin, Z.-H., Yao, X.-Y., Xu, J., Liu, Y., Dong, Y., and Shen, Y.-C., 2024, "The Progress of Optical Coherence Tomography in Industry Applications," Adv Devices Instrum, **5**, p. 0053.

[162] Wang, L., Xu, M., Zhang, L., Zhou, Q., and Luo, L., 2016, "Automated Quantitative Assessment of Three-Dimensional Bioprinted Hydrogel Scaffolds Using Optical Coherence Tomography," Biomed. Opt. Express, **7**(3), p. 894.

[163] Yang, S., Wang, L., Chen, Q., and Xu, M., 2021, "In Situ Process Monitoring and Automated Multi-Parameter Evaluation Using Optical Coherence Tomography during Extrusion-Based Bioprinting," Additive Manufacturing, **47**, p. 102251.

[164] Tashman, J. W., Shiwarski, D. J., Coffin, B., Ruesch, A., Lanni, F., Kainerstorfer, J. M., and Feinberg, A. W., 2022, "In Situ Volumetric Imaging and Analysis of FRESH 3D Bioprinted Constructs Using Optical Coherence Tomography," Biofabrication, **15**(1), p. 014102.

[165] Fan, B., Yang, S., Wang, L., and Xu, M., 2024, "Spatially Resolved Defect Characterization and Fidelity Assessment for Complex and Arbitrary Irregular 3D Printing Based on 3D P-OCT and GCode," Sensors, **24**(11), p. 3636.

[166] Shiwarski, D. J., Hudson, A. R., Tashman, J. W., Bakirci, E., Moss, S., Coffin, B. D., and Feinberg, A. W., 2025, "3D Bioprinting of Collagen-Based High-Resolution Internally Perfusable Scaffolds for Engineering Fully Biologic Tissue Systems," Science Advances, **11**(17), p. eadu5905.

[167] Yang, S., Li, Y., Ye, J., Wang, L., and Xu, M., 2025, "Three-Dimensional Bioprinting Utilizing Sacrificial Material Support and Longitudinal Printability Evaluation through Volumetric Imaging," Biomaterials Advances, **169**, p. 214188.

[168] Chen, E. P., Toksoy, Z., Davis, B. A., and Geibel, J. P., 2021, "3D Bioprinting of Vascularized Tissues for in Vitro and in Vivo Applications," Front. Bioeng. Biotechnol., **9**.

[169] Ricciardi, R., Auriemma, F., De Rosa, C., and Lauprêtre, F., 2004, "X-Ray Diffraction Analysis of Poly (Vinyl Alcohol) Hydrogels, Obtained by Freezing and Thawing Techniques," Macromolecules, **37**(5), pp. 1921–1927.

[170] Mansur, H. S., Oréfice, R. L., and Mansur, A. A., 2004, "Characterization of Poly (Vinyl Alcohol)/Poly (Ethylene Glycol) Hydrogels and PVA-Derived Hybrids by Small-Angle X-Ray Scattering and FTIR Spectroscopy," Polymer, **45**(21), pp. 7193–7202.

[171] Gorodzha, S., Douglas, T. E., Samal, S. K., Detsch, R., Cholewa-Kowalska, K., Braeckmans, K., Boccaccini, A. R., Skirtach, A. G., Weinhardt, V., and Baumbach, T., 2016, "High-resolution Synchrotron X-ray Analysis of Bioglass-enriched Hydrogels," Journal of Biomedical Materials Research Part A, **104**(5), pp. 1194–1201.

[172] Keklikoglou, K., Arvanitidis, C., Chatzigeorgiou, G., Chatzinikolaou, E., Karagiannidis, E., Koletsa, T., Magoulas, A., Makris, K., Mavrothalassitis, G., and Papanagnou, E.-D., 2021, "Micro-CT for Biological and Biomedical Studies: A Comparison of Imaging Techniques," Journal of imaging, **7**(9), p. 172.

[173] Moosmann, J., Ershov, A., Weinhardt, V., Baumbach, T., Prasad, M. S., LaBonne, C., Xiao, X., Kashef, J., and Hofmann, R., 2014, "Time-Lapse X-Ray Phase-Contrast Microtomography for in Vivo Imaging and Analysis of Morphogenesis," Nature Protocols, **9**(2), pp. 294–304.

[174] Tuan, H. S., and Hutmacher, D. W., 2005, "Application of Micro CT and Computation Modeling in Bone Tissue Engineering," Computer-Aided Design, **37**(11), pp. 1151–1161.

[175] Datta, S., Jana, S., Das, A., Chakraborty, A., Chowdhury, A. R., and Datta, P., 2020, "Bioprinting of Radiopaque Constructs for Tissue Engineering and Understanding Degradation Behavior by Use of Micro-CT," Bioactive Materials, **5**(3), pp. 569–576.

[176] Ning, L., Zhu, N., Smith, A., Rajaram, A., Hou, H., Srinivasan, S., Mohabatpour, F., He, L., Mclnnes, A., Serpooshan, V., Papagerakis, P., and Chen, X., 2021, "Noninvasive Three-Dimensional In Situ and In Vivo Characterization of Bioprinted Hydrogel Scaffolds Using the X-Ray Propagation-Based Imaging Technique," ACS Appl. Mater. Interfaces, **13**(22), pp. 25611–25623.

[177] Gureyev, T., Nesterets, Y. I., Baran, P., Taba, S., Mayo, S., Thompson, D., Arhatari, B., Mihocic, A., Abbey, B., and Lockie, D., 2019, "Propagation-based X-ray Phase-contrast Tomography of Mastectomy Samples Using Synchrotron Radiation," Medical physics, **46**(12), pp. 5478–5487.

[178] Appel, A., Anastasio, M. A., and Brey, E. M., 2011, "Potential for Imaging Engineered Tissues with X-Ray Phase Contrast," Tissue Engineering Part B: Reviews, **17**(5), pp. 321–330.

[179] Keklikoglou, K., Faulwetter, S., Chatzinikolaou, E., Wils, P., Brecko, J., Kvaček, J., Metscher, B., and Arvanitidis, C., 2019, "Micro-Computed Tomography for Natural History Specimens: A Handbook of Best Practice Protocols," European Journal of Taxonomy, (522).

[180] Ramirez, S. P., Hernandez, I., Balcorta, H. V., Kumar, P., Kumar, V., Poon, W., and Joddar, B., 2023, "Microcomputed Tomography for the Microstructure Evaluation of 3D Bioprinted Scaffolds," ACS Applied Bio Materials, **7**(12), pp. 7799–7808.

[181] Haleem, A., and Javaid, M., 2018, "Role of CT and MRI in the Design and Development of Orthopaedic Model Using Additive Manufacturing," Journal of Clinical Orthopaedics and Trauma, **9**(3), pp. 213–217.

[182] Fu, F., Qin, Z., Xu, C., Chen, X., Li, R., Wang, L., Peng, D., Sun, H., Tu, Y., Chen, C., Zhang, S., Zhao, M., and Li, X., 2017, "Magnetic Resonance Imaging-Three-Dimensional Printing Technology Fabricates Customized Scaffolds for Brain Tissue Engineering," Neural Regeneration Research, **12**(4), p. 614.

[183] Tomer, G., Newton, J. M., and Kinchesh, P., 1999, "Magnetic Resonance Imaging (MRI) as a Method to Investigate Movement of Water During the Extrusion of Pastes," Pharm Res, **16**(5), pp. 666–671.

[184] Schmieg, B., Gretzinger, S., Schuhmann, S., Guthausen, G., and Hubbuch, J., 2022, "Magnetic Resonance Imaging as a Tool for Quality Control in Extrusion-Based Bioprinting," Biotechnology Journal, **17**(5), p. 2100336.

[185] Chen, Z., Yan, C., Yan, S., Liu, Q., Hou, M., Xu, Y., and Guo, R., 2018, "Non-Invasive Monitoring of in Vivo Hydrogel Degradation and Cartilage Regeneration by Multiparametric MR Imaging," Theranostics, **8**(4), pp. 1146–1158.

[186] Gnanago, J.-L., Gerges, T., Chastagnier, L., Petiot, E., Semet, V., Lombard, P., Christophe, M., Cabrera, M., and Lambert, S. A., 2021, "Compact MRI Bioreactor for Real-Time Monitoring 3D Printed Tissue-Engineered Constructs."

[187] Theus, A. S., Ning, L., Kabboul, G., Hwang, B., Tomov, M. L., LaRock, C. N., Bauser-Heaton, H., Mahmoudi, M., and Serpooshan, V., 2022, "3D Bioprinting of Nanoparticle-Laden Hydrogel Scaffolds with Enhanced Antibacterial and Imaging Properties," iScience, **25**(9).

[188] Kim, K., and Wagner, W. R., 2016, "Non-Invasive and Non-Destructive Characterization of Tissue Engineered Constructs Using Ultrasound Imaging Technologies: A Review," Ann Biomed Eng, **44**(3), pp. 621–635.

[189] Dalecki, D., Mercado, K. P., and Hocking, D. C., 2016, "Quantitative Ultrasound for Nondestructive Characterization of Engineered Tissues and Biomaterials," Ann Biomed Eng, **44**(3), pp. 636–648.

[190] Zhou, Y., 2016, "The Application of Ultrasound in 3D Bio-Printing," Molecules, **21**(5).

[191] Walker, J. M., Myers, A. M., Schluchter, M. D., Goldberg, V. M., Caplan, A. I., Berilla, J. A., Mansour, J. M., and Welter, J. F., 2011, "Nondestructive Evaluation of Hydrogel Mechanical Properties Using Ultrasound," Ann Biomed Eng, **39**(10), pp. 2521–2530.

[192] Yang, T., Jin, Y., Smith, L. M., Dahotre, N. B., and Neogi, A., 2024, "Real-Time in-Situ Ultrasound Monitoring of Soft Hydrogel 3D Printing with Subwavelength Resolution," Commun Eng, **3**(1), p. 162.

[193] Mercado, K. P., Helguera, M., Hocking, D. C., and Dalecki, D., 2015, "Noninvasive Quantitative Imaging of Collagen Microstructure in Three-Dimensional Hydrogels Using High-Frequency Ultrasound," Tissue Engineering Part C: Methods, **21**(7), pp. 671–682.

[194] Gudur, M., Rao, R. R., Hsiao, Y.-S., Peterson, A. W., Deng, C. X., and Stegemann, J. P., 2012, "Noninvasive, Quantitative, Spatiotemporal Characterization of Mineralization in Three-Dimensional Collagen Hydrogels Using High-Resolution Spectral Ultrasound Imaging," Tissue Engineering Part C: Methods, **18**(12), pp. 935–946.

[195] Narayanan, L. K., Thompson, T. L., Shirwaiker, R. A., and Starly, B., 2018, "Label Free Process Monitoring of 3D Bioprinted Engineered Constructs via Dielectric Impedance Spectroscopy," Biofabrication, **10**(3), p. 035012.

[196] Narayanan, L. K., 2019, *Manufacturability Considerations in Biofabrication–Functional Mapping, Risk Assessment and Dielectric Impedance Spectroscopy-Based Non-Destructive Quality Evaluation*, North Carolina State University.

[197] Haring, A. P., Jiang, S., Barron, C., Thompson, E. G., Sontheimer, H., He, J.-Q., Jia, X., and Johnson, B. N., 2020, "3D Bioprinting Using Hollow Multifunctional Fiber Impedimetric Sensors," Biofabrication, **12**(3), p. 035026.

[198] Mojena-Medina, D., Hubl, M., Bäuscher, M., Jorcano, J. L., Ngo, H.-D., and Acedo, P., 2020, "Real-Time Impedance Monitoring of Epithelial Cultures with Inkjet-Printed Interdigitated-Electrode Sensors," Sensors, **20**(19), p. 5711.

[199] Shohan, S., Harm, J., Hasan, M., Starly, B., and Shirwaiker, R., 2021, "Non-Destructive Quality Monitoring of 3D Printed Tissue Scaffolds via Dielectric Impedance Spectroscopy and Supervised Machine Learning," Procedia Manufacturing, **53**, pp. 636–643.

[200] Matavosian, A. A., Griffin, A. C., Bhuiyan, D. B., Lyness, A. M., Bhatnagar, V., and Bonassar, L. J., 2025, "Real-Time Assessment of Cell Concentration and Viability Onboard a Syringe Using Dielectric Impedance Spectroscopy for Extrusion Bioprinting," Biofabrication, **17**(2), p. 025018.

[201] Strauß, S., Schroth, B., and Hubbuch, J., 2022, "Evaluation of the Reproducibility and Robustness of Extrusion-Based Bioprinting Processes Applying a Flow Sensor," Front. Bioeng. Biotechnol., **10**.

[202] Wenger, L., Strauß, S., and Hubbuch, J., 2022, "Automated and Dynamic Extrusion Pressure Adjustment Based on Real-Time Flow Rate Measurements for Precise Ink Dispensing in 3D Bioprinting," Bioprinting, **28**, p. e00229.

[203] Chen, X., O'Mahony, A., and Barber, T., 2022, "The Assessment of Average Cell Number inside In-Flight 3D Printed Droplets in Microvalve-Based Bioprinting," J. Appl. Phys., **131**(22), p. 224701.

[204] Zhang, J., Yu, K., Yao, Y., Lu, L., Gao, Q., Zhang, P., Shang, G., and Sing, S. L., 2026, "A Transformer-Based Framework for Cross-Material in Situ Monitoring in Extrusion-Based Bioprinting," Advanced Engineering Informatics, **71**, p. 104323.

[205] Ramya, V., Rohith, S. L., and Ananthi, G., 2024, "Automated Defect Classification in 3D Bioprinting Using Liquid Neural Networks," IEEE, pp. 1–5.

[206] Zhang, C., Elvitigala, K. C. M. L., and Sakai, S., 2026, "AI-Powered Printability Evaluation Framework for 3D Bioprinting Using Hausdorff Distance Metrics," Biofabrication, **18**(1), p. 015015.

[207] Bastianini, B., 2024, "Predictive Modeling and In-Situ Optimization of Two-Photon Bioprinting Using Deep Learning Techniques."

[208] Diamantides, N., Dugopolski, C., Blahut, E., Kennedy, S., and Bonassar, L. J., 2019, "High Density Cell Seeding Affects the Rheology and Printability of Collagen Bioinks," Biofabrication, **11**(4), p. 045016.

[209] Margarita, A., Gugliandolo, S. G., Santoni, S., Moscatelli, D., and Colosimo, B. M., 2025, "A Novel Solution for Real-Time in-Situ Cell Distribution Monitoring in 3D Bioprinting via Fluorescence Imaging," Biofabrication, **17**(2).

[210] Kim, S. H., Kwon, J. S., Cho, J. G., Park, K. G., Lim, T. H., Kim, M. S., Choi, H. S., Park, C. H., and Lee, S. J., 2021, "Non-Invasive in Vivo Monitoring of Transplanted Stem Cells in 3D-Bioprinted Constructs Using near-Infrared Fluorescent Imaging," Bioengineering & Translational Medicine, **6**(2), p. e10216.

[211] Chansoria, P., Narayanan, L. K., Schuchard, K., and Shirwaiker, R., 2019, "Ultrasound-Assisted Biofabrication and Bioprinting of Preferentially Aligned Three-Dimensional Cellular Constructs," Biofabrication, **11**(3), p. 035015.

[212] Bushnell, G. G., Hong, X., Hartfield, R. M., Zhang, Y., Oakes, R. S., Rao, S. S., Jeruss, J. S., Stegemann, J. P., Deng, C. X., and Shea, L. D., 2020, "High Frequency Spectral Ultrasound Imaging to Detect Metastasis in Implanted Biomaterial Scaffolds," Ann Biomed Eng, **48**(1), pp. 477–489.

[213] Yu, C., and Jiang, J., 2020, "A Perspective on Using Machine Learning in 3D Bioprinting," International Journal of Bioprinting, **6**(1), p. 253.

[214] Ruberu, K., Senadeera, M., Rana, S., Gupta, S., Chung, J., Yue, Z., Venkatesh, S., and Wallace, G., 2021, "Coupling Machine Learning with 3D Bioprinting to Fast Track Optimisation of Extrusion Printing," Applied Materials Today, **22**, p. 100914.

[215] Rafieyan, S., Ansari, E., and Vasheghani-Farahani, E., 2024, "A Practical Machine Learning Approach for Predicting the Quality of 3D (Bio) Printed Scaffolds," Biofabrication, **16**(4), p. 045014.

[216] Mohammadrezaei, D., Podina, L., Silva, J. D., and Kohandel, M., 2024, "Cell Viability Prediction and Optimization in Extrusion-Based Bioprinting via Neural Network-Based Bayesian Optimization Models," Biofabrication, **16**(2), p. 025016.

[217] Dey, M. K., Ikponmwoba, E., John, P., Belgodere, J. A., Semmes, I., Park, D. S., Monroe, W. T., and Devireddy, R., "Ai Driven Dual-Task Deep Learning Framework for Automated Scaffold Quality Assessment in Extrusion Based 3d Bioprinting," Available at SSRN 5374136.

[218] Zanderigo, G., Afghah, F., Colosimo, B. M., and Raman, R., 2025, "Modular and AI-Driven in Situ Monitoring Platform for Real-Time Process Analysis in Embedded Bioprinting," Device, **3**(11).

[219] Ning, H., Zhou, T., and Joo, S. W., 2023, "Machine Learning Boosts Three-Dimensional Bioprinting," Int J Bioprint, **9**(4), p. 739.

[220] Ke, D., 2025, "AI-Driven Closed-Loop Extrusion-Based Bioprinting System: From Dynamic Regulation to Medical Translation," Bioprinting, p. e00459.

[221] Kelly, D., Sergis, V., Ventura i Blanco, L., Mason, K., and Daly, A. C., 2025, "Autonomous Control of Extrusion Bioprinting Using Convolutional Neural Networks," Advanced Functional Materials, **35**(30), p. 2424553.

[222] Oh, D., Shirzad, M., Kim, M. C., Chung, E. J., and Nam, S. Y., 2023, "Rheology-Informed Hierarchical Machine Learning Model for the Prediction of Printing Resolution in Extrusion-Based Bioprinting," International Journal of Bioprinting, **9**(6), pp. 308–324.

[223] Fu, Z., Angeline, V., and Sun, W., 2021, "Evaluation of Printing Parameters on 3D Extrusion Printing of Pluronic Hydrogels and Machine Learning Guided Parameter Recommendation," International journal of bioprinting, **7**(4), p. 434.

[224] An, J., Chua, C. K., and Mironov, V., 2021, "Application of Machine Learning in 3D Bioprinting: Focus on Development of Big Data and Digital Twin," Int J Bioprint, **7**(1), p. 342.

[225] Zhang, Z., Zhou, X., Fang, Y., Xiong, Z., and Zhang, T., 2025, "AI-Driven 3D Bioprinting for Regenerative Medicine: From Bench to Bedside," Bioactive Materials, **45**, pp. 201–230.

[226] Upadhyay, S., and Gupta, A., 2025, "Machine Learning in 3D Bioprinting: Enhancing Biomaterials for Regenerative Medicine," *Advanced Technologies for Sustainable Biomedical Applications*, CRC Press, pp. 483–507.

[227] Mueller, E., Desai, S., Lundberg, M. S., Somara, S., Kengla, C., Schmidt, J., and Mitra, K., 2026, "Integrating 3D Bioprinting and AI in Healthcare," Current Stem Cell Reports, **12**(1), p. 1.

[228] Ramya, V., Vinothini, N., Levin Rohith, S., and Ananthi, G., 2026, "DenseNet-Driven Federated Learning for Enhanced Fault Detection in 3D Bioprinting," *Innovative and Intelligent Computing for Global Sustainability*, Springer, pp. 9–17.

[229] Guan, J., You, S., Xiang, Y., Schimelman, J., Alido, J., Ma, X., Tang, M., and Chen, S., 2022, "Compensating the Cell-Induced Light Scattering Effect in Light-Based Bioprinting Using Deep Learning," Biofabrication, **14**(1), p. 015011.

[230] Rafieyan, S., Ansari, E., and Vasheghani-Farahani, E., 2024, "A Practical Machine Learning Approach for Predicting the Quality of 3D (Bio) Printed Scaffolds," Biofabrication, **16**(4), p. 045014.

[231] Li, B., Wang, Z., Huang, C., Xu, L., Huang, S., Qu, M., Xu, Z., Zhang, D., Guo, B., and Jin, T., 2025, "A Comprehensive Review on the Printing Efficiency, Precision, and Cell Viability in 3D Bioprinting," Medical Engineering & Physics, p. 104448.

[232] Simińska-Stanny, J., Tournier, P., Shavandi, A., and Habib, S. J., 2026, "Geometrical Designs in Volumetric Bioprinting to Study Cellular Behaviors in Engineered Constructs," Advanced Healthcare Materials, **15**(6), p. e03550.

[233] Grigioni, M., Daniele, C., Morbiducci, U., D'Avenio, G., Di Benedetto, G., and Barbaro, V., 2004, "The Power-law Mathematical Model for Blood Damage Prediction: Analytical Developments and Physical Inconsistencies," Artificial organs, **28**(5), pp. 467–475.

[234] Grigioni, M., Morbiducci, U., D'Avenio, G., Benedetto, G. D., and Gaudio, C. D., 2005, "A Novel Formulation for Blood Trauma Prediction by a Modified Power-Law Mathematical Model," Biomechanics and Modeling in Mechanobiology, **4**(4), pp. 249–260.

[235] Müller, S. J., Fabry, B., and Gekle, S., 2023, "Predicting Cell Stress and Strain during Extrusion Bioprinting," Phys. Rev. Applied, **19**(6), p. 064061.

[236] Boularaoui, S., Al Hussein, G., Khan, K. A., Christoforou, N., and Stefanini, C., 2020, "An Overview of Extrusion-Based Bioprinting with a Focus on Induced Shear Stress and Its Effect on Cell Viability," Bioprinting, **20**, p. e00093.

[237] Huang, X., Ng, W. L., and Yeong, W. Y., 2024, "Predicting the Number of Printed Cells during Inkjet-Based Bioprinting Process Based on Droplet Velocity Profile Using Machine Learning Approaches," J Intell Manuf, **35**(5), pp. 2349–2364.

[238] Suh, Y. J., Lim, T. H., Choi, H. S., Kim, M. S., Lee, S. J., Kim, S. H., and Park, C. H., 2020, "3D Printing and NIR Fluorescence Imaging Techniques for the Fabrication of Implants," Materials, **13**(21), p. 4819.

[239] West-Livingston, L. N., Park, J., Lee, S. J., Atala, A., and Yoo, J. J., 2020, "The Role of the Microenvironment in Controlling the Fate of Bioprinted Stem Cells," Chemical reviews, **120**(19), pp. 11056–11092.

[240] Zhang, C., Elvitigala, K. C. M. L., Mubarok, W., Okano, Y., and Sakai, S., 2024, "Machine Learning-Based Prediction and Optimisation Framework for as-Extruded Cell Viability in Extrusion-Based 3D Bioprinting," Virtual and Physical Prototyping, **19**(1), p. e2400330.

[241] Ning, L., Betancourt, N., Schreyer, D. J., and Chen, X., 2018, "Characterization of Cell Damage and Proliferative Ability during and after Bioprinting," ACS Biomaterials Science & Engineering, **4**(11), pp. 3906–3918.

[242] Müller, S. J., Fabry, B., and Gekle, S., 2023, "Predicting Cell Stress and Strain during Extrusion Bioprinting," Physical Review Applied, **19**(6), p. 064061.

[243] Mladenovska, T., Choong, P. F., Wallace, G. G., and O'Connell, C. D., 2023, "The Regulatory Challenge of 3D Bioprinting," Regenerative Medicine, **18**(8), pp. 659–674.

[244] Li, P., Faulkner, A., and Medcalf, N., 2020, "3D Bioprinting in a 2D Regulatory Landscape: Gaps, Uncertainties, and Problems," Law, Innovation and Technology, **12**(1), pp. 1–29.

[245] Hourd, P., Medcalf, N., Segal, J., and Williams, D. J., 2015, "A 3D Bioprinting Exemplar of the Consequences of the Regulatory Requirements on Customized Processes," Regenerative Medicine, **10**(7), pp. 863–883.

[246] "3D Bio-Printed Products: ICMRA Members Discuss Potential Regulatory Frameworks."